NSMB

NETHERLANDS SHIP MODEL BASIN
P.O. BOX 28 · WAGENINGEN · THE NETHERLANDS

Report No. 67-163-AH

Contract No. N 62558-4555

Series of Model Tests on Ducted Propellers.

Final Report

November 1967.

SERIES OF MODEL TESTS ON DUCTED PROPELLERS.

(Final Report)

by:

Ir. M.W.C. Oosterveld

This research was carried out under the Naval Ship Systems Command General Hydromechanics Research Program SR 009-01-01, administered by the Naval Ship Research and Development Center. Prepared under the Office of Naval Research Contract

N62558-4555

Contents:

Abstract
Administrative information

1. Introduction
2. Method for the calculation of systematic nozzle series
3. Experiments with systematic series of nozzles shapes
   3.1. Nozzle shapes selected for the experiments
   3.2. Open water tests
   3.3. Cavitation tests
   3.4. Presentation of the tests results
4. Discussion of the theoretical and experimental results
5. Conclusions

References
List of Figures
List of Tables
List of Symbols
Appendix A

Abstract.

This report presents the results of open water tests and observation of the cavitation characteristics of systematic series of flow decelerating type of nozzles (or pumpjets). The tested nozzle shapes have been derived theoretically. The results of these theoretical calculations and of the experiments, are presented in a non-dimensional form in graphs and tables.
A discussion of the results is given.

Administrative information.

This research was carried out under the Naval Ship Systems Command, General Hydromechanics Research Program SR 009 01 01, administered by the Naval Ship Research and Development Center. Prepared under the Office of Naval Research Contract

N 62558 4555

1. Introduction.

Important parameters for the design of the nozzle of a ducted propeller are (see also Fig. 1):

the thrust coefficient, $C_T = T/\frac{1}{2}\rho V_e^2 \frac{\pi}{4}D^2$

the propeller thrust - total thrust ratio, $\tau = T_P/T$

and further the nozzle length - diameter ratio L/D, the thickness distribution and maximum thickness of the nozzle profile S/L, the percentage of nozzle length in front of the propeller a/L, and the hub-diameter ratio d/D.

The ducted propeller with the accelerating flow type of nozzle has been tested extensively in the past and is now frequently used in cases where the ship screw is heavily loaded. A positive thrust is developed on the accelerating nozzle ($\tau < 1$). For heavy screw loads ($C_T > 2$-3) an accelerating nozzle can improve the efficiency of the propulsion system.

The application of the flow decelerating nozzle may be attractive if retardation of propeller cavitation phenomena is desired. This retardation of propeller cavitation will also lead to a reduction in noise level which may be of importance for tactical reasons.

The reduction of the flow rate inside the decelerating type of nozzle, results in an increment of the static pressure at the impeller. This increment is attractive from a point of view of retardation of screw cavitation. The duct itself, however, will produce a negative thrust ($\tau > 1$). In order to compensate for this thrust loss (induced nozzle drag), the screw loading must be increased. An improvement of cavitation properties of the screw will therefore only be obtained if the gain in static pressure at least compensates the unfavourable effect of the increased screw loading.

The present report presents the results of investigations into suitable nozzle shapes for flow decelerating nozzles. These investigations are a continuation of the investigation which has been carried out under the Bureau of Ship's, General Hydrodynamic Research Program, S-R009-01-01, administered by the Naval Ship Research and Development Center, contract number N 62558-3960 and which covered the following details (see also Ref. [1]):

- Development of a simplified method for the calculation of nozzle shapes based on vortex theory. The effect of a finite hub and the thickness of the nozzle profile was taken into account.
- Selection of three nozzle shapes with the aid of the above theory, each designed for operating at the same thrust coefficient C_T ($C_T \approx 0.95$), but for different propeller thrust-total thrust ratios τ ($\tau \approx 1.00$; 1.15 and 1.30). Measurements in the cavitation tunnel were performed with these nozzles.
- Investigation of the validity of the approximate method for the calculation of the nozzle propeller performance by a comparison with the results of the measurements in the cavitation tunnel.

The present report gives the results of the calculations of suitable nozzle shapes for flow decelerating nozzles in a more detailed way.
A number of nozzle shapes with the following variation of the design parameters have been manufactured and tested:

Nozzle No.	C_T	τ	L/D	a/L	S/L	d/D
30	0.95	1.00	0.6	0.5	0.15	0.20
31	0.95	1.15	0.6	0.5	0.15	0.20
32	0.95	1.30	0.6	0.5	0.15	0.20
33	1.00	1.20	0.6	0.5	0.15	0.20
34	1.00	1.20	0.6	0.5	0.09	0.20
35	1.00	1.20	0.9	0.5	0.10	0.20
36	1.00	1.20	1.2	0.5	0.075	0.20

The experiments with these nozzles in combination with a screw series designed for nozzle no. 31, were carried out both in the towing tank and in the cavitation tunnel. The results of the open water tests (with all nozzles shapes) and of the flow observations in the cavitation tunnel (with nozzles nos. 33 and 36) are shown graphically in non-dimensional form. A discussion of the results is given.

2. Method for the calculation of systematic nozzle series.

A simplified method has been used, based on vortex theory, to enable the calculation of the nozzle propeller characteristics of systematic series of nozzle shapes. The calculations were based on the assumption that the forward velocity of the ducted propeller system was sufficiently large and the impeller and nozzle loading were sufficiently low to permit the application of a linearized theory.

The ducted propeller system considered was assumed to consist of an annular airfoil surrounding an impeller having an infinite number of blades. The impeller is regarded as a uniformely loaded actuator disc, set normal to the free stream. It is driven to rotate in its own plane with angular velocity ω .

The nozzle was represented by source and vortex rings, axially distributed at the nozzle mean radius. The source distribution represents the thickness effect of the nozzle; the vortex density along the nozzle, representing the nozzle loading, was chosen sinusoidal with zero strength at the leading and trailing edges of the nozzle.

The total induced velocities due to the different vortex and source distributions representing the impeller and the nozzle can be calculated according to the law of Biot-Savart if the main dimensions of the system (L/D, a/L, d/L, S/L and the thickness distribution of the nozzle), the advance coefficient of the screw ($J = V_e/nD$), and the loading of the impeller and nozzle are given. The impeller thrust and torque, the thrust on the nozzle and the ideal efficiency of the system can be calculated now for the chosen values of the design parameters.
In addition, the shape of the nozzle and the pressure distribution along the nozzle can be computed.
The method for the calculation of the ducted propeller characteristics is, in a more detailed way, given in Appendix A.

It is shown in Appendix A, that for the chosen load distributions of impeller and nozzle, the shape of the nozzle is completely determined by the values of the thrust coefficient C_{T_o} , the impeller thrust - total thrust thrust ratio τ_o and the main dimensions of the ducted propeller system. Here, the subscript "o" denotes that ducted propeller system is considered with an impeller rotating at infinite angular velocity or with an advance coefficient equal to zero. Then, the tangentially induced velocities and consequently the losses due to the rotation of the fluid are zero. The case that the impeller rotates with an infinite angular velocity coincides with the case that the impeller rotates with finite angular velocity while a stator is used to eliminate the rotational losses.

Starting from given thrust coefficients C_{T_o} , thrust ratios τ_o (thus at $J = 0$), and the main dimensions, the characteristics of a number of ducted propellers were calculated. It must be noted that for the thickness distribution of the nozzle profiles of all nozzles given in this report the NACA four-digit wing section basic thickness form was used.
First, the shape and the pressure distribution along these nozzles were derived. Secondly, the thrust coefficient C_T , thrust ratio τ and the ideal efficiency η_i of these ducted propellers were calculated over a range of advance coefficients J .

The data used for the computations and the results are given in the Tables A_1, A_2 and A_3 of Appendix A. Some results are presented in the Figs. 2 through 9. Figs. 2 and 3 show the effect of the thrust ratio τ_o on the shape of the nozzle and the characteristics of ducted propeller systems.
The effect of the nozzle length diameter ratio L/D and the thickness ratio of the nozzle profile S/L are shown in the Figs. 4 and 5 and the Figs. 6 and 7 respectively. The pressure distributions along the interior and the exterior surface of various nozzles are given in the Figs. 8 and 9.

The afore mentioned method for the calculation of the ducted propeller characteristics enables the analysis of the sectional lift coefficient C_L of the nozzle under design condition. Analyses of the sectional lift coefficient C_L have been made for nozzles with different thrust ratios τ_o , different thickness ratios, S/L and different nozzle length diameter ratios L/D . The results which are independent of the value of the thrust coefficient C_{T_o} , are presented in Fig. 10. The minimum pressure at the exterior surface of the nozzle and the mean pressure at the impeller plane are presented in non-dimensional form in Fig. 11, as a function of τ_o , L/D and S/L

Finally, an approximate method of calculation has been followed in order to determine whether an improvement of the screw cavitation characteristics can be obtained by application of a nozzle. A comprehensive set of data on the cavitation properties of propellers designed according to the vortex theory (see Ref. [2]) permits the introduction of the following empirical relation for the minimum pressure on the screw blades:

$$\left[C_{p_{min}}\right]_{screw} = \frac{P_{min} - P_\infty}{\frac{1}{2}\rho V_e^2} = -\frac{\pi\left[2.4 + 0.6Z\right]C_T}{8\left[A_e/A + 0.2\right]}$$

where the blade-area ratio and the number of blades of the screw are denoted by A_e/A and Z respectively. The ducted propeller may now be regarded as operating in open-water with an equivalent uniform stream velocity ($V_e + U_n$) and an equivalent static pressure of the undisturbed stream $\left[P_\infty + \frac{1}{2}\rho V_e^2 - \frac{1}{2}\rho(V_e + U_n)^2\right]$. Term U_n denotes the mean axial velocity at the impeller due to the nozzle action. The relation between U_n , C_T and τ has been calculated with the aid of the vortex theory given before.

Hence, the minimum static pressure coefficient on the impeller blades of the ducted propeller may be written as:

$$\left[C_{p_{min}}\right]_{\substack{ducted \\ propeller}} = \frac{P_{min} - P_\infty}{\frac{1}{2}\rho V_e^2} = -\frac{\pi\left[2.4 + 0.6Z\right]\tau\, C_T}{8\left[A_e/A + 0.2\right]} + 1 - \left(1 + \frac{U_n}{V_e}\right)^2$$

Analyses of the pressure coefficient $C_{p_{min}}$ corresponding to ducted propellers with different thrust coefficients C_T and thrust ratios τ , and for $A_e/A = 1$ and $Z = 5$ were made. The result is presented in Fig. 12.

3. Experiments with systematic series of nozzle shapes.

3.1. Nozzle shapes selected for the experiments.

The main dimensions and the assumed impeller and nozzle loading of the nozzles selected for the experiments were mentioned already in the introduction and are given in Table I.
The following variations of the design coefficients of the nozzles were considered:

- variations in the thrust ratio τ_o at the design thrust coefficient C_{T_o} (nozzles nos. 30,31 and 32)
- variations in the length-diameter ratio L/D (nozzles nos. 33, 35 and 36)
- variations in the thickness ratio of the nozzle profiles S/L (nozzles nos. 33 and 34)

The nozzle shapes are presented in the Figs. 13, 14 and 15 and are tabulated in Table II.

The experiments were all carried out with a series of five bladed Kaplan type screws (Kd 5-100 series). The Kd 5-100 series screws were designed in combination with nozzle no. 31. The pitch distributions of the screws depend on the velocities induced by the nozzle at the impeller plane and on the radial load distributions of the screws. Particulars of the screw models are given in Table III and in Fig.16. The screws were located in the nozzles with a uniform tip clearance of 1 mm. (about 0.4 percent of the screw diameter D).

3.2. Open-water tests.

The tests were carried out with the usual tank apparatus for open-water tests of ducted propellers.

Fig. 17 shows the measuring equipment which is fixed under the carriage running over the tank during the tests. The usual routine of open-water tests was followed; the RPM of the screw was kept constant and by varying the speed of advance the desired value of the advance coefficient J was obtained. The RPM was chosen as high as possible to obtain a high Reynolds number. Speeds above 3 m/sec could not be investigated on account of the towing carriage. The tests were normally made at 350 RPM of the screw.

3.3. Cavitation tests.

The nozzles nos. 33 and 36 were tested in the NSMB cavitation tunnel no. 1, having a 90cm x 90cm closed working section and a uniform flow distribution. A description of this facility is given in Ref. [6] . The nozzles were fitted to the tunnel wall by means of faired struts.
During the tests the RPM of the screw was kept constant and by varying the pressure and the water velocity in the tunnel the region of bubble cavitation at the exterior surface of the nozzle was determined. The tests were normally made at 1200 RPM of the screw. Corrections were applied to the velocity and the pressure for tunnel wall interference. These corrections were based on the thrust identity of the screws in the tunnel and in the open-water condition.

3.4. Presentation of the test results.

All the open-water test results were faired by computer and plotted in the conventional way with the coefficients:

$$K_T = \frac{T}{\rho n^2 D^4}$$

$$K_{T_n} = \frac{T_n}{\rho n^2 D^4}$$

$$K_Q = \frac{Q}{\rho n^2 D^4}$$

$$\eta_p = \frac{J}{2\pi} \frac{K_T}{K_Q}$$

as functions of the advance coefficient $J=\frac{V_e}{nD}$. The diagrams are given as Figs. 18 through 23. It must be noted that in the presentation of the test results (Figs. 18 through 23) the diameter D denotes now the tip diameter of the impeller.
In addition the test results were plotted with the coefficients:

$$C_T = \frac{T}{\frac{1}{2}\rho V_e^2 \pi/4 D^2} = \frac{8}{\pi}\cdot\frac{K_T}{J^2}$$

$$\tau = \frac{T_p}{T}$$

$$\eta_p = \frac{J}{2\pi}\cdot\frac{K_T}{K_Q}$$

as functions of the advance coefficient J . These diagrams are given in the Figs. 25 through 31.
The experimentally obtained relations between the thrust coefficient C_T and the thrust ratio τ of the various nozzles are given in the Figs. 32 and 33. In addition, the design thrust coefficient C_T and the design thrust ratio τ are given in these Figures.

For design purpose, various practical results can be derived from these diagrams. For instance, in the case where the torque Q of a screw and V_e and n are given, the determination of the optimum diameter from a point of view of efficiency of the ducted propeller system can be solved by plotting η_p and δ ($\delta=\frac{101.27}{J}$) as functions of:

$$\frac{K_Q}{J^5} = \frac{n^3 Q}{\rho V_e^5} = \frac{n^2 P}{2\pi\rho V_e^5}$$

The well-known coefficient B_p is related to the above expression by the equation:

$$B_p = 33.08\,\frac{K_Q^{1/2}}{J^{5/2}}$$

For all the nozzles the coefficients η_p and δ are given for optimum diameter in the Figs. 34 and 35 on a basis of B_p. In addition, the relation between B_p and C_T for the different nozzles are given in these diagrams.

As a compasrison, the optimum curves for efficiency η_p, diameter coefficient δ and thrust ratio τ of the Ka 4-70 screw series in nozzle no. 19A, the B 4-70 screw series and the Kd 5-100 screw series in nozzle no. 33 are given in Fig. 36 on a basis of B_p. Nozzle no. 19A is the standard nozzle profile applied by the NSMB in the case of heavy loaded screws. This nozzle is of the accelerating flow type (see Ref. [4] and [5]). Screws of the B 4-70 screw series are usually applied behind single screw ships. (see for instance Ref. [7]).

Finally, the results of investigations in the cavitation tunnel with the nozzles nos. 33 and 36 are given in Fig. 37. In this diagram, the faired curves for the onset of bubble cavitation at the exterior surface of the nozzles are given as a function of C_T.
The cavitation number σ was based on the speed of advance of the ducted propeller system:

$$\sigma = \frac{P_e - P_v}{\frac{1}{2}\rho V_e^2}$$

where P_e denotes the vapour pressure of the water.

4. Discussion of the theoretical and experimental results.

A large number of theoretical investigations have been conducted on ducted propellers during the past thirty years. A general review of recent studies on ducted propellers has been given by Morgan and Voigt [3] .

They classified the calculations of ducted propellers into two types:

- The direct problem of the ducted propellers, in which the geometry of the ducted propeller system is given and the pressure distribution and force on the duct must be determined
- The inverse problem of ducted propellers, in which a certain combination of impeller forces and duct forces are given and the shape of the nozzle must be determined.

The present investigation is concerned with the inverse problem although a slightly different approach has been chosen. In this approach the nozzle shape was determined for a given uniform loading of the actuator disc representing the impeller and for a given circulation of the nozzle. From a point of view of simplicity in computation this method is very attractive, however, it gives only the possibility of determining nozzle shapes which will operate satisfactory for a given flow condition.

Some of the more general results of the computations were presented in the Figs. 10, 11 and 12.
The result of the analysis of the sectional lift coefficient C_L of nozzles was given in Fig. 10. The value of the lift coefficient of the nozzle will give a rough indication with respect to the danger of flow separation on the nozzle.
From two-dimensional airfoil flow it is well known that flow separation will occur when the lift coefficient C_L exceeds a value of about 1. From Fig. 10 it can be seen that the risk of flow separation on the exterior surface of the nozzle is small, even in the case of large thrust ratios τ . The application of the decelerating type of nozzle results in an increment of the pressure at the impeller and a reduction of the pressure at the exterior surface of the nozzle. Minimum pressures which may occur at the exterior surface of the decelerating nozzle were given in Fig. 11.

The effect of nozzle length and maximum thickness of the nozzle profile on the minimumpressure were shown in this diagram. The result of the analysis of the minimum pressure at the impeller blades of a ducted propeller was presented in Fig. 12. This diagram shows that, for the particular screw considered ($A_e/A = 1$ $Z = 5$), only for low values of C_T , the flow decelerating type of nozzle affects favourably the cavitation properties of the screw. If ducted propellers with larger blade area ratios of the impeller or with more rotor rows are considered, the flow decelerating type of nozzle may even for larger values of the thrust coefficient C_T favourably affect the cavitation properties of the screw.

The results of the experimental investigations were shown in the Figs. 18 through 37.
The relationship between the thrust coefficient C_T and the thrust ratio τ of nozzle no. 33 in combination with the various screws of the Kd 5-100 screw series was shown in Fig. 33. It can be seen from this diagram, that, as might be expected, this relationship is approximately independent of the pitch ratio of the screws. The small differences which occur may be explained by the differences in rotational losses and radial load distributions of the screws and by frictional effects. The relationships between C_T and τ of nozzles nos. 30, 31 and 32 (Fig. 32) and nozzles nos. 34, 35 and 36 (Fig. 33) was, therefore, only given for the screw with a pitch ratio of 1.4. In addition, the design thrust coefficients C_T and thrust ratios τ at $J = 0$ and $J = 1.0$ of the various nozzles were given in the Figs. 32 and 33. Although a number of simplifying assumptions were made in the development of the theory for the numerical calculations of the nozzle shapes, (it was a linearized theory, the impeller was represented by a uniformly loaded actuator disc, tip clearance effects were not taken into account, the effect of friction was neglected) a reasonable agreement between the calculated relationship of C_T and τ of the various nozzles and the one obtained by the open-water tests was found.

The open-water efficiency η_p and the diameter coefficient δ of the various nozzles were given for optimum condition from the view point of efficiency in the Figs. 34 and 35 on a base of B_p . In combination with the Figs. 32 and 33, these diagrams show clearly that, by comparing the properties of the different nozzles, the open-water efficiency η_p decreases with increasing thrust ratio τ . The diameter coefficients of the various nozzles are nearly the same.

Optimum curves for open-water efficiency η_p , diameter coefficient δ and thrust ratio τ of the Ka 4-70 screw series in nozzle no. 19A, the Kd 5-100 screw series in nozzle no. 33 and the B 4-70 screw series are presented in Fig. 36.
Typical B_p - values for different ship types are:

torpedo's	$B_p < 10$ -	or $C_T < 0.5$
twin-screw ships	≤ 10 - 15	≤ 0.5 - 1.0
fast warships (frigates)	≤ 10 - 25	≤ 0.5 - 1.5
single-screw cargo ships	≤ 15 - 35	≤ 1.0 - 2.5
tankers	≤ 35 - 70	≤ 2.5 - 4.0
towing vessels (tugs, pushboats)	> 80	> 5.0

The lightly loaded screws of fast ships are on the left hand side of Fig. 36 while the heavily loaded propellers of towing vessels are on the right.

The propulsive efficiency of a ship depends on the open-water efficiency of the screw and the mutual interference of screw and ship. A screw behind a ship normally causes an increase in the drag of the ship because of the low pressure due to the acceleration of the flow in front of the screw. This increase in drag is called "thrust deduction".
The accelerating nozzle (nozzle no 19A), if compared with a conventional screw propeller (B 4-70 screw series) gives raise to an improvement in open-water efficiency η_p in the case of heavy screw loads (see Fig. 36). However, from the viewpoint of

thrust deduction, the application of this nozzle type is questionable. The decelerating nozzle (nozzle no. 33) has a relatively low open-water efficiency; with regard to thrust deduction, the application of this nozzle type may be attractive. In the case of heavy screw loads (all types of towing vessels) the attractiveness with regard to propulsive efficiency of application of the accelerating nozzle has been demonstrated in practice in the course of the past thirty years. For middle and lower screw loads (tankers and single-screw cargo ships) the increase in propulsive efficiency through application of an accelerating nozzle strongly depends on the stern-nozzle configuration.
In this range of screw loads, however, the application of a decelerating nozzle may also become attractive when other than hydrodynamic factors influence the choice.

It can be seen from Fig. 36 that at low B_p-values the open-water efficiency of both the accelerating and the decelerating nozzle decrease with respect to the efficiency of the B 4-70 screw series. This fact can be explained by the relative increase of the frictional and the induced drag of the nozzle. The curves of the diameter coefficient δ of the accelerating and the decelerating nozzle almost coincide; the B 4-70 screw series has a larger optimum screw diameter. It is interesting to note that the curves of the diameter coefficient based on the maximum diameter of the system δ^* of both the accelerating and the decelerating nozzle and of the B 4-70 screw series almost coincide.

The cavitation numbers at which incipient bubble cavitation at the exterior surface of the nozzle nos. 33 and 36 was observed, are presented in Fig. 37. Comparing the results given in this diagram with those of the rough analysis of the minimum pressure at the impeller blades of a ducted propeller (with $A_e/A = 1$ and $Z = 5$) it can be concluded that only at very low screw loads

($C_T > 0.6$), cavitation phenomena at the exterior surface will occur before the screw cavitation. If impellers with a larger blade area ratio or with more rotor rows are used, then the ducted propeller system will become more critical for cavitation phenomena at the exterior surface of the nozzle.

Finally, it must be noted that no experiments were carried out to determine the effect of a small angle of attack on the cavitation performance of the tested nozzle shapes. The equipment for performing these experiments did not operate satisfactory.

5. Conclusions.

As a result of the investigations the following conclusions can be made:

- The risk of flow separation on the exterior surface of the flow decelerating type of nozzle is small, even in the case of large thrust ratios.
- Whether an improvement of the screw cavitation properties can be obtained by application of the decelerating nozzle, depends on the particulars of the screw considered. A rough analysis shows, that for screws with $A_e/A = 1$ and $Z = 5$, the flow decelerating nozzle favourably affects the cavitation properties of the screw only at low values of the thrust coefficient C_T ($C_T < 1.5$). In the case of large thrust coefficients, the flow decelerating nozzle will favourably affect the cavitation properties of the screw if ducted propeller systems with larger blade area ratios of the screw or with more rotor rows are used.
- Although a number of simplifications were used in the development of the theory for numerical calculation of the nozzle shapes, a reasonable agreement was found between the computed properties of the nozzles and those obtained by the open-water tests.

- There exists a fixed relation between the thrust coefficient C_T and the thrust ratio τ of a nozzle, which relation is approximately independent of the particulars of the screw considered. This property determines the range of application of the nozzle.
- By comparing the open-water efficiency for optimum condition of various ducted propellers, it was found that the efficiency of the system decreases with increasing value of the thrust ratio τ. The optimum diameters of the various systems were about equal. It was interesting to note that for optimum condition the maximum diameter of both the accelerating and the decelerating nozzle and the considered screw series were nearly the same.

References.

[1] Oosterveld, M.W.C., "Series of Model Tests on Ducted Propellers". N.S.M.B., Report on Contract No. N 62558-4555 (October 1967).

[2] Keller, J. auf'm, "Enige aspecten bij het ontwerp van scheepsschroeven", Schip en Werf (December 1966).

[3] Morgan, W.B. and Voigt, R.G., "The Inverse Problem of the Annular Airfoil and Ducted Propeller", David Taylor Model Basin, Report 2251 (September 1966).

[4] van Manen, J.D., "Effect of Radial Load Distribution on the Performance of Shrouded Propellers", Paper No. 7, R.I.N.A. (March 1962).

[5] van Manen, J.D. and Oosterveld, M.W.C., "Analysis of Ducted Propeller Design", Paper No. 13, S.N.A.M.E. (November 1966).

[6] Witte, J.H. and Esveldt, J., "Recent Improvements in the Large Cavitation Tunnel of the Netherlands Ship Model Basin", International Shipbuilding Progress, Vol. 13, No. 146 (October 1966).

[7] "Principles of Naval Architecture", Published by the Society of Naval Architects and Marine Engineers, New York (1967).

List of Figures

Figure 1. Ducted Propeller

2. Mean lines and characteristics of systematic series of nozzles with $C_{T_o} = 0.5$ and $\tau_o = 1.0$; 1.2 and 1.4.

3. Mean lines and characteristics of systematic series of nozzles with $C_{T_o} = 1.0$ and $\tau_o = 1.0$; 1.2 and 1.4.

4. Mean lines and characteristics of systematic series of nozzles with $C_{T_o} = 0.5$; $\tau_o = 1.2$ and different L/D ratios ($L/D = 0.3$; 0.6 and 0.9).

5. Mean lines and characteristics of systematic series of nozzles with $C_{T_o} = 1.0$; $\tau_o = 1.2$ and different L/D ratios ($L/D = 0.3$; 0.6 and 0.9).

6. Mean lines and characteristics of systematic series of nozzles with $C_{T_o} = 0.5$; $\tau_o = 1.2$ and different thickness ratios S/L. ($S/L = 0$; 0.05; 0.10 and 0.15).

7. Mean lines and characteristics of systematic series of nozzles with $C_{T_o} = 1.0$; $\tau_o = 1.2$ and different thickness ratios S/L. ($S/L = 0$; 0.05; 0.10 and 0.15).

8. Pressure distribution along interior and exterior surface of nozzles with $C_{T_o} = 0.5$ and $\tau_o = 1.0$; 1.2 and 1.4.

9. Pressure distribution along interior and exterior surface of nozzles with $C_{T_o} = 1.0$ and $\tau_o = 1.0$; 1.2 and 1.4.

10. Sectional lift coefficient C_L of the nozzle as a function of τ_o, L/D and S/L

11. Mean static pressure at propeller plane and minimum static pressure at exterior surface of nozzle as a function of τ_o, L/D and S/L.

Figure 12. Minimum pressure at the impeller blades of a ducted propeller.

13. Particulars of nozzles nos. 30, 31 and 32.

14. Particulars of nozzles nos. 33, 35 and 36.

15. Particulars of nozzles nos. 33 and 34.

16. Particulars of screw models of the K_d 5-100 screw series.

17. Measuring equipment for open water tests with ducted propellers.

18. Open water test results of nozzle no. 30 (K_T; K_{T_n}; K_Q and η_p as functions of J).

19. Open water tests results of nozzle no. 31 (K_T; K_{T_n}; K_Q and η_p as functions of J).

20. Open water test results of nozzle no. 32 (K_T; K_{T_n}; K_Q and η_p as functions of J).

21. Open water test results of nozzle no. 33 (K_T; K_{T_n}; K_Q and η_p as functions of J).

22. Open water test results of nozzle no. 34 (K_T; K_{T_n}; K_Q and η_p as functions of J).

23. Open water test results of nozzle no. 35 (K_T; K_{T_n}; K_Q and η_p as functions of J).

24. Open water test results of nozzle no. 36 (K_T; K_{T_n}; K_Q and η_p as functions of J).

25. Open water test results of nozzle no. 30 (C_T, τ and η_p as functions of J).

26. Open water test results of nozzle no. 31 (C_T, τ and η_p as functions of J).

27. Open water test results of nozzle no. 32 (C_T, τ and η_p as functions of J).

28. Open water test results of nozzle no. 33 (C_T, τ and η_p as functions of J).

29. Open water test results of nozzle no. 34 (C_T, τ and η_p as functions of J).

Figure 30. Open water test results of nozzle no. 35 (C_T, τ and η_p as functions of J).

31. Open water test results of nozzle no. 36 (C_T, τ and η_p as functions of J).

32. Relationship between C_T and τ of nozzles nos. 30, 31 and 32.

33. Relationship between C_T and τ of nozzles nos. 33, 34, 35 and 36.

34. Optimum relationship between η_p, δ and B_p of nozzles nos. 30, 31 and 32.

35. Optimum relationship between η_p, δ and B_p of nozzles nos. 33, 34, 35 and 36.

36. Optimum relationship between η_p, δ, τ and B_p of an accelerating nozzle (nozzle no. 19A), a decelerating nozzle (nozzle no. 33) and the B 4-70 screw series in open water.

37. Incipient cavitation phenomena at the exterior surface of the nozzles nos. 33 and 36.

List of Tables

Table I : Design parameters of the tested nozzle shapes.

II : Mean lines of the tested nozzle shapes.

III : Particulars of the K_d 5-100 screw series.

List of symbols.

a	nozzle length in front of propeller disk
B_p	design coefficient, $\frac{K_Q^{1/2}}{J^{5/2}}$
C_L	sectional lift coefficient of the nozzle
C_p	pressure coefficient, $\frac{P - P_\infty}{\frac{1}{2}\rho V_e^2}$
C_T	thrust coefficient, $\frac{T}{\frac{1}{2}\rho V_e^2 \pi/4 D^2}$
d	hub diameter
D	nozzle diameter (see Fig. 1) ; impeller diameter
A_e/A	blade area ratio of the screw
J	advance coefficient, $\frac{V_e}{n D}$
K_T	thrust coefficient, $\frac{T}{\rho n^2 D^4}$
K_Q	torque coefficient, $\frac{Q}{\rho n^2 D^5}$
n	number of revolutions per second of the screw
P	local static pressure
P_∞	static pressure in the undisturbed stream
P_v	vapour pressure
Q	torque
R	propeller radius
S	maximum thickness of the nozzle profile
S(x)	shape of the mean line of the nozzle profile (see also Fig. 1)
T	thrust
V_e	undisturbed stream velocity
Z	number of screw blades
δ	diameter coefficient, $\frac{101.27}{J}$
ρ	specific mass of fluid
σ	cavitation number of the undisturbed fluid, $\frac{P_\infty - P_v}{\frac{1}{2}\rho V_e^2}$

η_p open water efficiency

η_i ideal efficiency

τ impeller thrust - total thrust ratio

ω rotational velocity of the screw

Subscripts:

p propeller

n nozzle

o value of the coefficient at J = 0

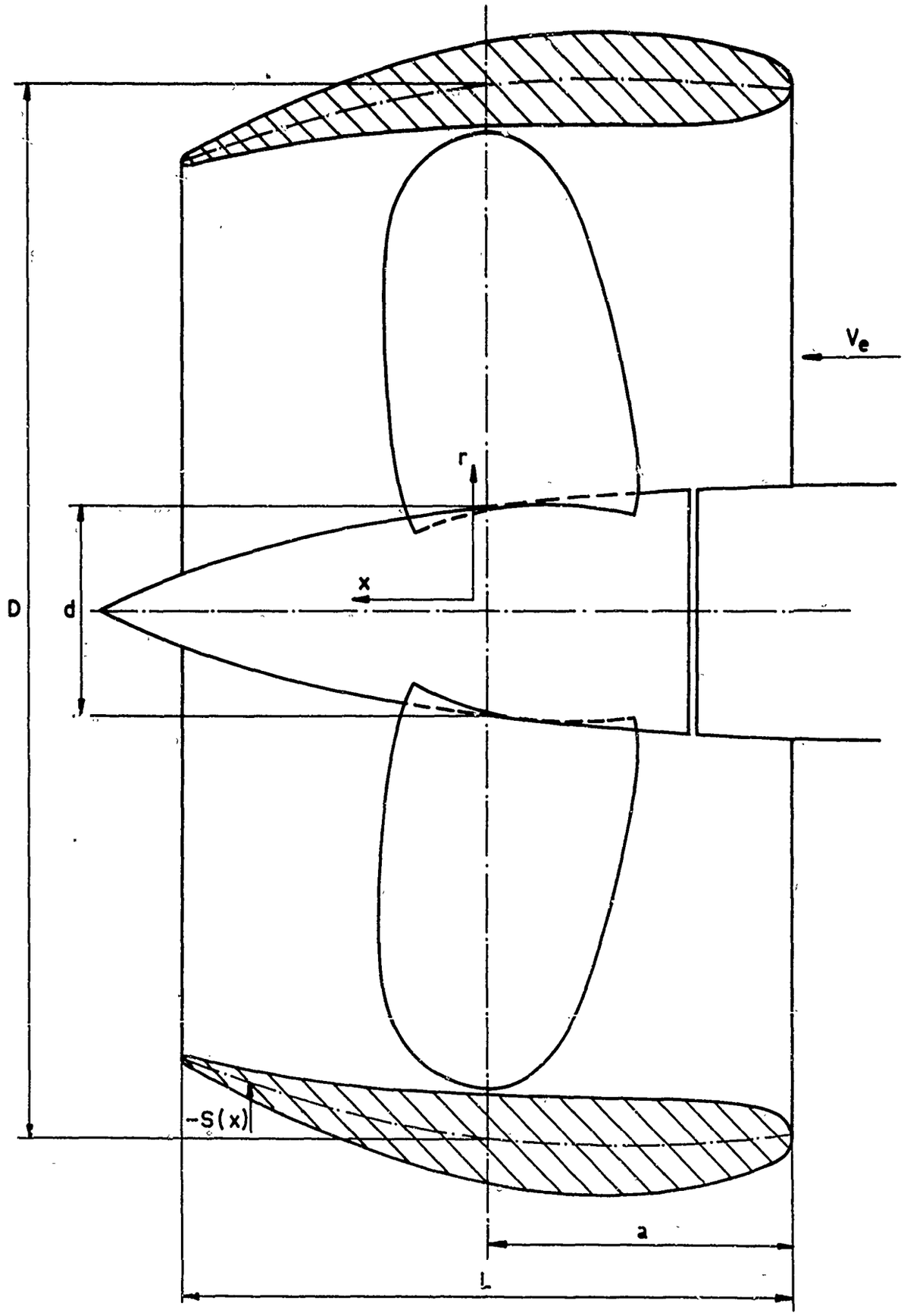

Fig.1 Ducted Propeller

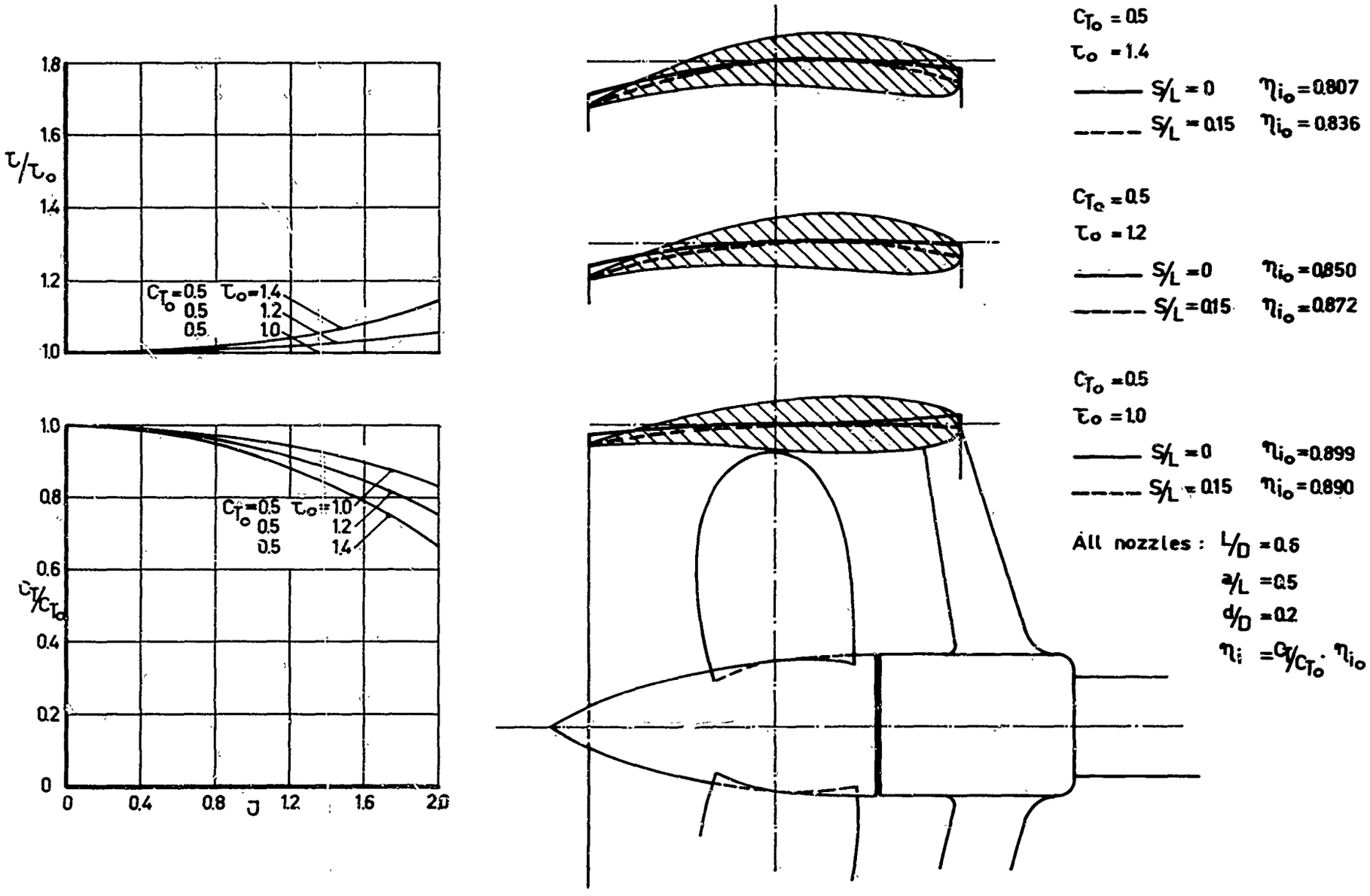

Fig. 2 Meanlines and characteristics of systematic series of nozzles with C_{T_o}=0.5 and τ_o=1.0; 1.2 and 1.4.

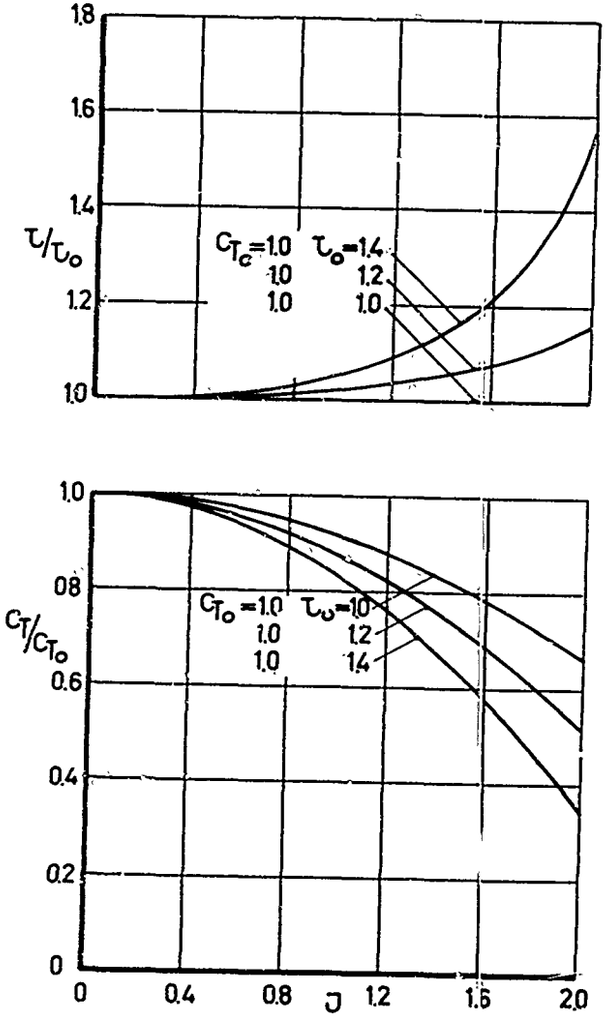

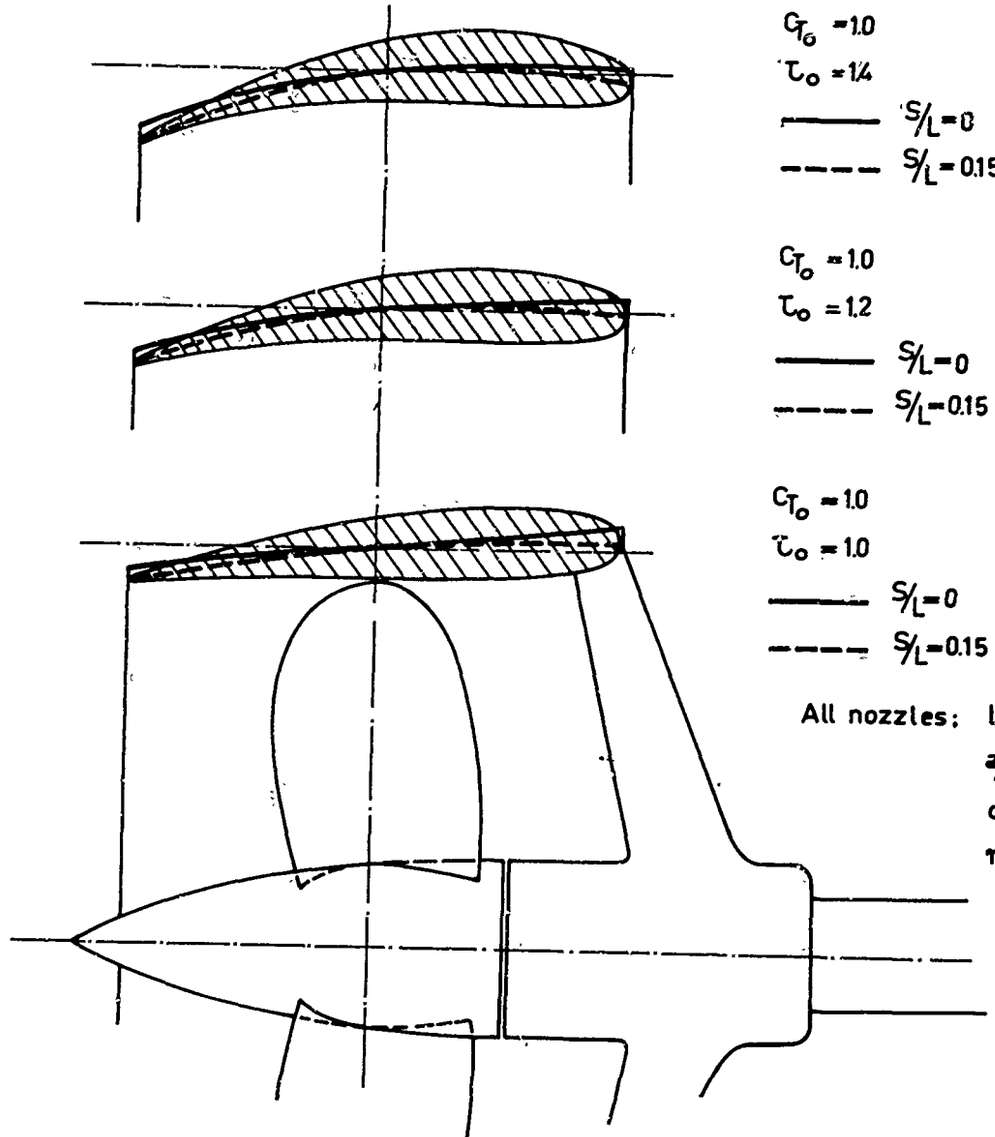

C_{T_o} = 1.0
τ_o = 1.4
——— S/L = 0 η_{i_o} = 0.674
– – – – S/L = 0.15 η_{i_o} = 0.684

C_{T_o} = 1.0
τ_o = 1.2
——— S/L = 0 η_{i_o} = 0.736
– – – – S/L = 0.15 η_{i_o} = 0.745

C_{T_o} = 1.0
τ_o = 1.0
——— S/L = 0 η_{i_o} = 0.801
– – – – S/L = 0.15 η_{i_o} = 0.804

All nozzles: l/D = 0.6
a/L = 0.5
d/D = 0.2
$\eta_i = C_T/C_{T_o} \cdot \eta_{i_o}$

Fig.3 Meanlines and characteristics of systematic series of nozzles with C_{T_o}=1.0 and τ_o=1.0; 1.2 and 1.4.

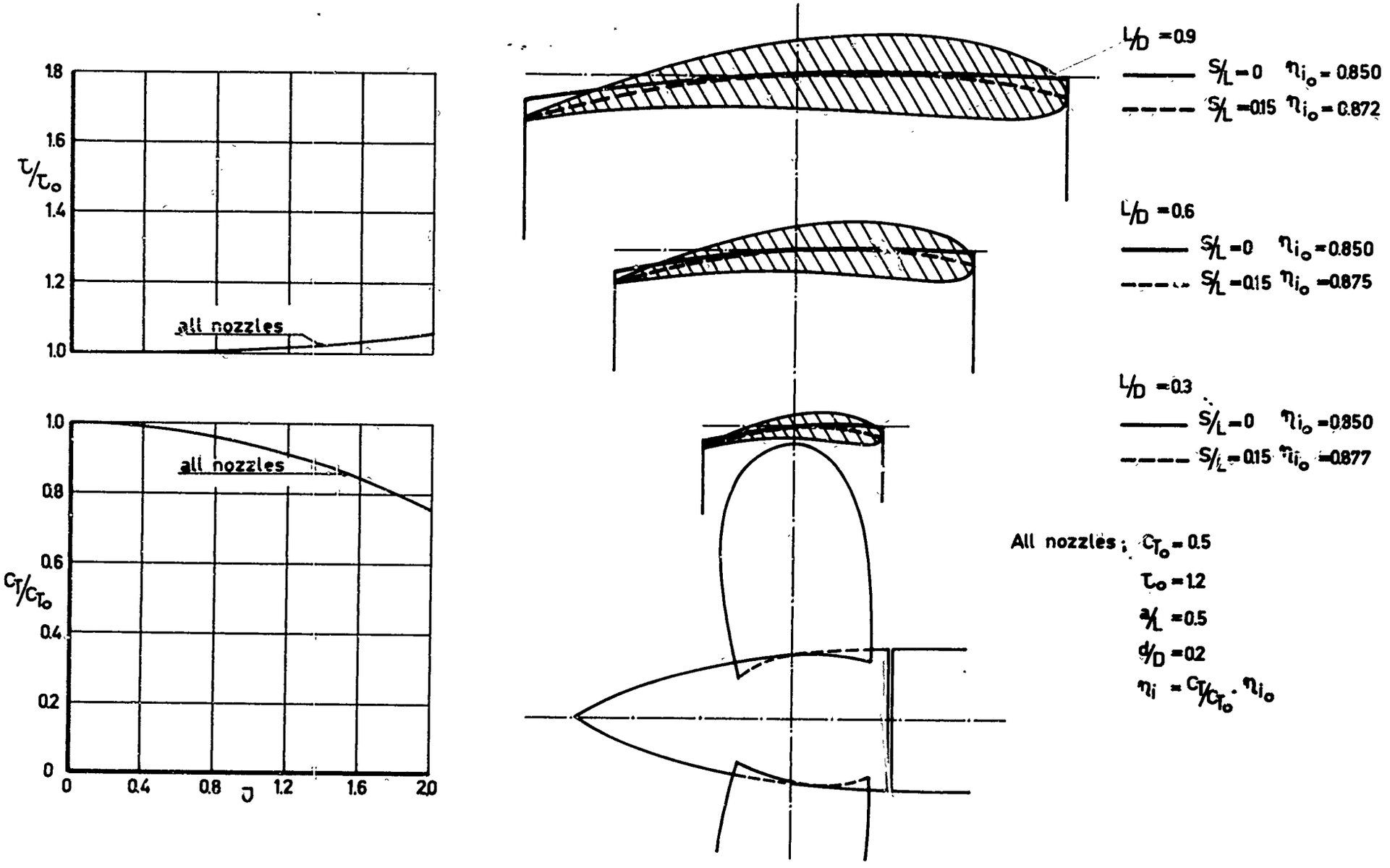

Fig.4 Meanlines and characteristics of systematic series of nozzles with $C_{T_o}=0.5$; $\tau_o=1.2$ and different L/D ratios ($L/D=0.3$; 0.6 and 0.9).

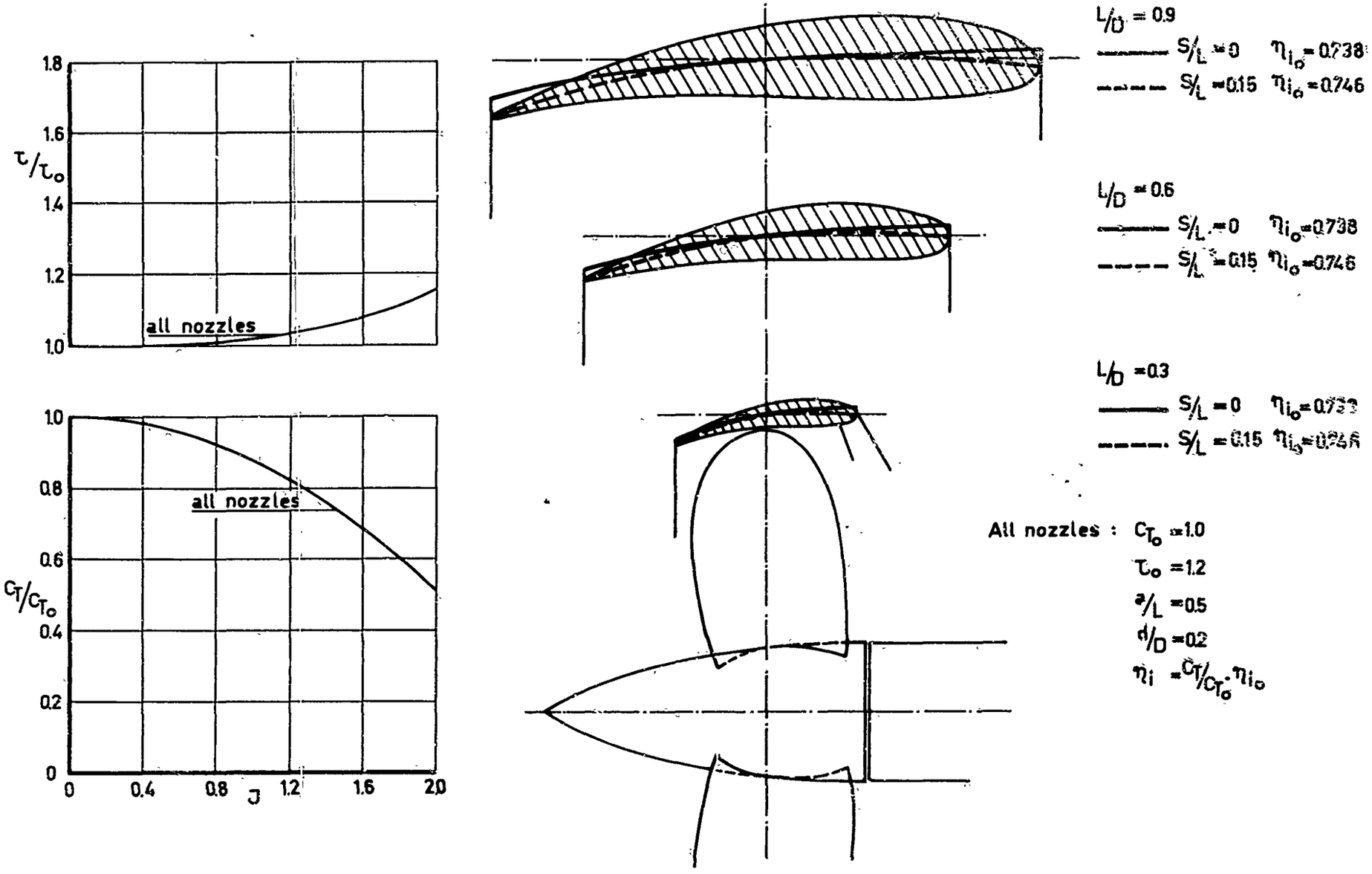

Fig.5 Meanlines and characteristics of systematic series of nozzles with $C_{T_o}=1.0$; $\tau_o=1.2$ and different L/D ratios ($L/D=0.3$; 0.6 and 0.9).

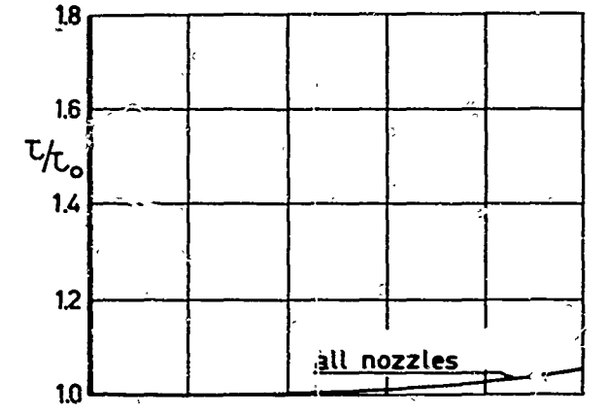

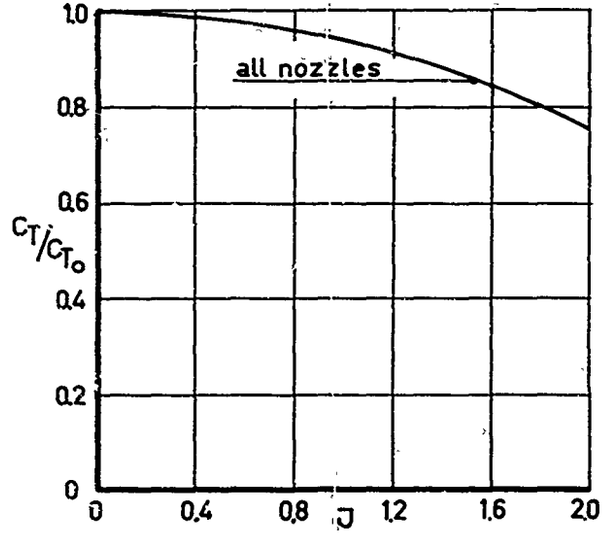

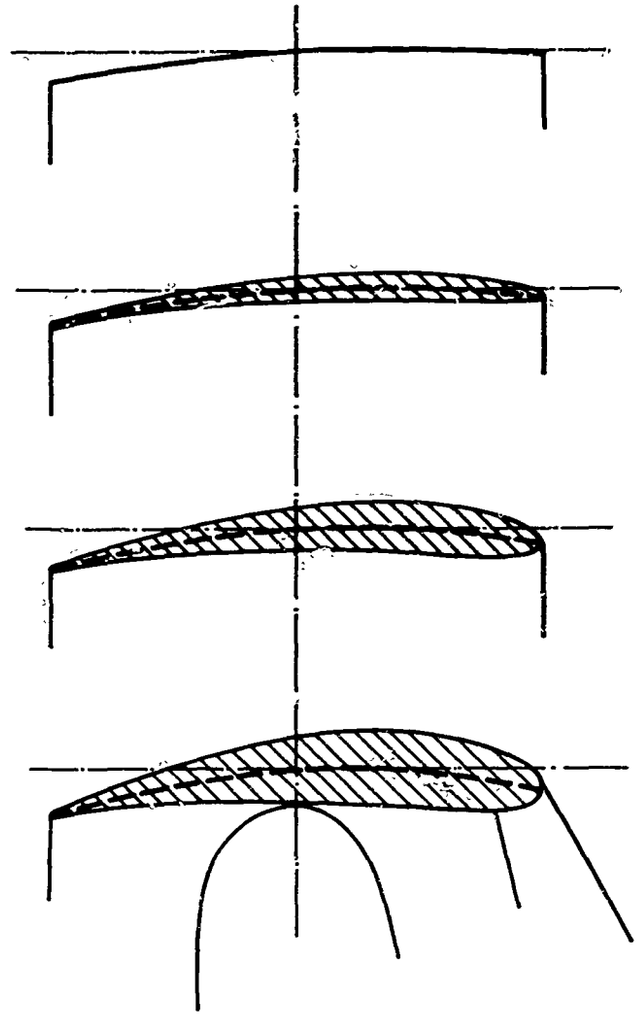

S/L =0 η_{i_o}=0.850

S/L =0.05 η_{i_o}=0.857

S/L =0.10 η_{i_o}=0.865

S/L =0.15 η_{i_o}=0.872

All nozzles: C_{T_o} =0.5
τ_o =1.2
L/D =0.6
a/L =0.5
d/D =0.2
$\eta_i = C_T/C_{T_o} . \eta_{i_o}$

Fig.6 Meanlines and characteristics of systematic series of nozzles with C_{T_o}=0.5 ; τ_o=1.2 and different thickness ratios S/L. (S/L=0; 0.05; 0.10 and 0.15).

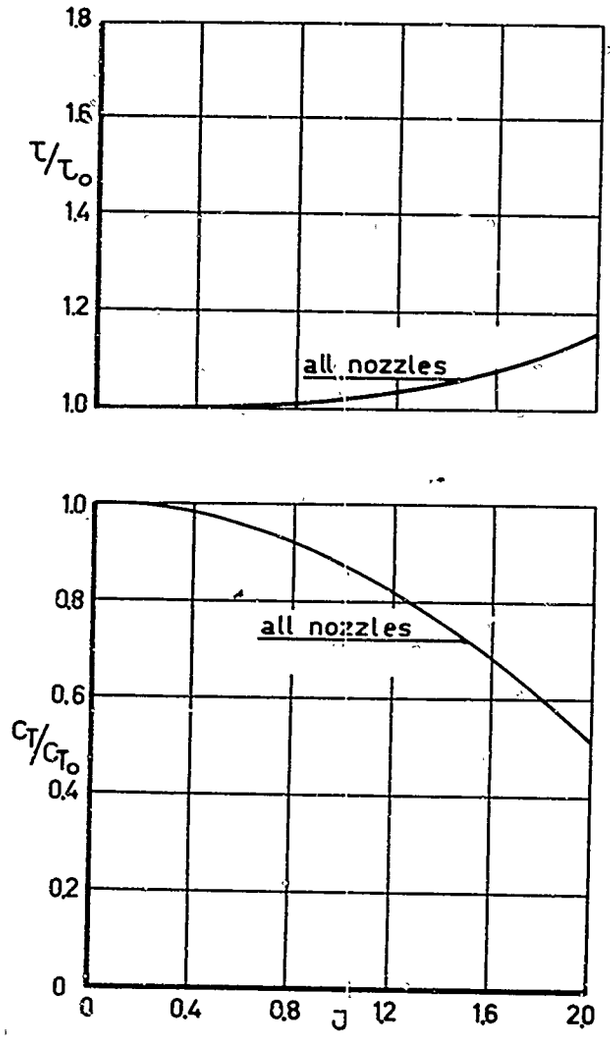

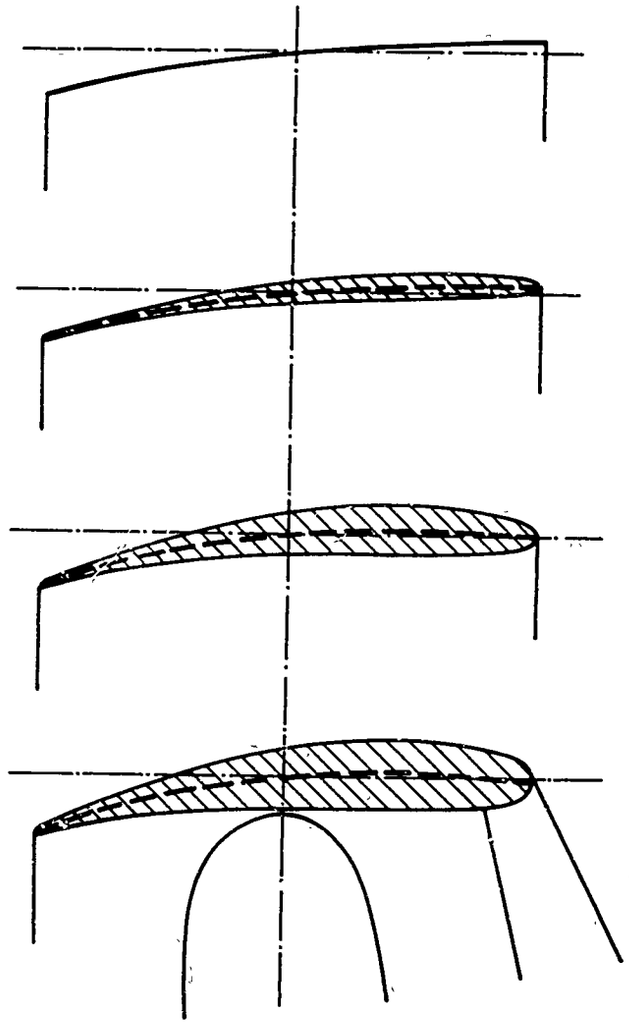

Fig.7 Meanlines and characteristics of systematic series of nozzles with $C_{T_o}=1.0$; $\tau_o=1.2$ and different thickness ratios S/L ($S/L=0$; 0.05 ; 0.10 and 0.15).

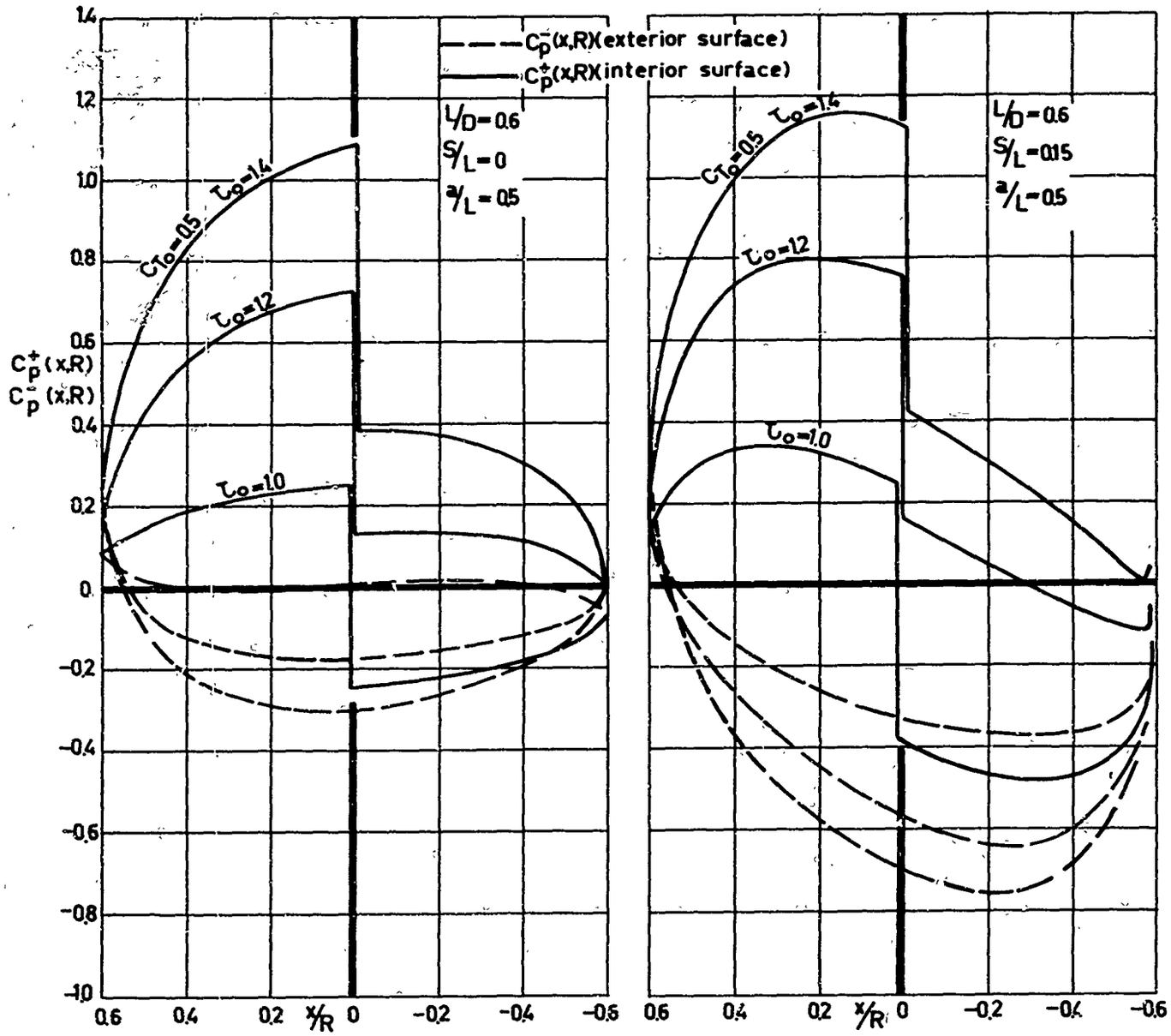

Fig.8 Pressure distribution along interior and exterior surface of nozzles with $C_{T_o}=0.5$ and $\tau_o=1.0$; 1.2 and 1.4.

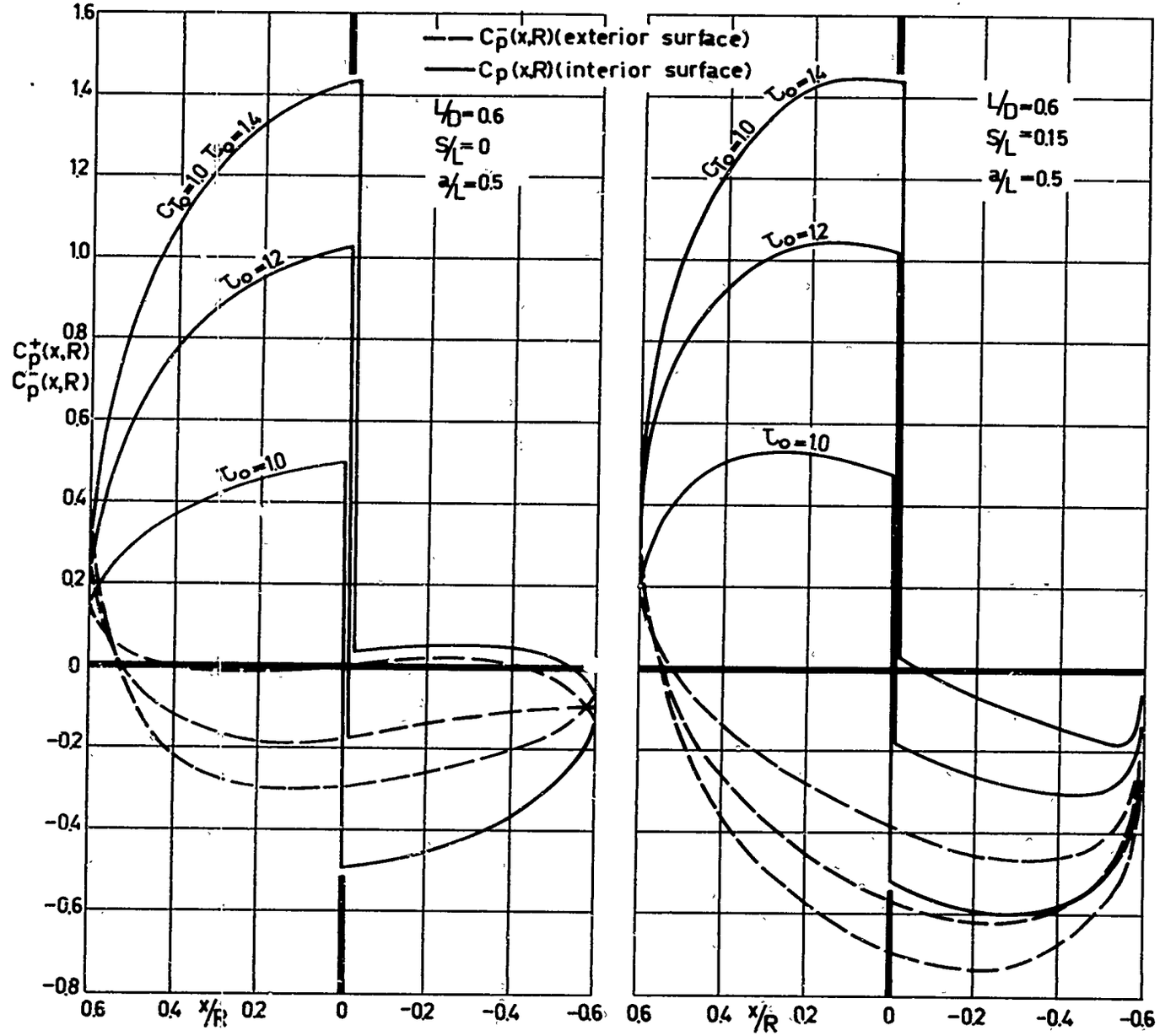

Fig.9 Pressure distribution along interior and exterior surface of nozzles with C_{T_o}=1.0 and τ_o=1.0 , 1.2 and 1.4 .

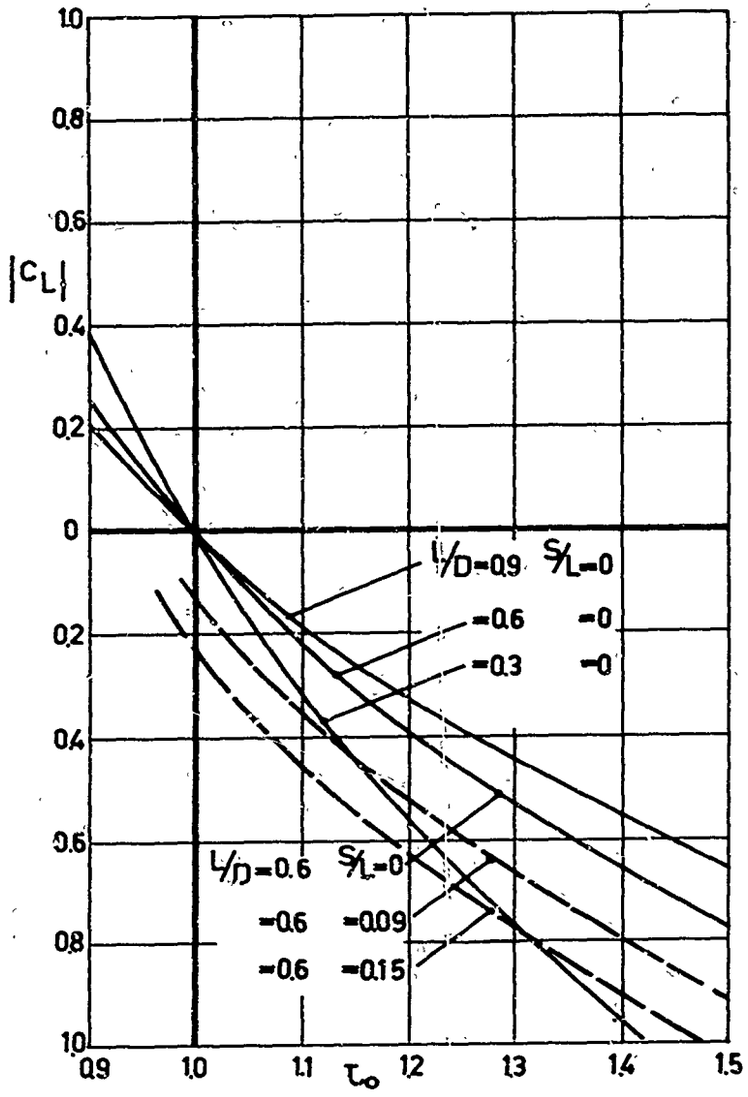

Fig.10 Sectional lift coefficient C_L of the nozzle as a function of τ_o, L/D and S/L.

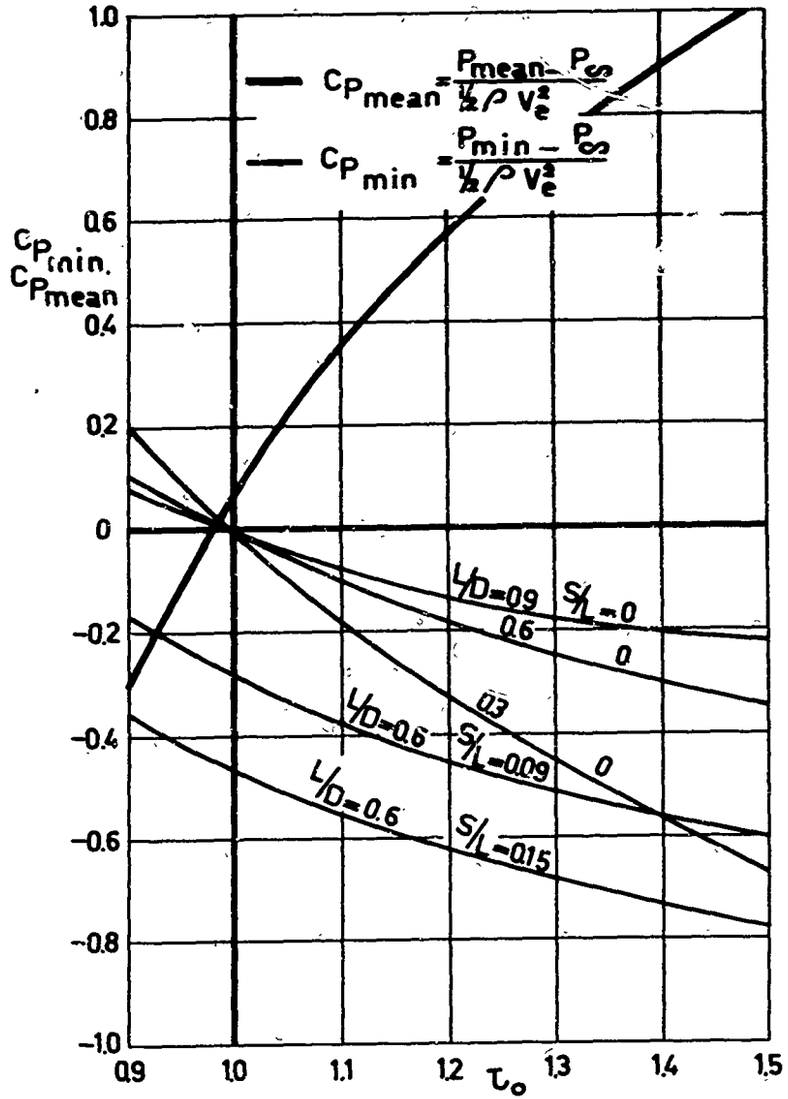

Fig.11 Mean static pressure at propeller plane and minimum static pressure at exterior surface of nozzle is a function of τ_o, L/D and S/L.

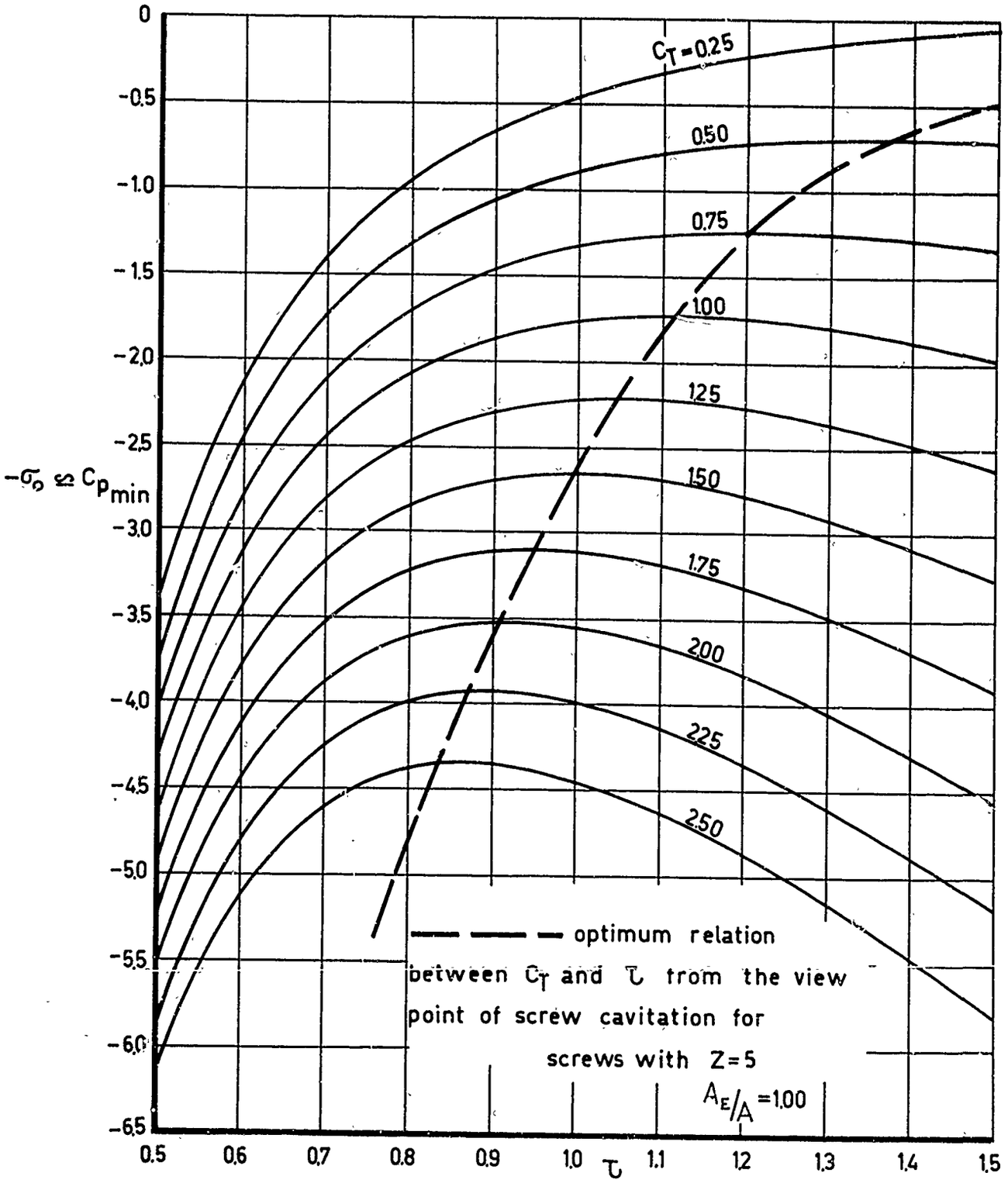

Fig.12 Minimum pressure at the impeller blades of a ducted propeller.

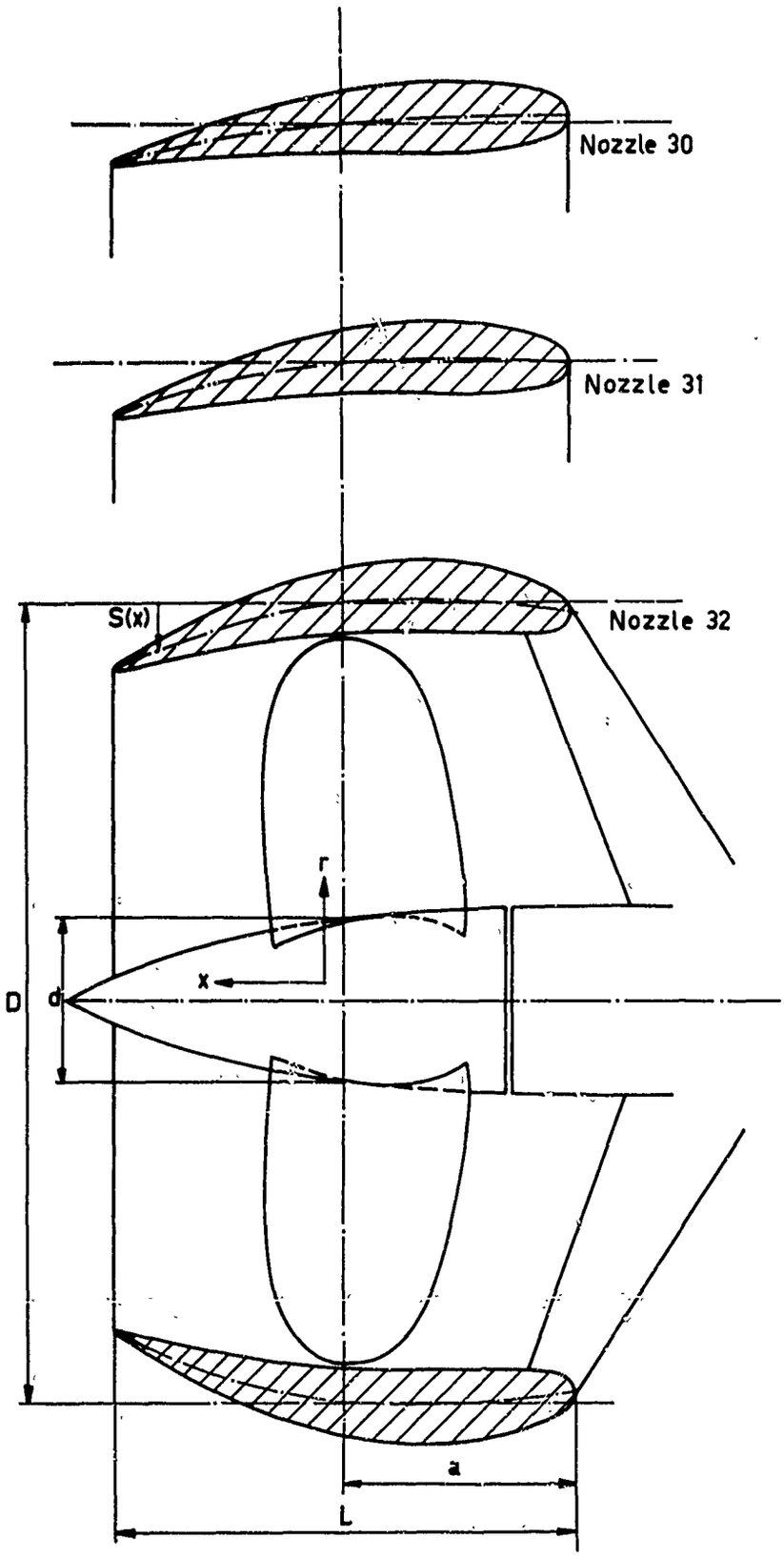

Fig.13 Particulars of nozzles nos.30, 31 and 32.

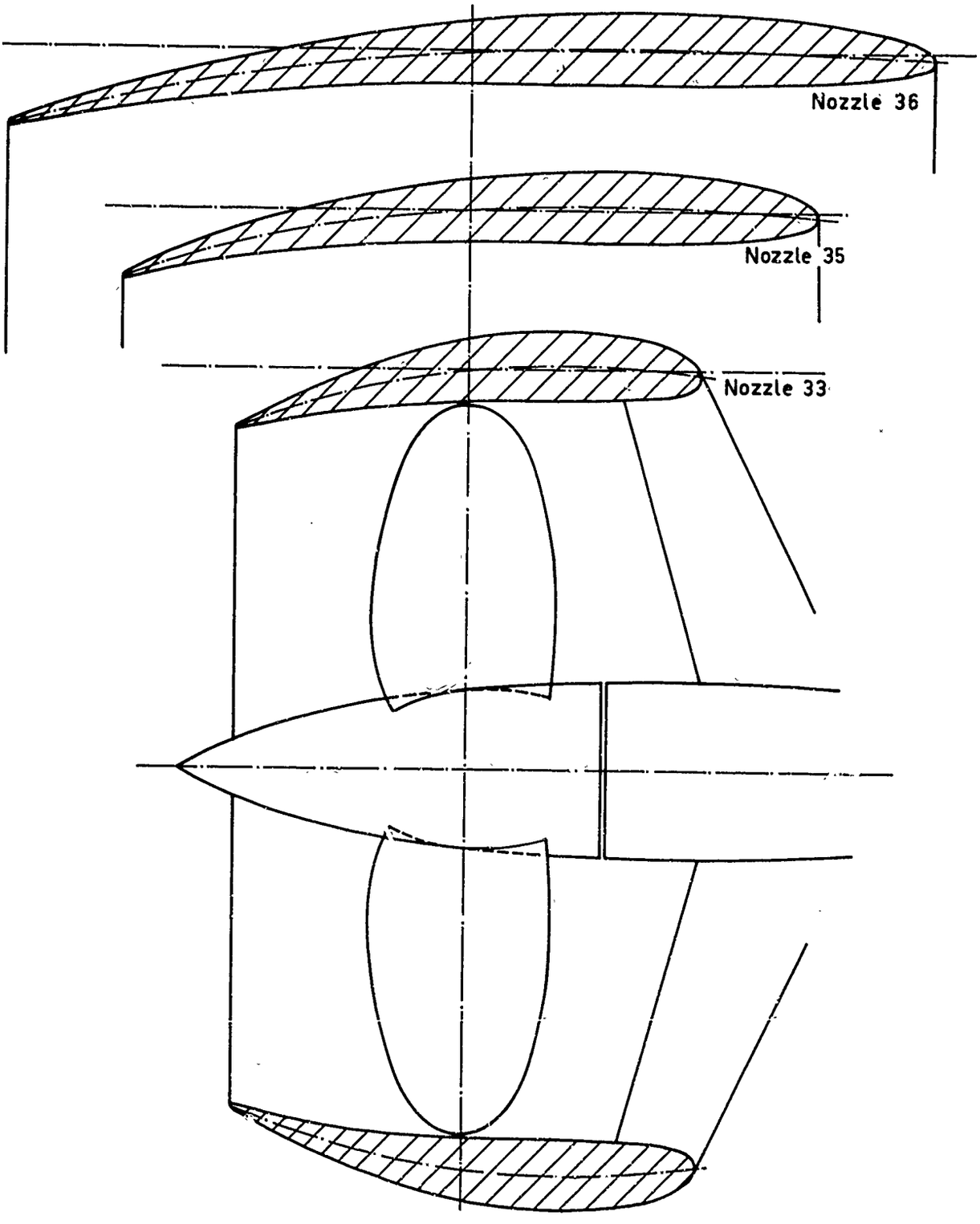

Fig.14 Particulars of nozzles nos. 33, 35 and 36.

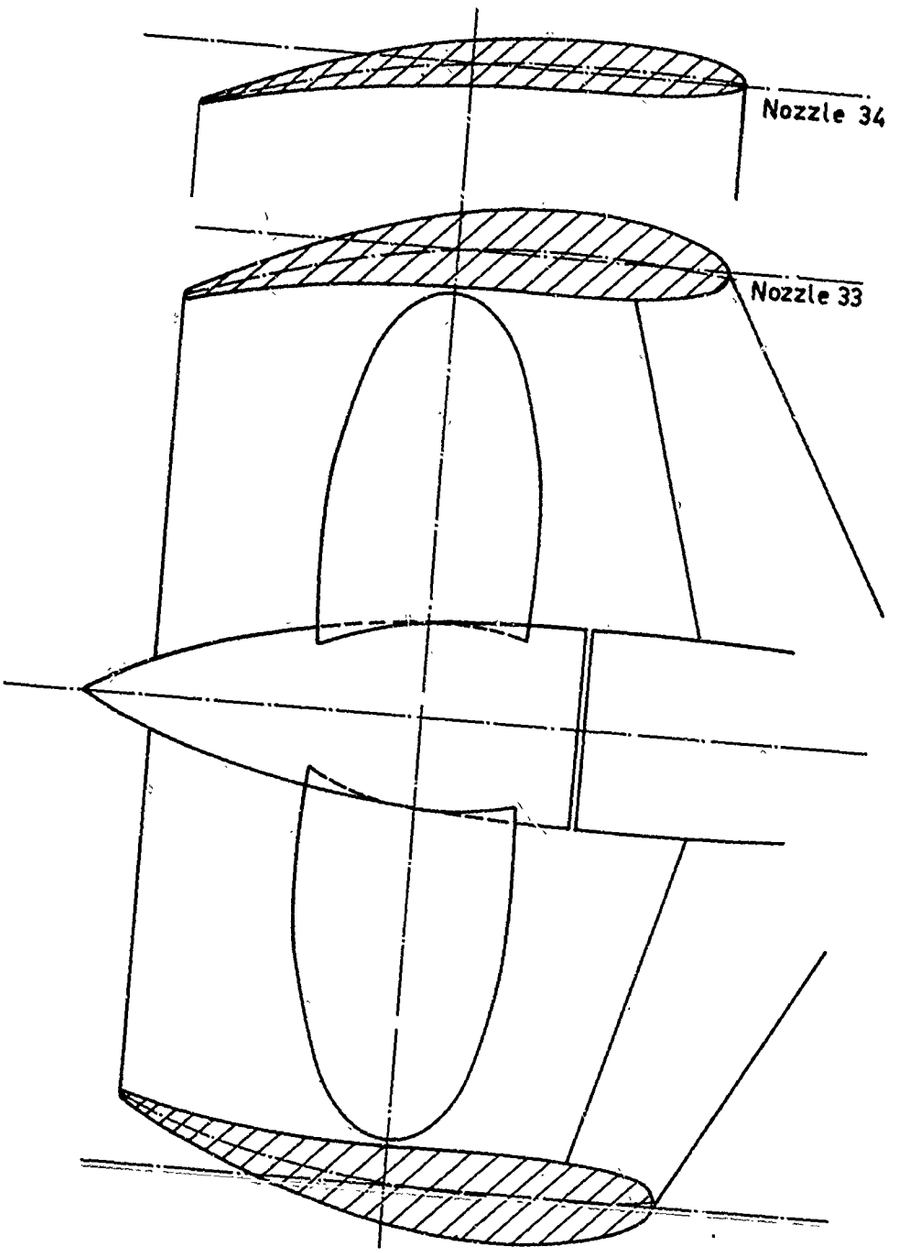

Fig. 15 Particulars of nozzles nos. 33 and 34.

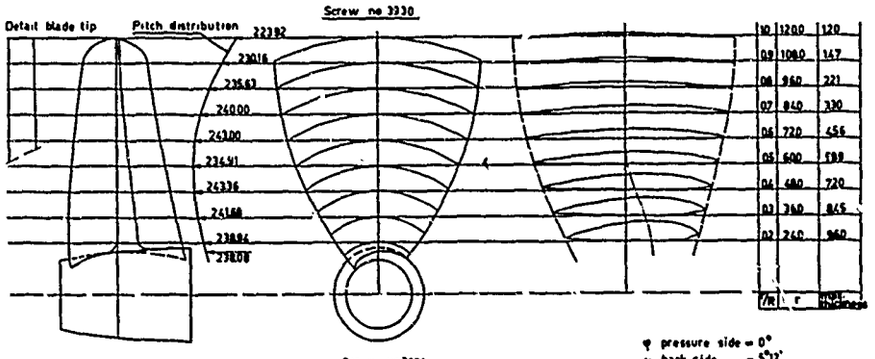

φ pressure side = 0°
φ back side = 5°12'

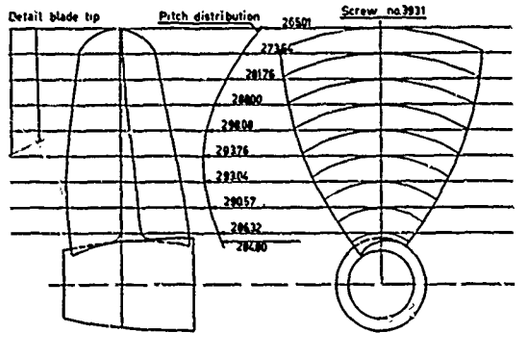

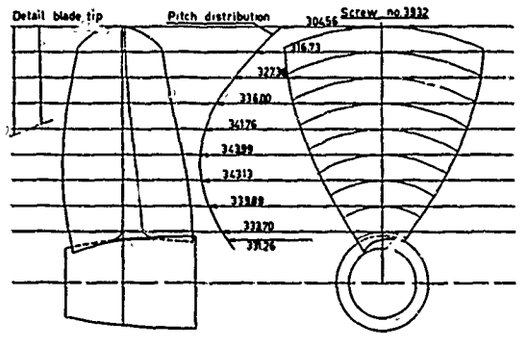

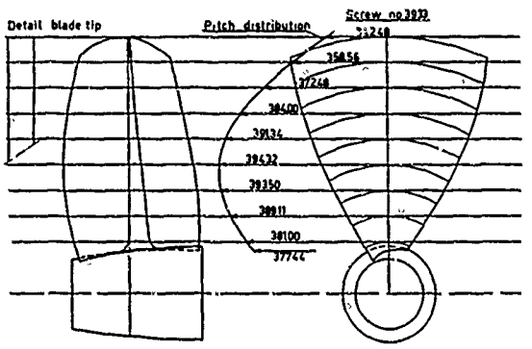

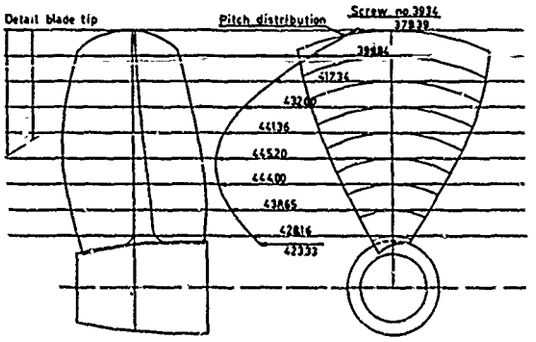

Particulars

All screws:
D = 240 mm
Z = 5
$\frac{d}{D}$ = 0.167
$\frac{A_e}{A_0}$ = 1.0

Screw no 3930 $\frac{P}{D}$ = 1.0 (at 0.7 R)
" no 3931 " = 1.2 "
" no 3932 " = 1.4 "
" no 3933 " = 1.6 "
" no 3934 " = 1.8 "

Fig 16 Particulars of screw models of the $K_0 5$-100 screw series.

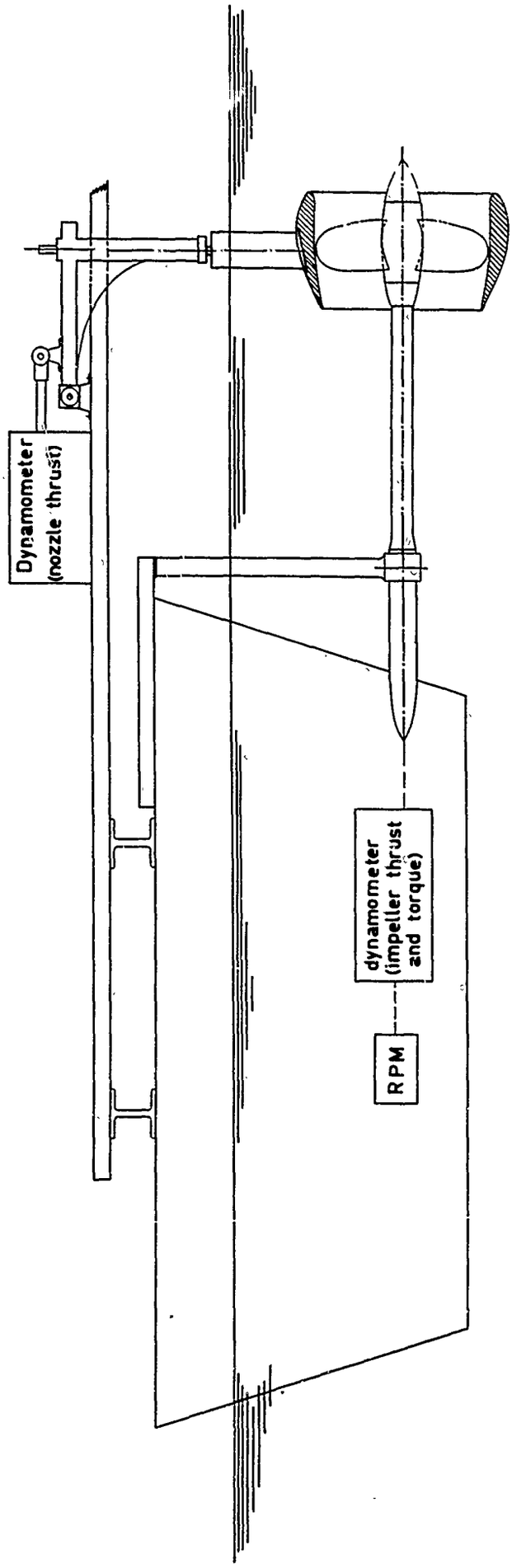

Fig 17 Measuring equipment for open water tests with ducted propeller

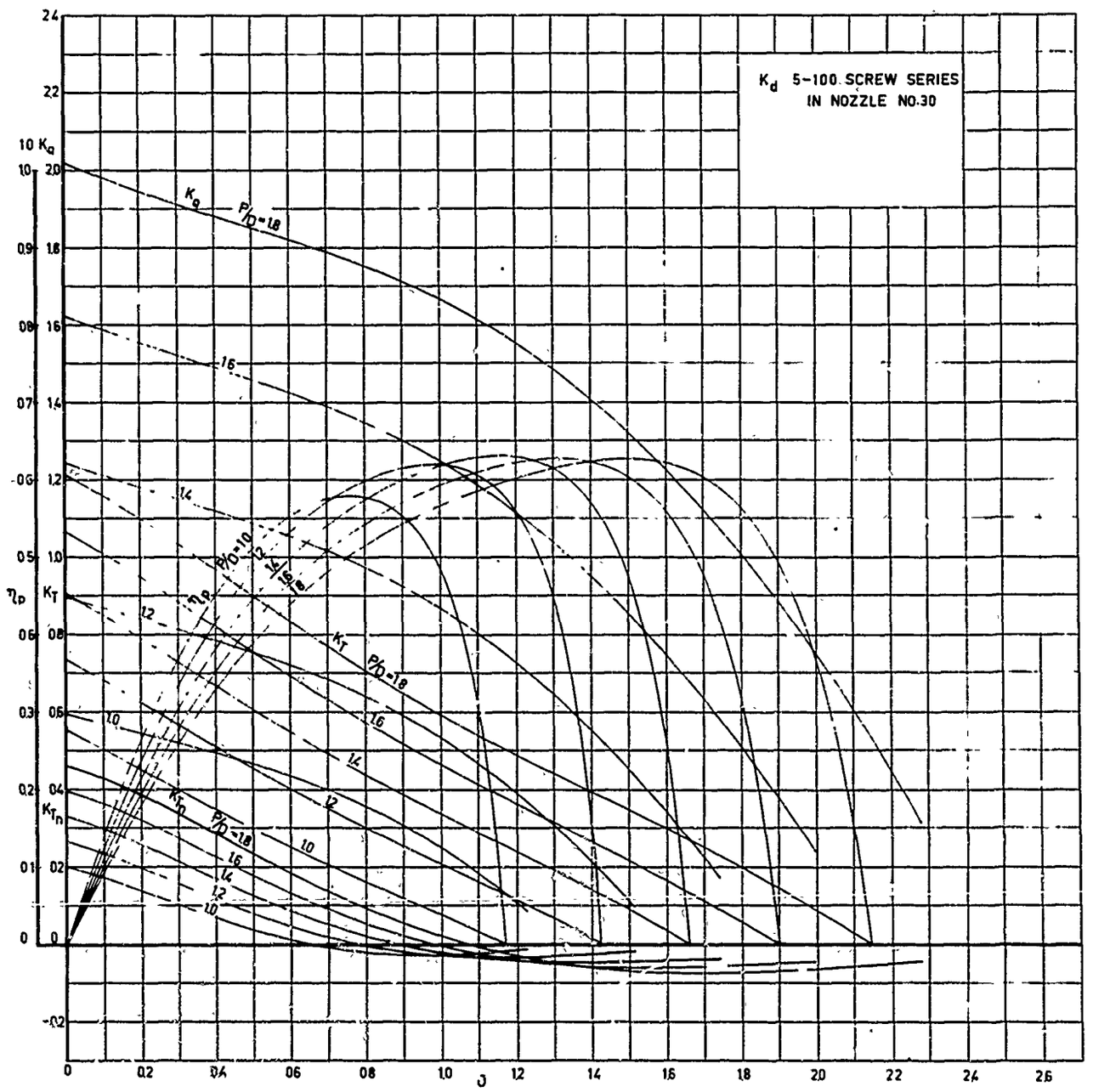

Fig.18 Open water test results of nozzle no.30 (K_T; K_{T_n}; K_Q and η_p as functions of J).

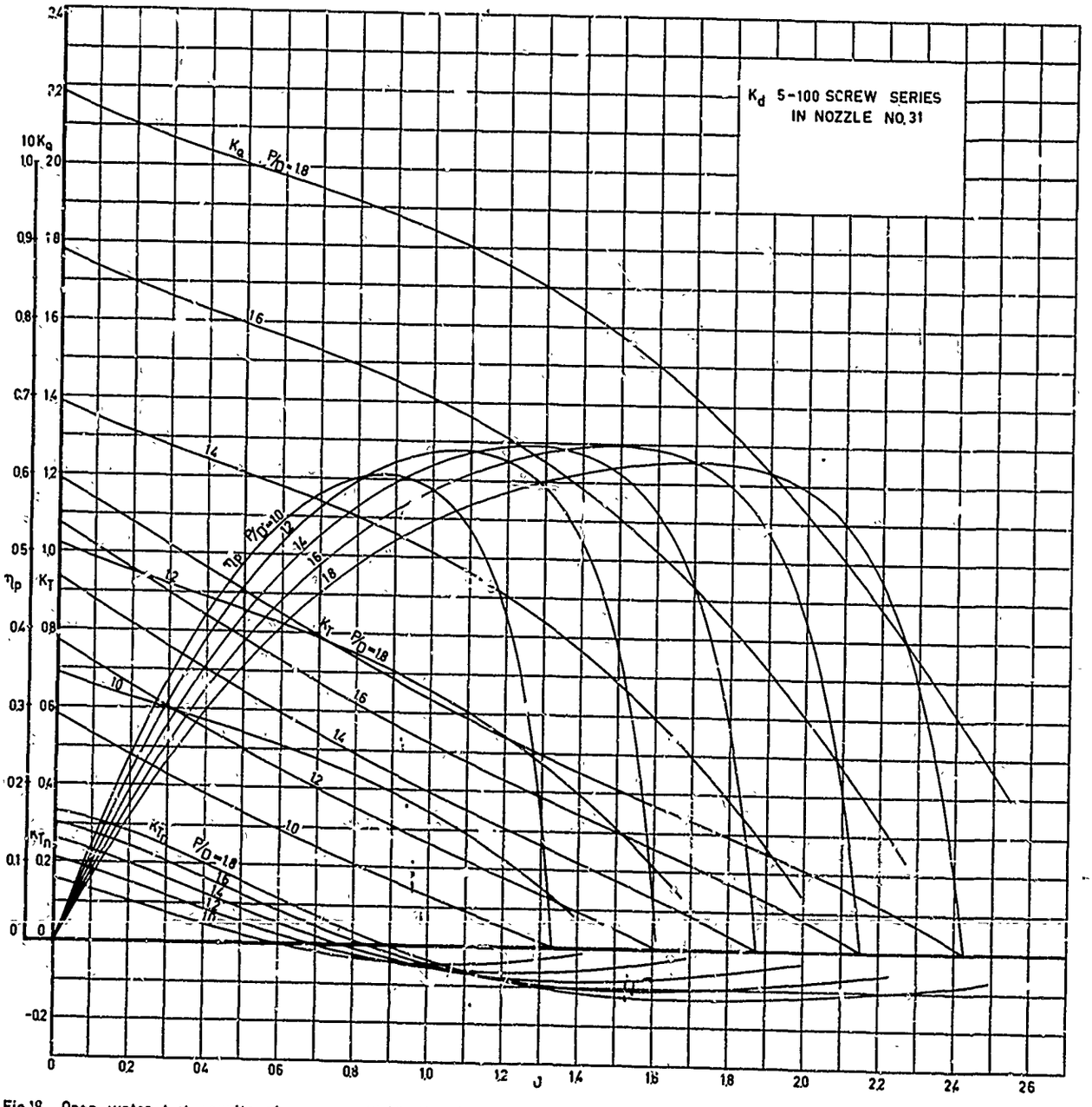

Fig.19 Open water test results of nozzle no.31 (K_T; K_{T_n}; K_Q and η_p as functions of J).

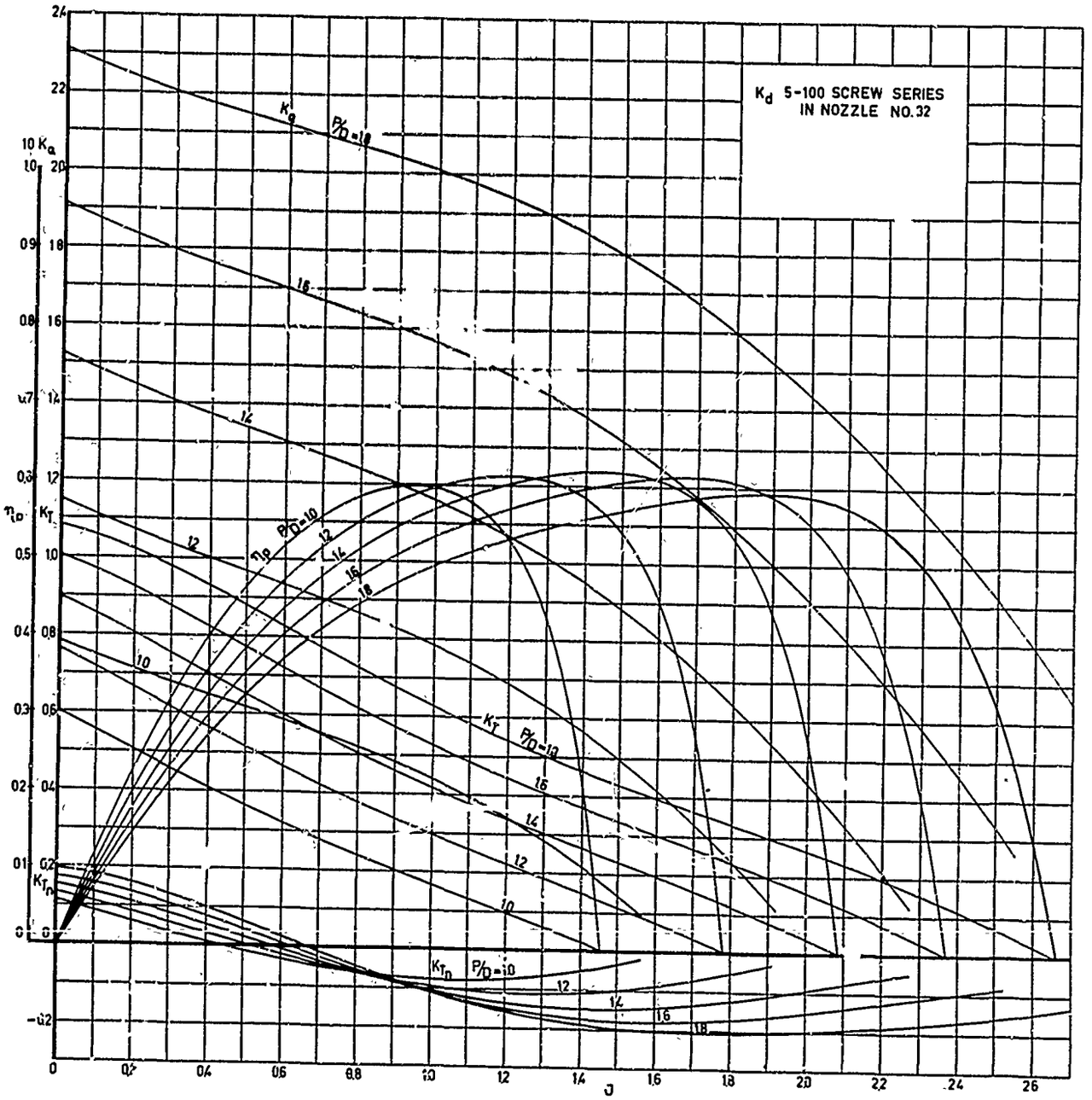

Fig. 20 Open water test results of nozzle no.32 ; K_T; K_{T_n}; K_Q and η_p as functions of J).

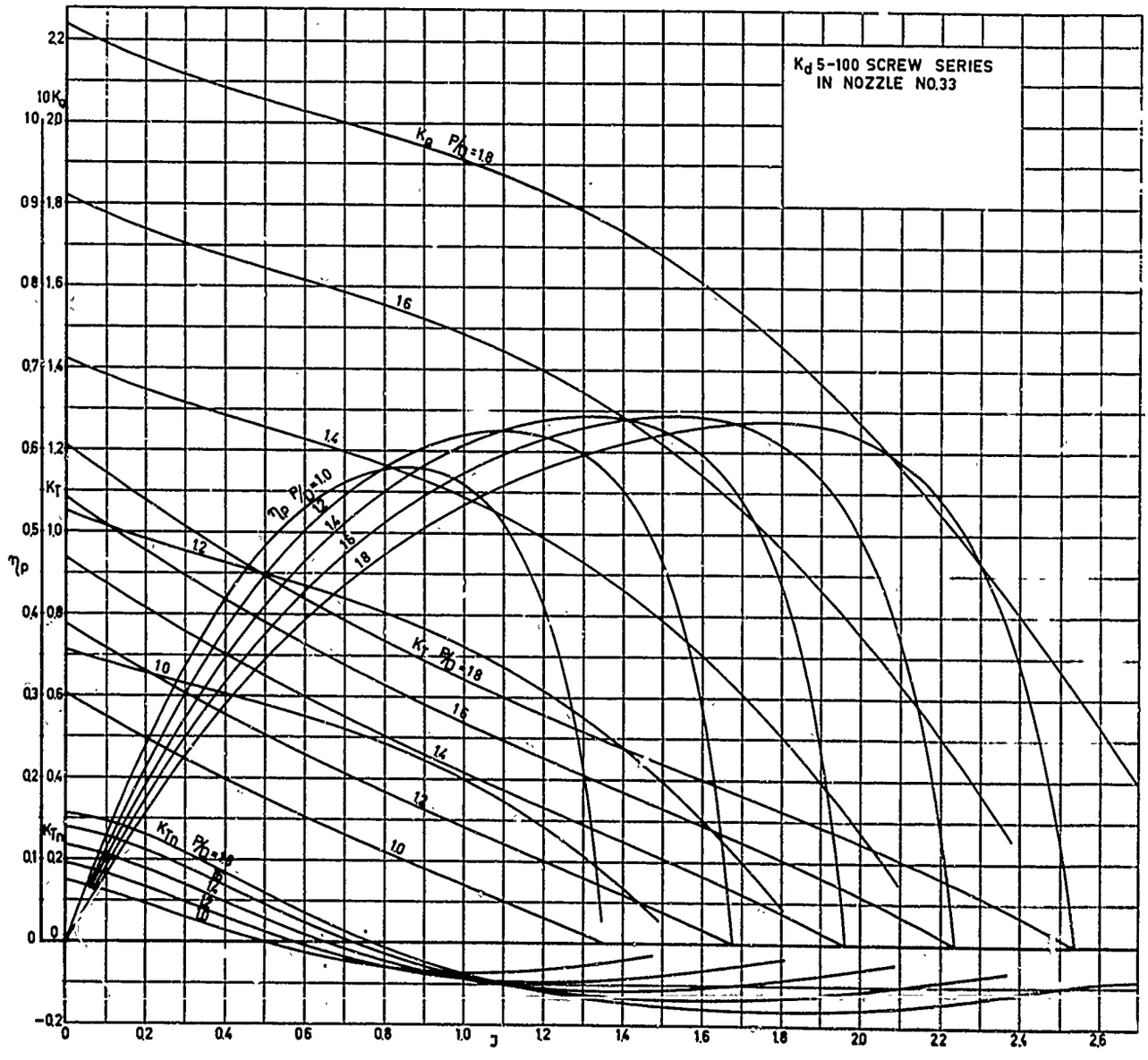

Fig.21 Open water test results of nozzle no.33 (K_T; K_{T_n}; K_q and η_p as functions of J).

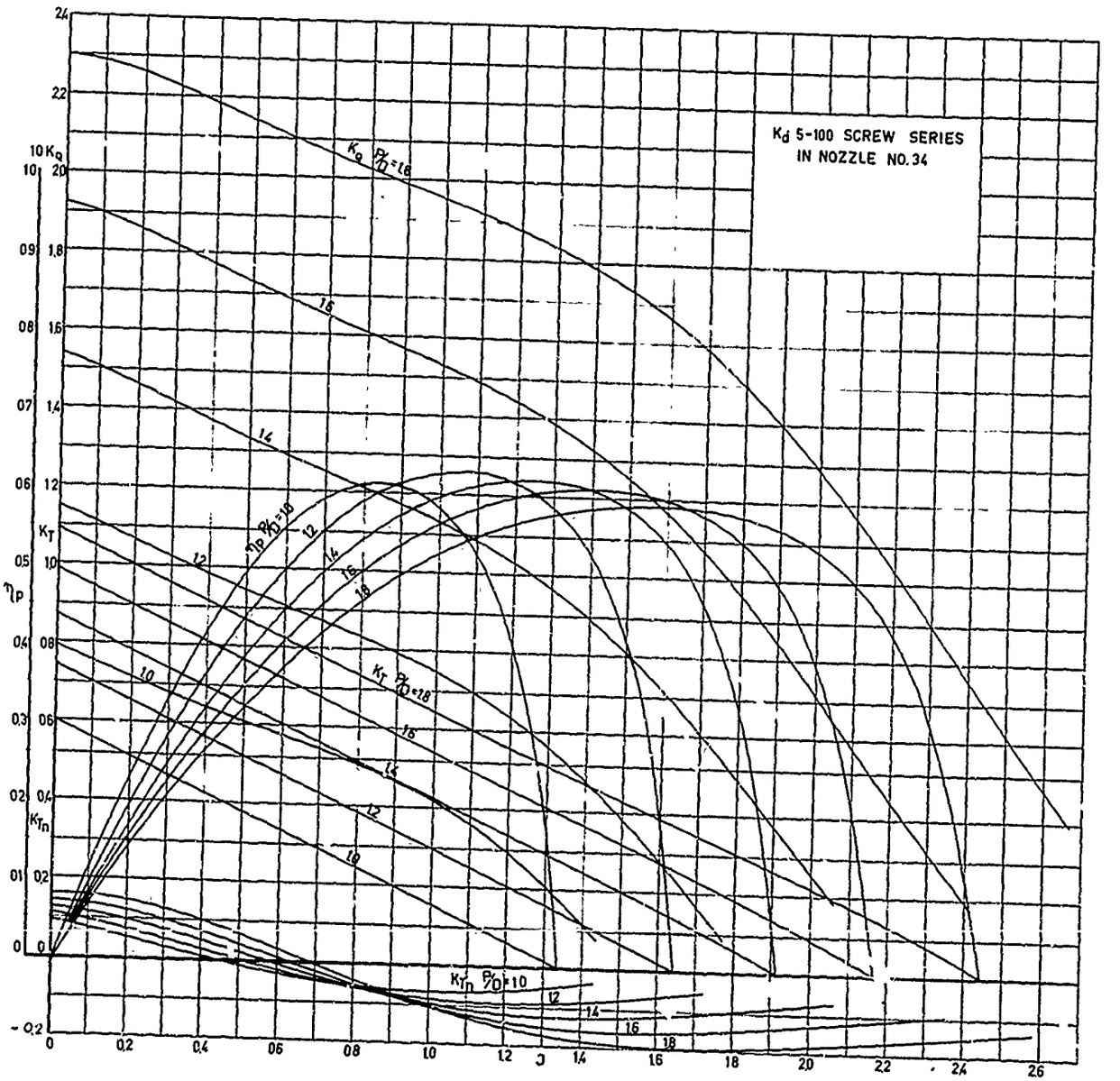

Fig.22 Open water test results of nozzle no.34 (K_T; K_{T_n}; K_Q and η_P as functions of J).

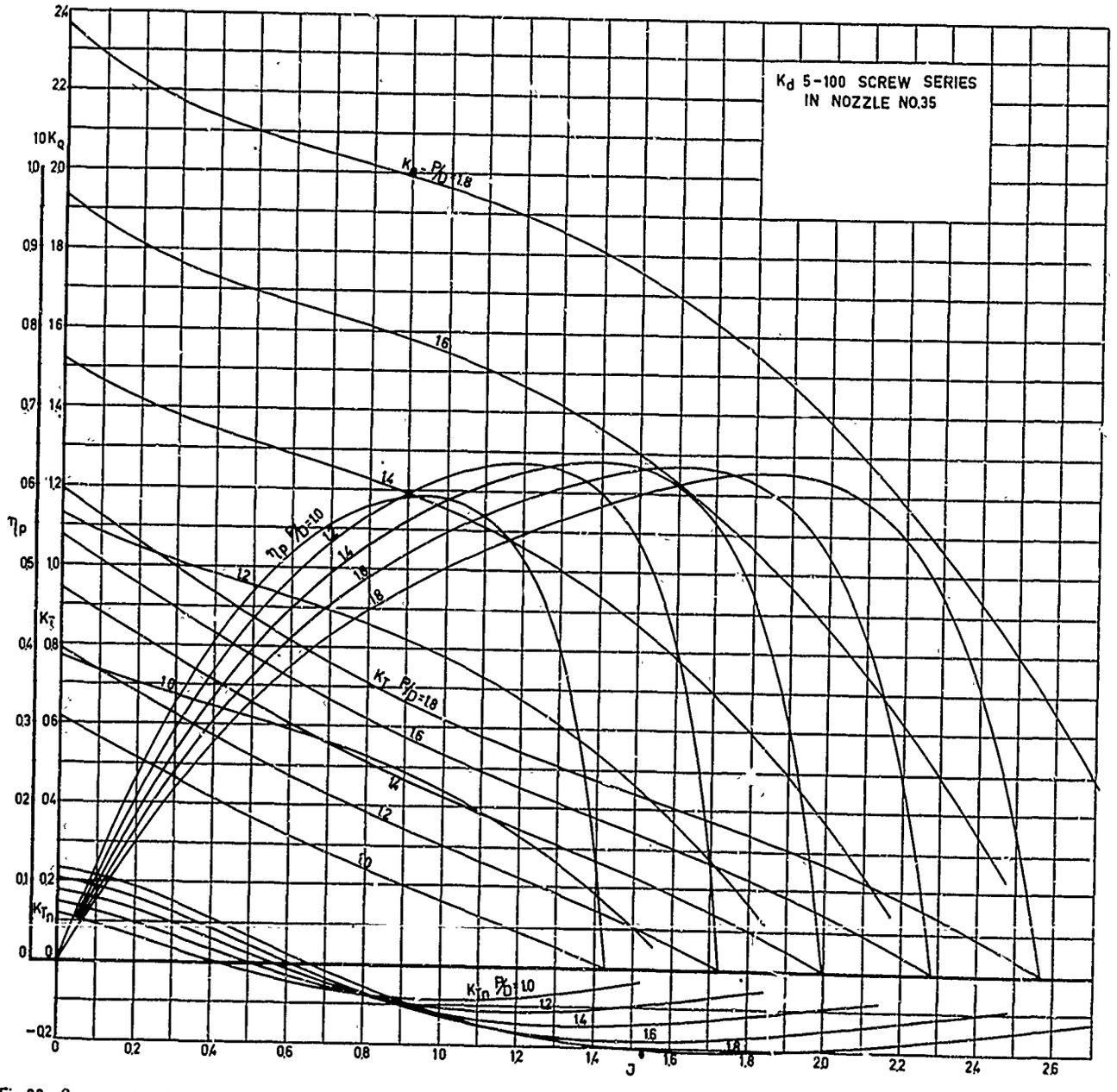

Fig.23 Open water test results of nozzle no.35 (K_T; K_{T_n}; K_Q and η_p as functions of J)

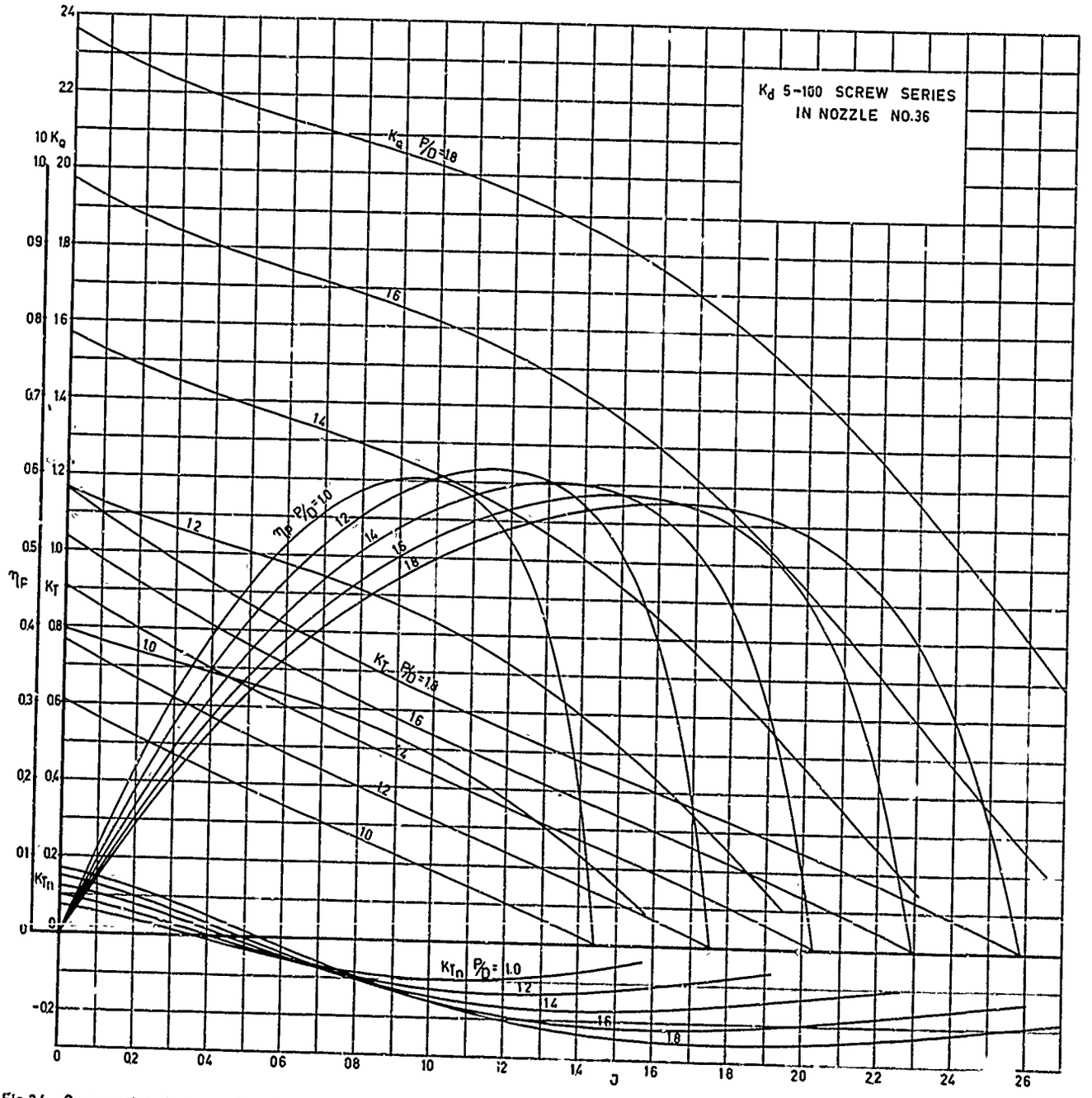

Fig.24 Open water test results of nozzle no.36 (K_T, K_{T_n}, K_Q and η_p as functions of J)

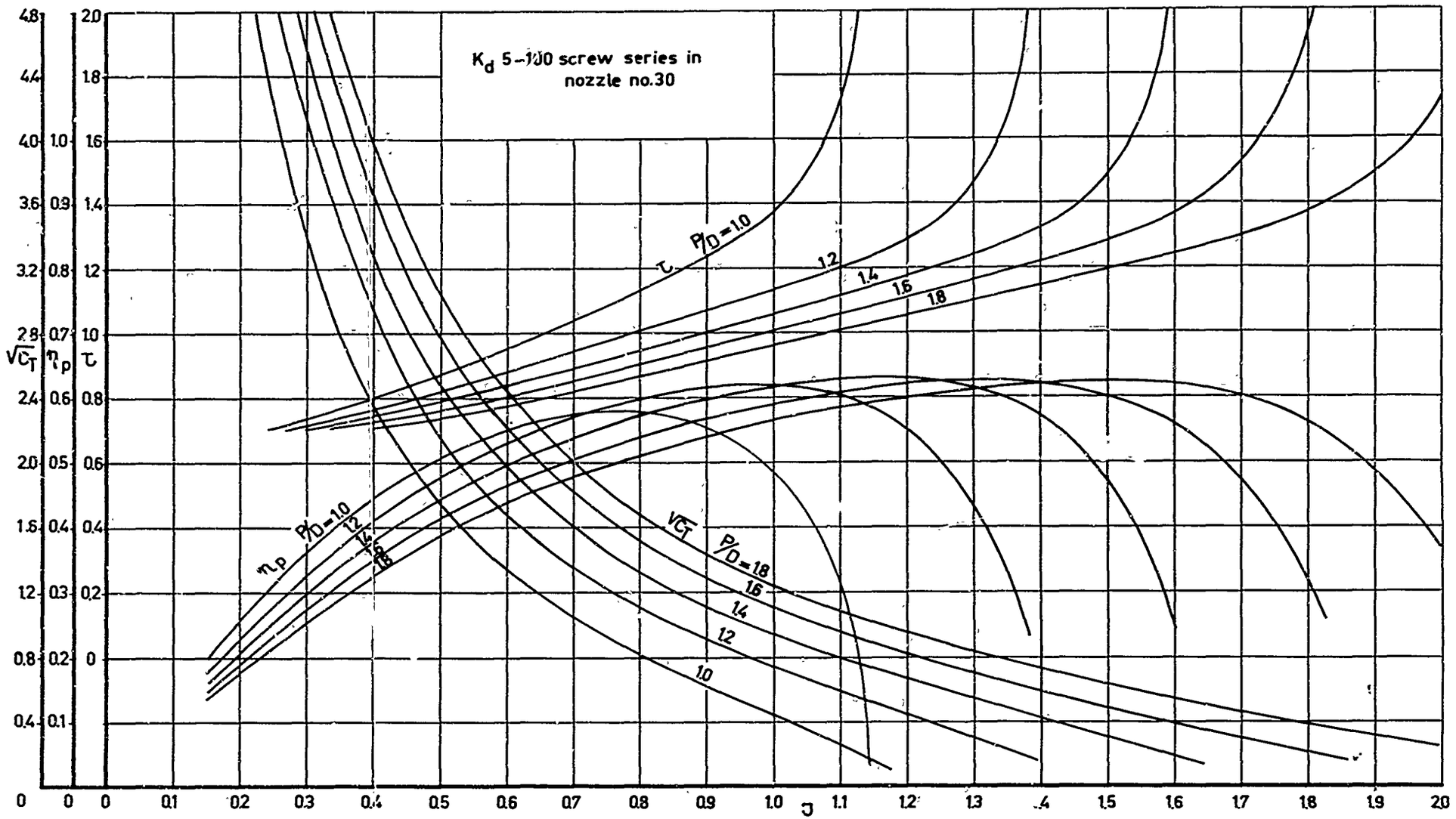

Fig. 25 Open water test results of nozzle no.30 (C_T, τ and η_p as functions of J).

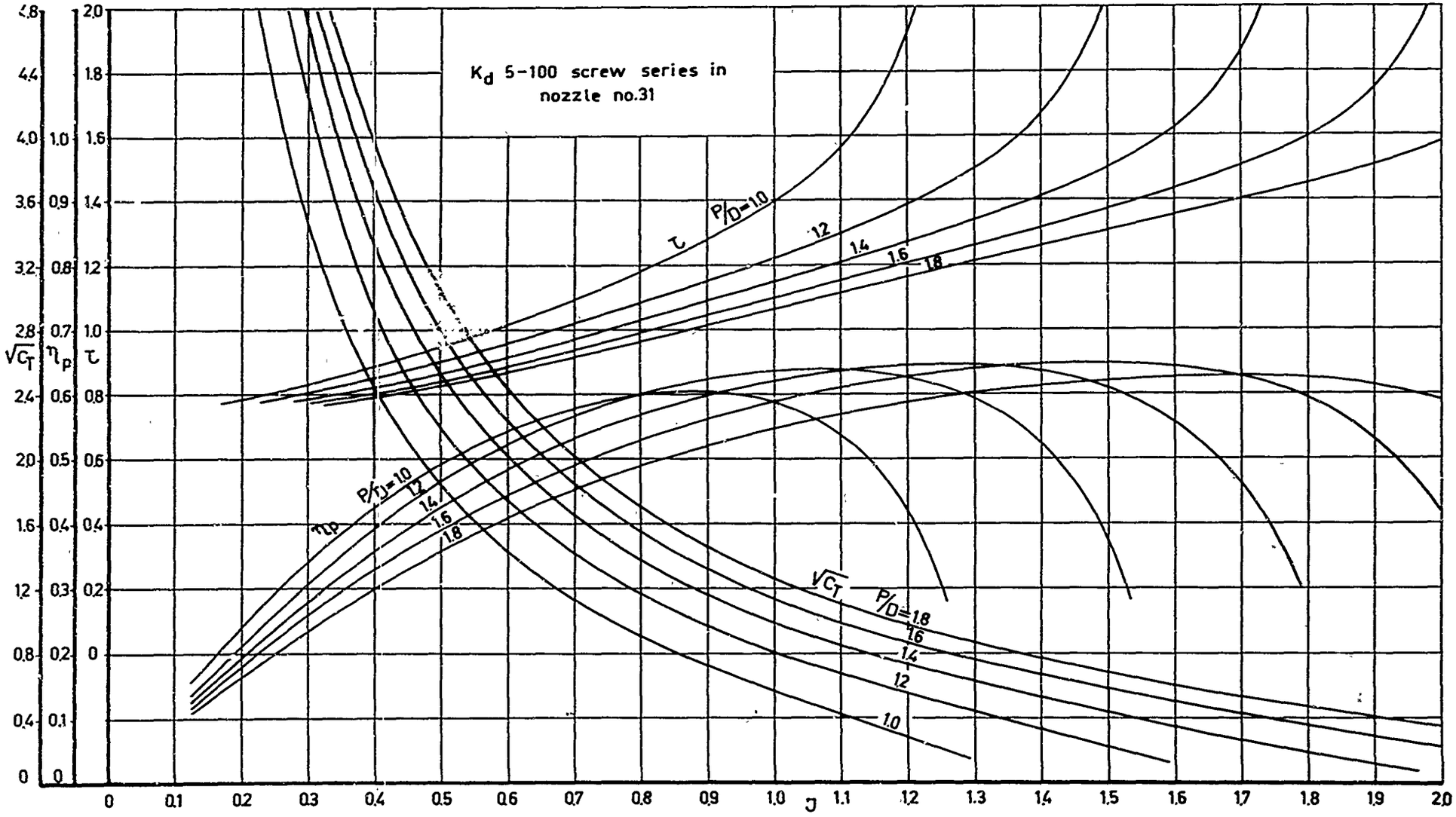

Fig.26 Open water test results of nozzle no.31 (C_T, τ and η_p as functions of J).

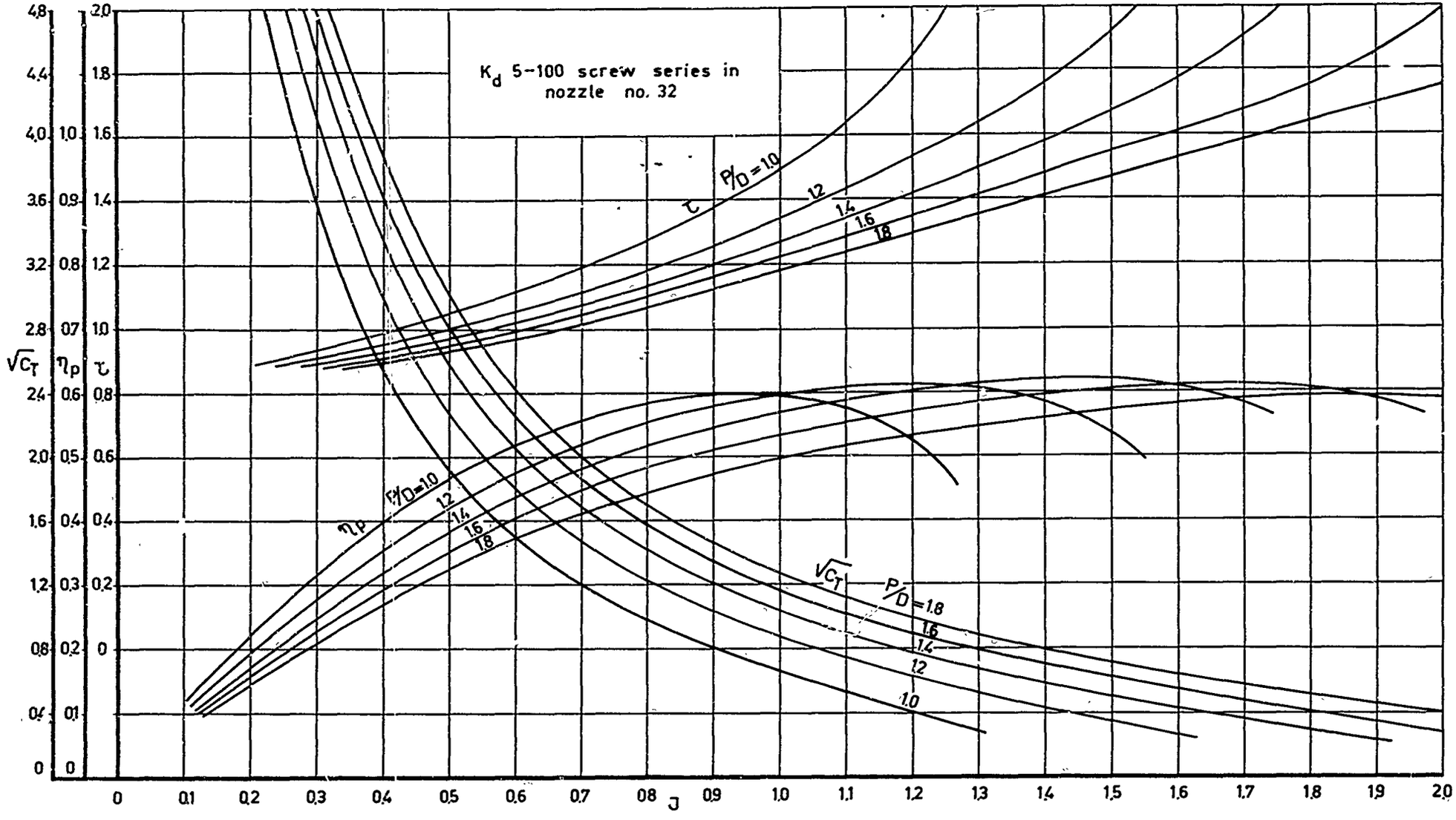

Fig.27 Open water test results of nozzle no.32 (C_T, τ and η_p as functions of J).

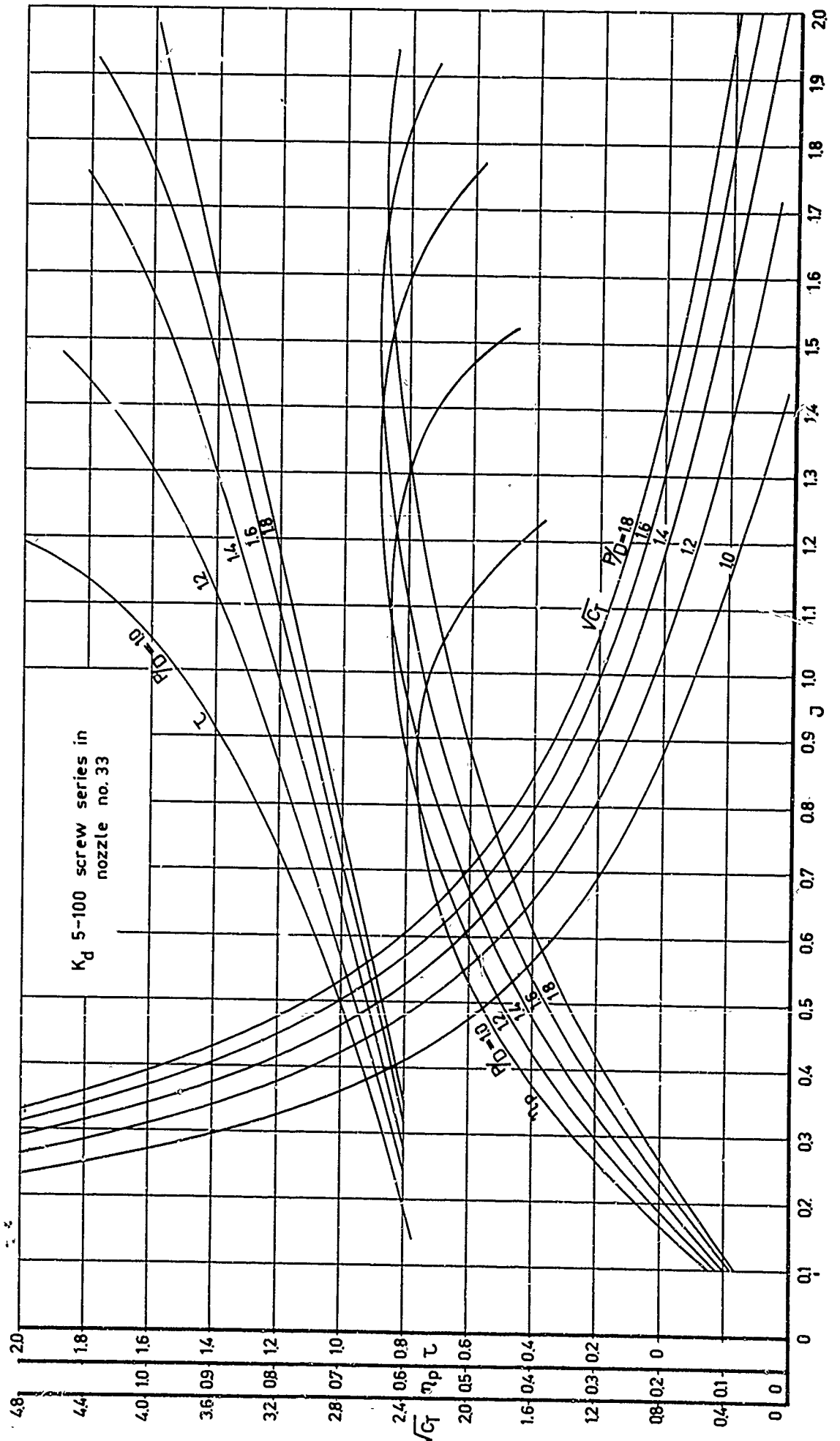

Fig.28 Open water test results of nozzle no.33 (C_T, τ and η_p as functions of J).

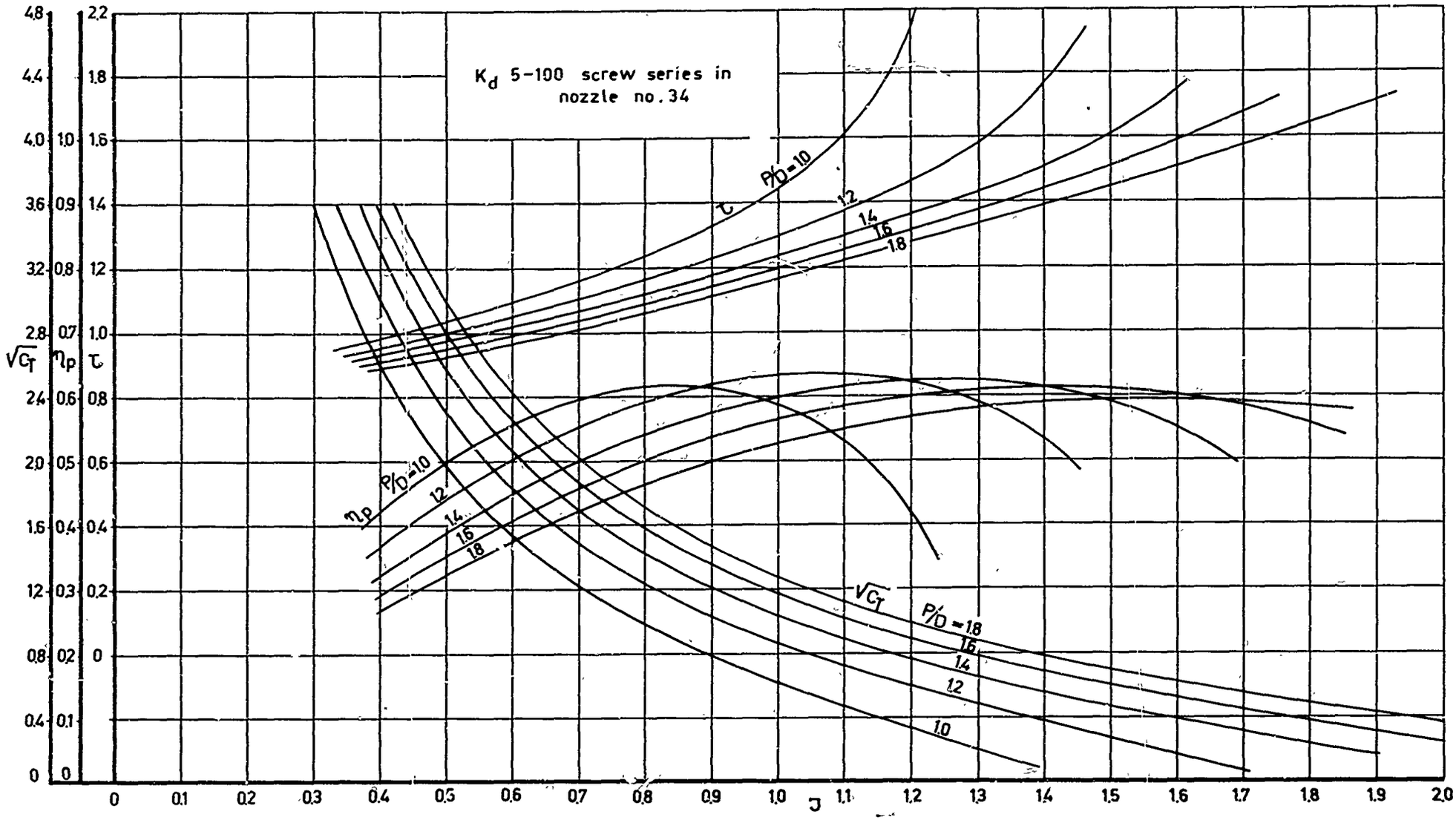

Fig.29 Open water test results of nozzle no.34 (C_T, τ and η_p as functions of J).

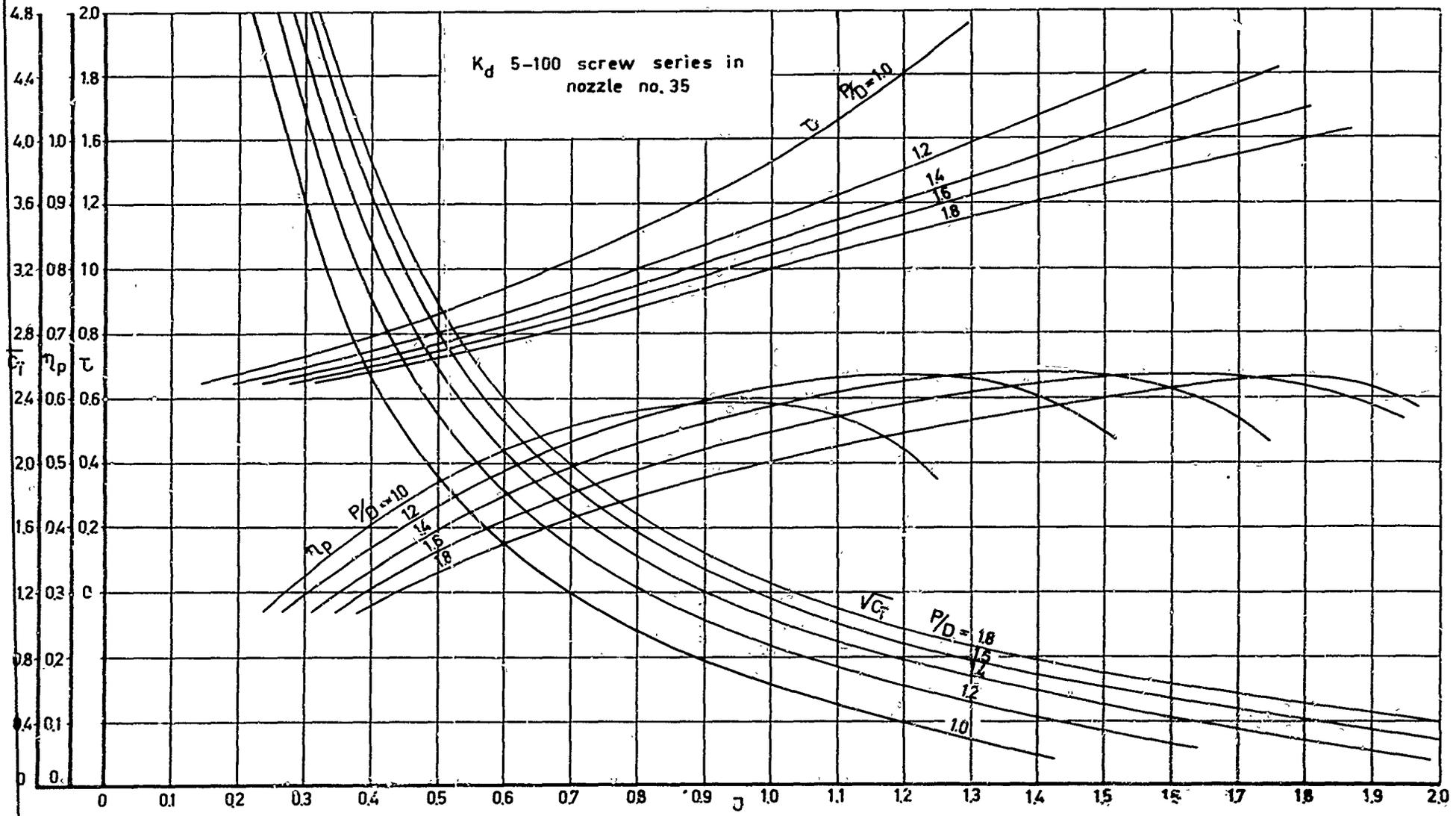

Fig.30 Open water test results of nozzle no.35 (C_T, τ and η_p as functions of J.).

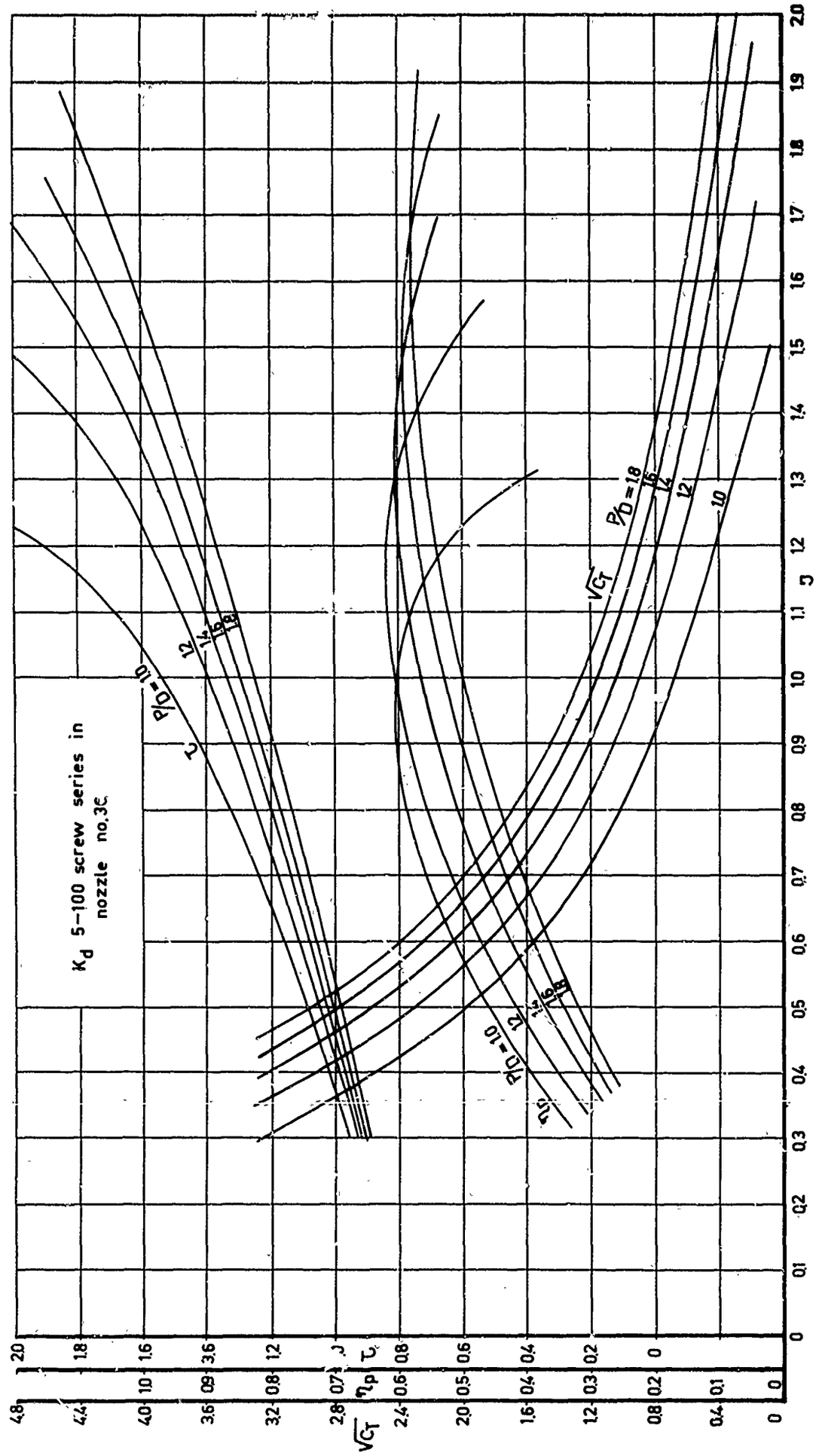

Fig.31 Open water test results of nozzle no.36 (C_T, τ and η_p as functions of J).

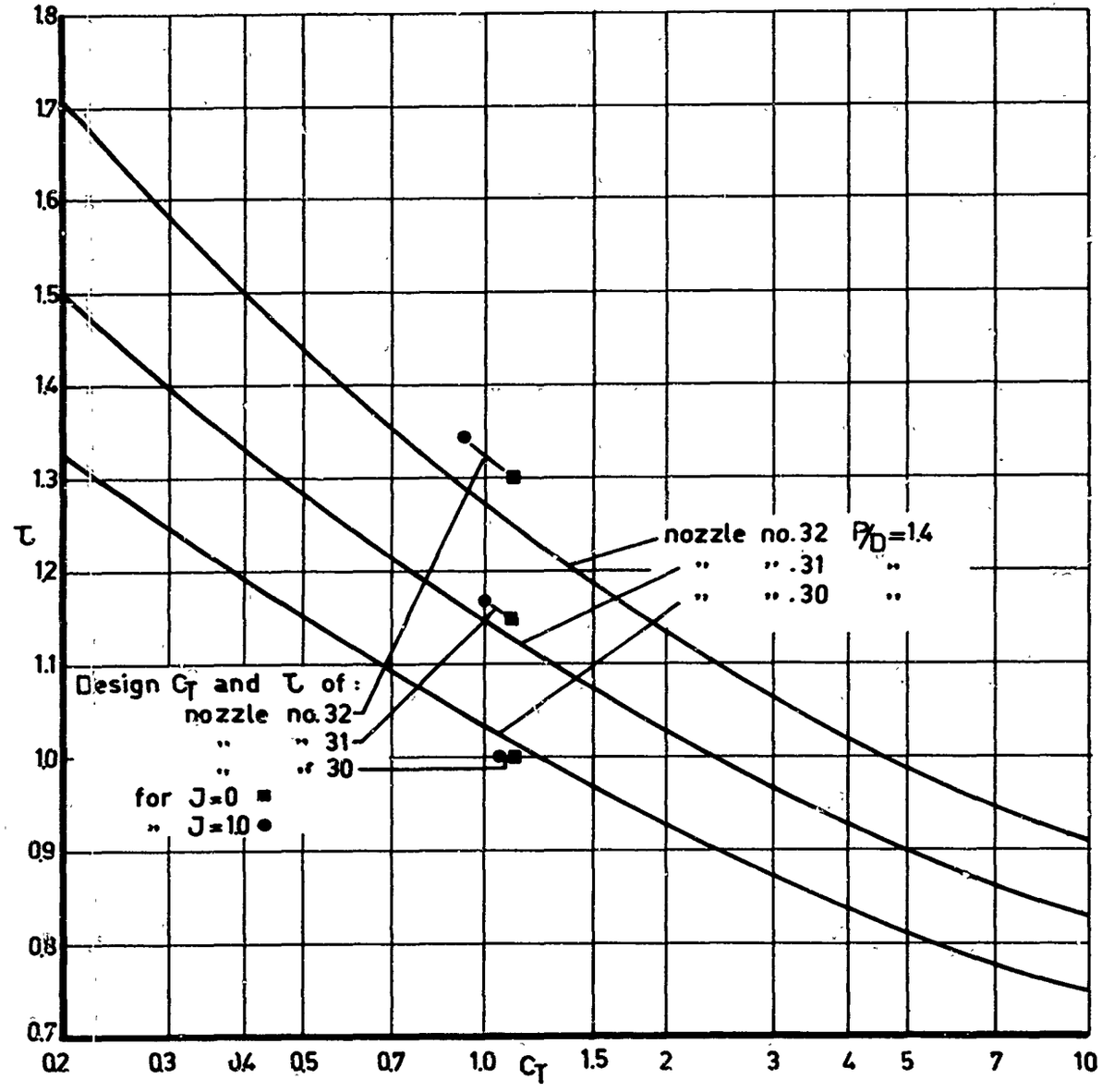

Fig.32 Relationship between C_T and τ of nozzles nos.30,31 and 32.

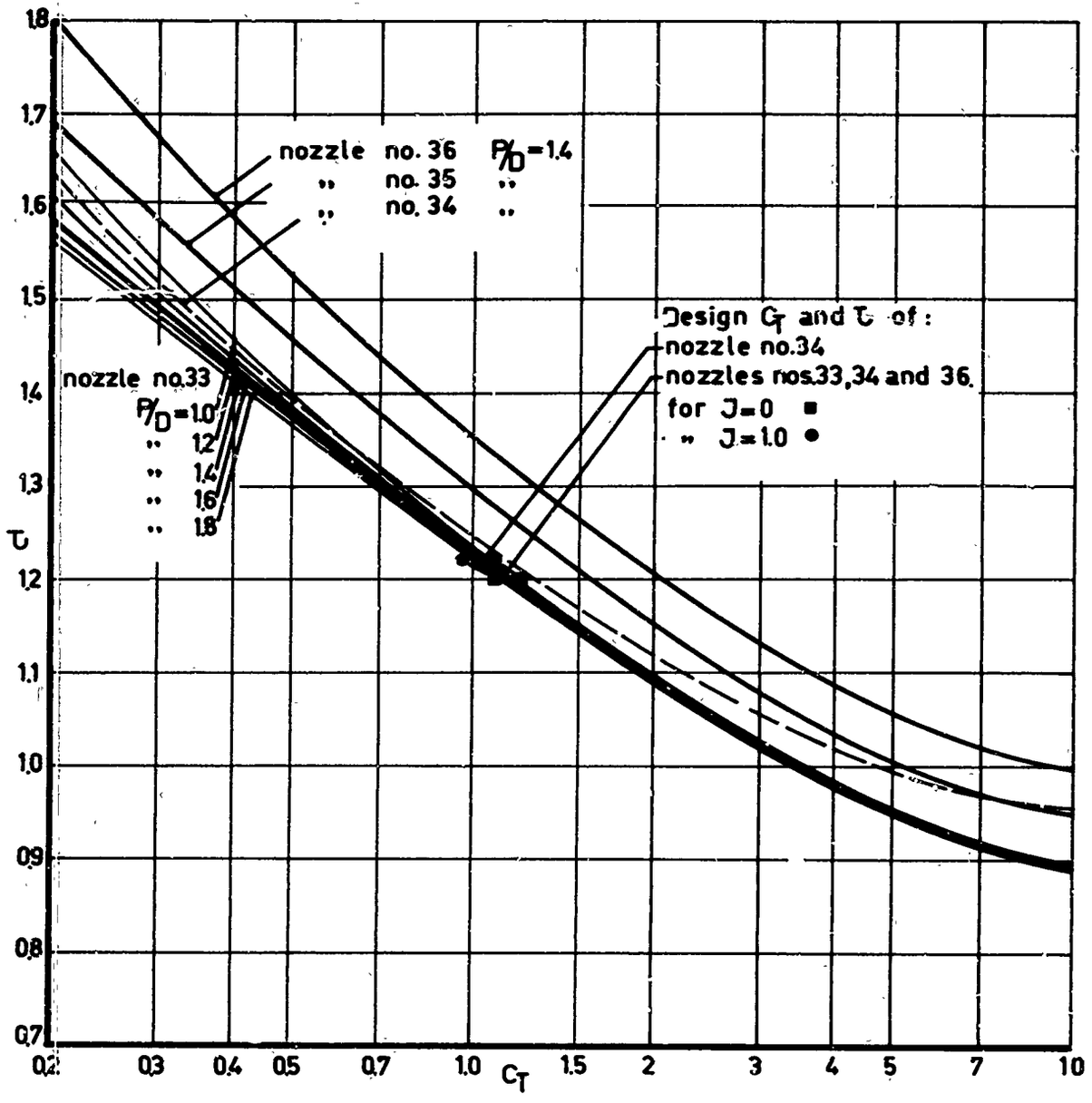

Fig.33 Relationship between C_T and τ of nozzles nos. 33, 34, 35 and 36.

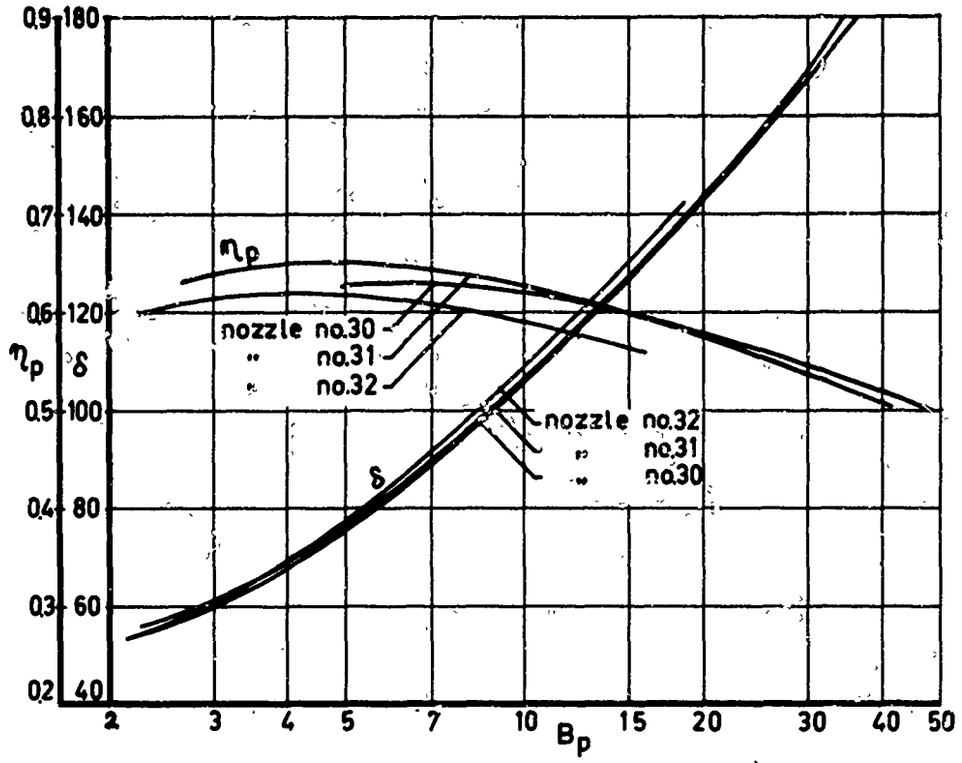

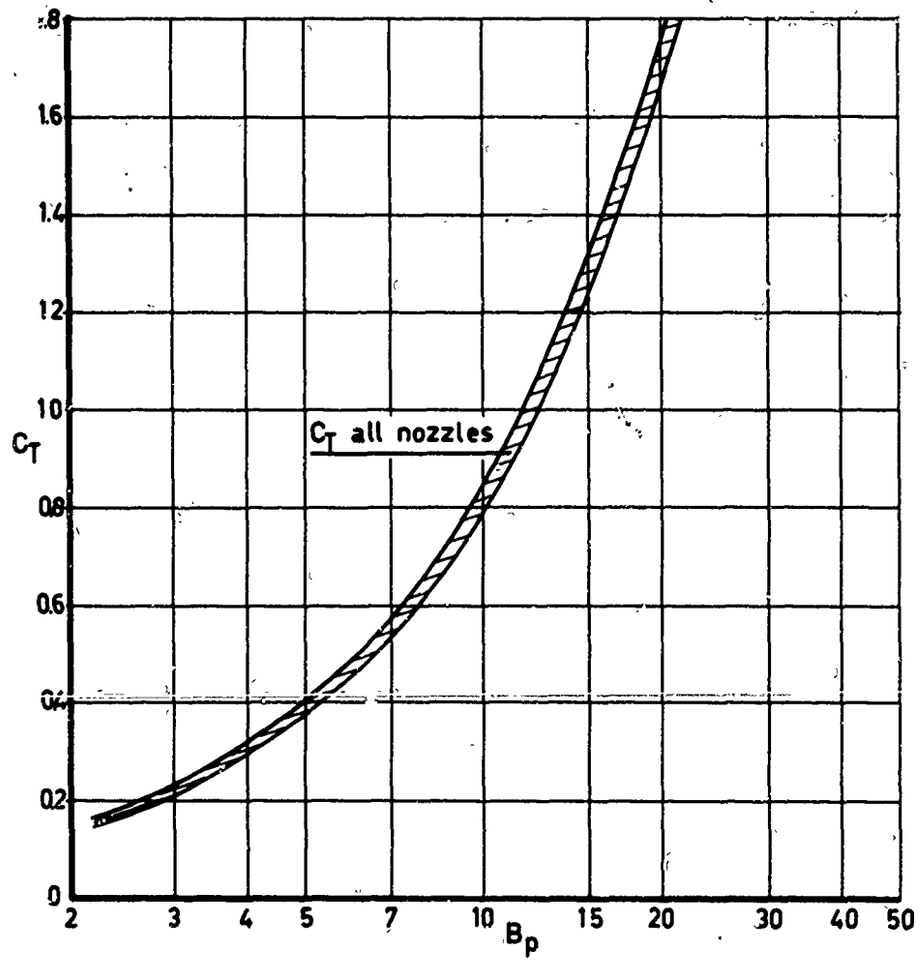

Fig.34 Optimum relationship between η_p, δ and B_p of nozzles nos. 30, 31 and 32.

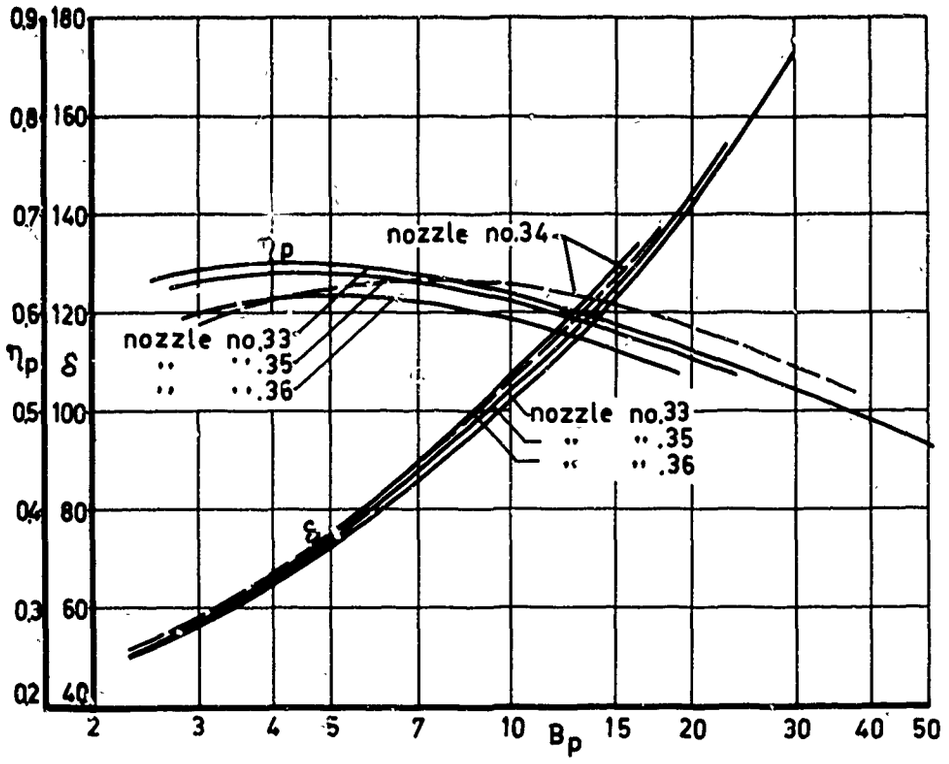

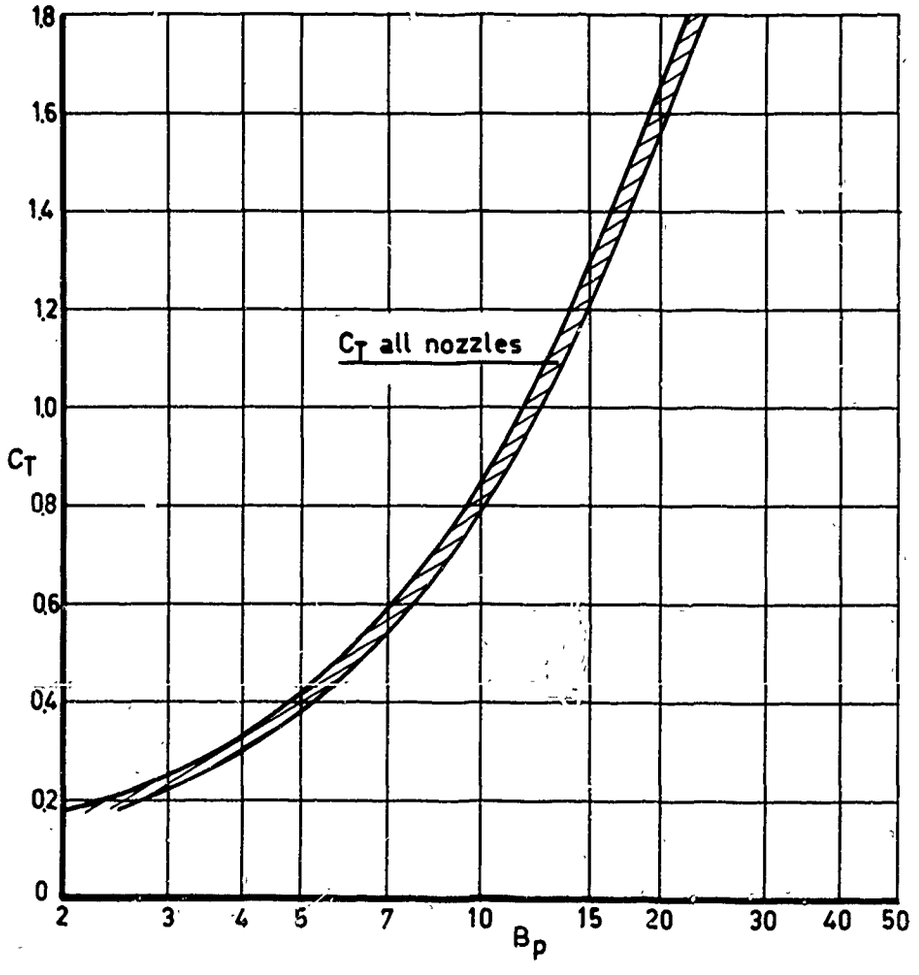

Fig. 35 Optimum relationship between η_p, δ and B_p of nozzles nos. 33, 34, 35 and 36.

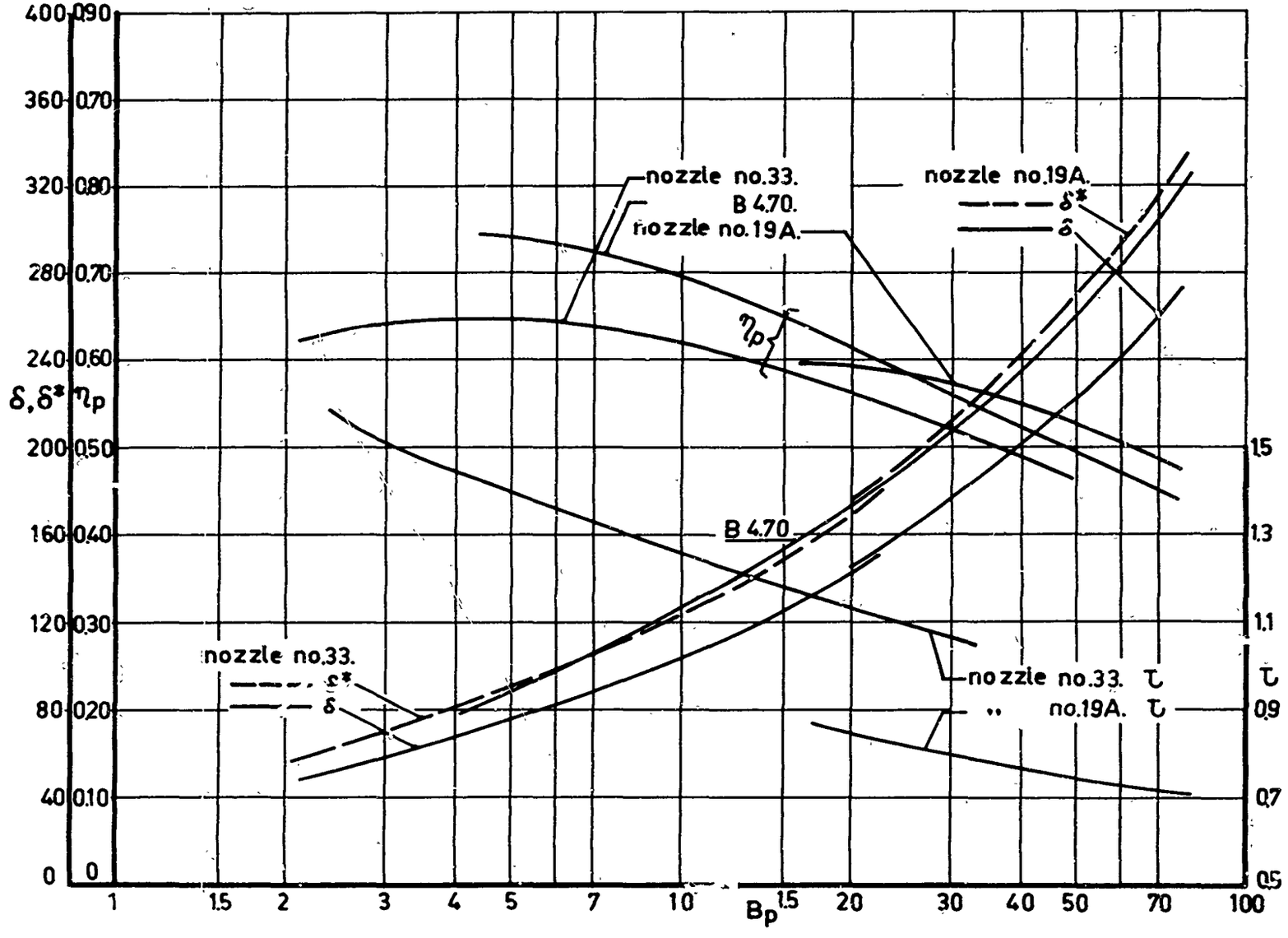

Fig.36 Optimum relationship between η_p, δ and B_p of an accelerating nozzle (nozzle no.19A), a decelerating nozzle (nozzle no.33) and the B 4.70 screw series in open water.

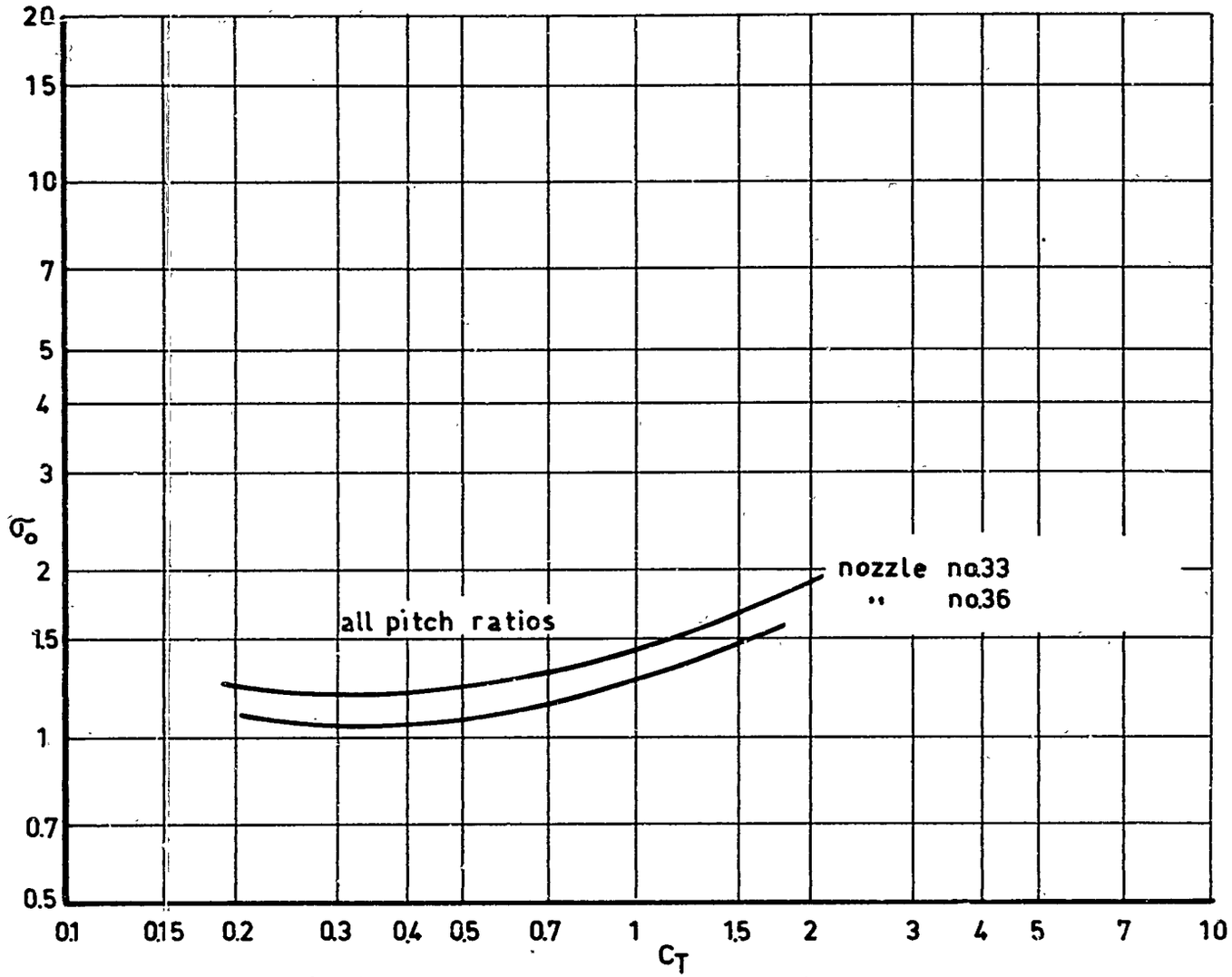

Fig.37 Incipient cavitation phenomena at the exterior surface of the nozzles no.33 and 36.

nozzle number	C_{T_o}	v_o	L/D	a/L	S/L	d/D
30	0.95	1.00	0.6	0.5	0.15	0.20
31	0.95	1.15	0.6	0.5	0.15	0.20
32	0.95	1.30	0.6	0.5	0.15	0.20
33	1.0	1.2	0.6	0.5	0.15	0.20
34	1.0	1.2	0.6	0.5	0.09	0.20
35	1.0	1.2	0.9	0.5	0.10	0.20
36	1.0	1.2	1.2	0.5	0.075	0.20

Table I : Design parameters of the tested nozzle shapes.

x/L	S(x)/L						
	nozzle number 30	31	32	33	34	35	36
- 0.500	+ 0.0112	- 0.0073	- 0.0232	- 0.0083	+ 0.0005	- 0.0067	- 0.0091
- 0.416	+ 0.0130	+ 0.0008	- 0.0096	+ 0	+ 0.0007	- 0.0008	- 0.0034
- 0.333	+ 0.0139	+ 0.0067	+ 0.0006	+ 0.0058	+ 0.0008	+ 0.0033	- 0.0008
- 0.250	+ 0.0128	+ 0.0093	+ 0.0067	+ 0.0083	+ 0.0011	+ 0.0056	+ 0.0004
- 0.167	+ 0.0102	+ 0.0091	+ 0.0085	+ 0.0083	+ 0.0012	+ 0.0055	+ 0.0012
- 0.084	+ 0.0059	+ 0.0060	+ 0.0063	+ 0.0058	+ 0.0011	+ 0.0037	+ 0.0003
+ 0	0	+ 0	+ 0	+ 0	+ 0	0	0
+ 0.084	- 0.0081	- 0.0096	- 0.0112	- 0.0010	- 0.0009	- 0.0064	- 0.0054
+ 0.167	- 0.0186	- 0.0229	- 0.0276	- 0.0023	- 0.0021	- 0.0152	- 0.0158
+ 0.250	- 0.0316	- 0.0404	- 0.0496	- 0.0042	- 0.0038	- 0.0389	- 0.0279
+ 0.333	- 0.0476	- 0.0622	- 0.0773	- 0.0066	- 0.0053	- 0.0460	- 0.0417
+ 0.416	- 0.0661	- 0.0881	- 0.1106	- 0.0092	- 0.0083	- 0.0675	- 0.0582
+ 0.500	- 0.0874	- 0.1162	- 0.1498	- 0.0124	- 0.0112	- 0.0951	- 0.0816

Table II : Mean lines of the tested nozzle shapes

Diameter	D	240 mm
Number of blades	Z	5
Pitch ratio (at 0.7 D)	$P/_D$	1.0-1.2-1.4-1.6-1.8
Blade area ratio	A_e/A	1.00
Blade outline		Kaplan type
Blade section		NASA 16-parabolic camberline
Propellers indicated by nos.		3930-3931-3932-3933-3934

Table III : Particulars of the K_d 5-100 screw series

Appendix A.

Theoretical analysis of ducted propellers

1. Representation of ducted propellers by vortex distributions.

The calculations of the ducted propellers were based on the following assumptions. The forward velocity was assumed to be sufficiently large, the nozzle loading and the blade loading of the impeller sufficiently low to permit the application of the linearized theory. The effect of the hub shape on the flow field was neglected. The ducted propeller system considered consists of an annular airfoil of finite length and zero thickness and of an impeller having an infinite number of blades.

The mathematical model of the ducted propeller configuration can be composed by means of vortex distributions.
The impeller was regarded as a uniformly loaded actuator disk set normal to the free stream. It was driven to rotate with an angular velocity ω. Free trailing vortices started from the propeller disk at hub and tip radius. The flow around the nozzle was represented by a sinusoidal bound ring vortex distribution with zero strength at the leading and the trailing edges and by a ring vortex distribution with zero strength at the leading edge and equal to the strength of the circumferential component of the helical trailing vortices at the impeller disk. The resulting mathematical model is summarized in Fig. a.

Assume the vortex strength per unit impeller disk area at the impeller tip to be equal to $\gamma(R_1)$, the strength of the different vortex distributions then becomes:

- vortex strength per unit impeller disk area

$$\gamma(r) = \frac{R_i}{r}\gamma(R_1)$$

- strength per unit area of the trailing vortex sheet starting from the impeller disk at the tip radius

$$\sqrt{1+\mu^2}\,\gamma(R_1)$$

- strength per unit area of the trailing vortex sheet starting from the impeller disk at the hub radius

$$\sqrt{1+\lambda^2\mu^2}\,\frac{1}{\lambda}\,\gamma(R_1)$$

- strength per unit area of the bound ring vortex distribution along the nozzle

$$\mu\,\gamma(R_1)\,\frac{\sin\theta}{2\sqrt{a(1-a)}} \qquad (\text{for } -aL < x < 0)$$

$$\gamma(R_1)\,\sin\theta \qquad (\text{for } -aL < x < (1-a)L)$$

where,

$$\mu = \frac{\omega R_1}{V_e}\ , \quad \lambda = \frac{R_o}{R_1}\ , \quad x+(a-0{,}5)L = -0{,}5\,L\cos\theta$$

and the definitions of R_o, R_i, r, x, L, a and so on, are given in Figure a.

2. Calculations of the flow field

The total induced velocities can be calculated according to the law of Biot-Savart if the main dimensions of the ducted propeller system (R_o, R_i, L and a), the loading of duct and impeller ($\gamma(R_1)$ and $\gamma_i(R_1)$), the rotational velocity of the impeller (ω) and the undisturbed stream velocity (V_e) are given. In the following, we will give the induced velocities in the point (x, r) of the flow field due to the various vortex distributions.
The relations are made non-dimensional in the following way:

$$\bar{x} = \frac{x}{R_1} \;,\; \bar{\xi} = \frac{\xi}{R_1} \;,\; \bar{r} = \frac{r}{R_1} \;,\; \lambda = \frac{R_0}{R_1} \;,\; \eta = \frac{L}{R_1}$$

$$\bar{\gamma} = \frac{\gamma(R_1)}{V_e} \;,\quad \bar{\gamma}_1 = \frac{\gamma_1(R_1)}{V_e}$$

$$\bar{w}_{a,t,or,r} = \frac{w_{a,t,or\,r}}{V_e}$$

where a , t and r denote the axial, tangential and radial induced velocities respectively.

(1) Induced velocities due to the vortices representing the impeller disk

$$\bar{w}_a^{(1)}(\bar{x},\bar{r}) = 0$$

$$\bar{w}_T^{(1)}(\bar{x},\bar{r}) = \bar{\gamma}\, A_{1,1}(\bar{x},\bar{r}) \qquad A_{1,1}(\bar{x},\bar{r}) = \frac{1}{\pi}\int_{\lambda}^{1} d\bar{r}_1 \int_0^{\pi/2} d\psi \, \frac{\bar{x}\cos 2\psi}{\left[\bar{x}^2 + (\bar{r}_1+\bar{r})^2 - 4\bar{r}_1\bar{r}\sin^2\psi\right]^{3/2}}$$

$$\bar{w}_r^{(1)}(\bar{x},\bar{r}) = 0$$

(2) Induced velocities due to the trailing vortex sheet starting from the impeller disk at the tip radius

$$\bar{w}_a^{(2)}(\bar{x},\bar{r}) = \mu\bar{\gamma} A_{2,1}(\bar{x},\bar{r}) \qquad A_{2,1}(\bar{x},\bar{r}) = \frac{1}{\pi}\int_0^{\infty} d\tau \int_0^{\pi/2} d\psi \, \frac{\mu^2(1+\bar{r}\cos 2\psi)}{\left[\left\{\mu\bar{x}-\tau\right\}^2 + \mu^2\left\{(1+\bar{r})^2 - 4\bar{r}\sin^2\psi\right\}\right]^{3/2}}$$

$$\bar{w}_T^{(2)}(\bar{x},\bar{r}) = \bar{\gamma} A_{2,2}(\bar{x},\bar{r}) \qquad A_{2,2}(\bar{x},\bar{r}) = \frac{1}{\pi}\int_0^{\infty} d\tau \int_0^{\pi/2} d\psi \, \frac{\mu(\bar{r}+\cos 2\psi)}{\left[\text{---------------}\right]^{3/2}}$$

$$\bar{w}_r^{(2)}(\bar{x},\bar{r}) = \mu\bar{\gamma} A_{2,3}(\bar{x},\bar{r}) \qquad A_{2,3}(\bar{x},\bar{r}) = -\frac{1}{\pi}\int_0^{\infty} d\tau \int_0^{\pi/2} d\psi \, \frac{\mu\left[\mu\bar{x}-\tau\right]\cos 2\psi}{\left[\text{---------------}\right]^{3/2}}$$

(3) Induced velocities due to the trailing vortex sheet starting from the impeller disk at the hub radius:

$$w_a^{(3)}(\bar{x},\bar{r}) = \mu\bar{\gamma} A_{3,1}(\bar{x},\bar{r}) \qquad A_{3,1}(\bar{x}\bar{r}) = -\frac{1}{\pi}\int_0^{\infty} d\tau \int_0^{\pi/2} d\psi \, \frac{\lambda\mu^2(\lambda+\bar{r}\cos 2\psi)}{\left[\left\{\mu\bar{x}-\tau\right\}^2 + \mu^2\left\{(\lambda+\bar{r})^2 - 4\lambda\bar{r}\sin^2\psi\right\}\right]^{3/2}}$$

$$w_T^{(3)}(\bar{x},\bar{r}) = \bar{\gamma} A_{3,2}(\bar{x},\bar{r}) \qquad A_{3,2}(\bar{x},\bar{r}) = -\frac{1}{\pi}\int_0^{\infty} d\tau \int_0^{\pi/2} d\psi \, \frac{\mu^2(\bar{r}+\lambda\cos 2\psi)}{\left[\text{---------------}\right]^{3/2}}$$

$$w_r^{(3)}(\bar{x},\bar{r}) = \mu\bar{\gamma} A_{3,3}(\bar{x},\bar{r}) \qquad A_{3,3}(\bar{x},\bar{r}) = \frac{1}{\pi}\int_0^{\infty} d\tau \int_0^{\pi/2} d\psi \, \frac{\lambda\mu\left[\mu\bar{x}-\tau\right]\cos 2\psi}{\left[\text{---------------}\right]^{3/2}}$$

4 Induced velocities due to the discontinuous ring vortex distributions along the nozzle

$$w_a^{(4)}(\bar{x},\bar{r}) = \mu\bar{\gamma}\, A_{4,1}(\bar{x},\bar{r}) \qquad A_{4,1}(\bar{x},\bar{r}) = \frac{1}{2\pi\sqrt{a(1-a)}} \int_{-a\eta}^{0} d\bar{\xi} \int_{0}^{\pi/2} d\psi \, \frac{(1+\bar{r}\cos 2\psi)\sin\theta}{\left[(\bar{x}-\bar{\xi})^2+(1+\bar{r})^2-4\bar{r}\sin^2\psi\right]^{3/2}}$$

$$w_T^{(4)}(\bar{x},\bar{r}) = 0$$

$$w_r^{(4)}(\bar{x},\bar{r}) = \mu\bar{\gamma}\, A_{4,3}(\bar{x},\bar{r}) \qquad A_{4,3}(\bar{x},\bar{r}) = \frac{-1}{2\pi\sqrt{a(1-a)}} \int_{-a\eta}^{0} d\bar{\xi} \int_{0}^{\pi/2} d\psi \, \frac{(\bar{x}-\bar{\xi})\cos 2\psi}{\left[\text{-----------------}\right]^{3/2}}$$

5 Induced velocities due to the sinusoidal ring vortex distribution along the nozzle:

$$w_a^{(5)}(\bar{x},\bar{r}) = \bar{\gamma}_1 A_{5,1}(\bar{x},\bar{r}) \qquad A_{5,1}(\bar{x},\bar{r}) = \frac{1}{\pi} \int_{-a\eta}^{(1-a)\eta} d\bar{\xi} \int_{0}^{\pi/2} d\psi \, \frac{(1+\bar{r}\cos 2\psi)\sin\theta}{\left[(\bar{x}-\bar{\xi})^2+(1+\bar{r})^2-4\bar{r}\sin^2\psi\right]^{3/2}}$$

$$w_T^{(5)}(\bar{x},\bar{r}) = 0$$

$$w_r^{(5)}(\bar{x},\bar{r}) = \bar{\gamma}_1 A_{5,3}(\bar{x},\bar{r}) \qquad A_{5,3}(\bar{x},\bar{r}) = -\frac{1}{\pi} \int_{-a\eta}^{(1-a)\eta} d\bar{\xi} \int_{0}^{\pi/2} d\psi \, \frac{(\bar{x}-\bar{\xi})\cos 2\psi \sin\theta}{\left[\text{-----------------}\right]^{3/2}}$$

The total induced velocities may be written as:

$$\bar{w}_a(\bar{x},\bar{r}) = \mu\bar{\gamma} A_1(\bar{x},\bar{r}) + \bar{\gamma}_1 A_2(\bar{x},\bar{r}) \qquad A_1(\bar{x},\bar{r}) = A_{2,1}(\bar{x},\bar{r}) + A_{3,1}(\bar{x},\bar{r}) + A_{4,1}(\bar{x},\bar{r})$$
$$A_2(\bar{x},\bar{r}) = A_{5,1}(\bar{x},\bar{r})$$

$$\bar{w}_T(\bar{x},\bar{r}) = \bar{\gamma}\, A_3(\bar{x},\bar{r}) \qquad A_3(\bar{x},\bar{r}) = A_{1,2}(\bar{x},\bar{r}) + A_{2,2}(\bar{x},\bar{r}) + A_{3,2}(\bar{x},\bar{r})$$

$$\bar{w}_r(\bar{x},\bar{r}) = \mu\bar{\gamma} A_4(\bar{x},\bar{r}) + \bar{\gamma}_1 A_5(\bar{x},\bar{r}) \qquad A_4(\bar{x},\bar{r}) = A_{2,3}(\bar{x},\bar{r}) + A_{3,3}(\bar{x},\bar{r}) + A_{4,3}(\bar{x},\bar{r})$$
$$A_5(\bar{x},\bar{r}) = A_{5,3}(\bar{x},\bar{r})$$

where the coefficients A are functions of $\bar{x}, \bar{r}$ and the main dimensions of the ducted propeller system (thus R_0, R_1, L and a) only. These coefficients are independent of the vortex densities $\gamma(R_1)$ and $\gamma_1(R_1)$ and the advance coefficient μ.

3. Calculation of the camberline of the nozzle profile

The shape of the camberline of the nozzle profile can be obtained from the relation:

$$\frac{dS(x)}{dx} = \frac{Wr(x,R_1)}{V_e} \qquad \text{or} \qquad S(x) = \int_0^x \frac{Wr(\xi,R_1)}{V_e}\, d\xi$$

where the definitions of $S(x)$ is given in Fig. 1. This relation may also be written as:

$$\bar{S}(\bar{x}) = \frac{S(x)}{R_1} = \mu\bar{\gamma}\, B_1(\bar{x},1) + \bar{\gamma}_1\, B_2(\bar{x},1) \qquad (1)$$

where,

$$B_1(\bar{x},1) = \int_0^{\bar{x}} A_4(\bar{\xi},1)\, d\bar{\xi}$$

$$B_2(\bar{x},1) = \int_0^{\bar{x}} A_5(\bar{\xi},1)\, d\bar{\xi}$$

4. Pressure distribution along the nozzle

With the aid of Bernoulli's theorem the pressure distribution along the nozzle can be calculated. The static pressure coefficients $c_p^+(x)$ and $c_p^-(x)$ are defined by:

$$c_p^+(x) = \frac{p^+(x)-p_\infty}{\frac{1}{2}\rho V_e^2}$$

$$c_p^-(x) = \frac{p^-(x)-p_\infty}{\frac{1}{2}\rho V_e^2}$$

p_∞ and V_e are the static pressure and the velocity of the undisturbed flow,

$p^+(x)$ and $p^-(x)$ are the static pressure at respectively the inner and the outer side of the nozzle as a function of the location.

Calculation of the pressure distribution along the nozzle gives:

$$C_p^+(\bar{x}) = \mu\bar{\gamma}\, B_3(\bar{x},1) + \bar{\gamma}_1\, B_4(\bar{x},1). \qquad (2)$$

$$C_p^-(\bar{x}) = \mu\bar{\gamma}\, B_5(\bar{x},1) + \bar{\gamma}\, B_6(x,1). \qquad (3)$$

where,

$$B_3(\bar{x},1) = \frac{R_1 \sin\theta}{2\sqrt{a(1-a)}} + R_2 - 2A_1(\bar{x},1).$$

$$B_4(\bar{x},1) = \sin\theta - 2A_2(\bar{x},1).$$

$$B_5(\bar{x},1) = -\frac{R_1 \sin\theta}{2\sqrt{a(1-a)}} - R_2 - 2A_1(\bar{x},1)$$

$$B_6(\bar{x},1) = -\sin\theta - 2A_2(\bar{x},1)$$

and

$R_1 = 1 \quad R_2 = 0 \qquad$ for $\quad -a\eta < \bar{x} < 0$

$R_1 = 0 \quad R_2 = 1 \qquad$ for $\quad 0 < \bar{x} < (1-a)\eta$

5. Calculation of thrust, torque and efficiency

The non-dimensional thrust and torque coefficients are defined by:

$$C_T = \frac{T}{\frac{1}{2}\rho V_e^2 \frac{\pi}{4} D^2} \qquad C_{T_{P \text{ or } n}} = \frac{T_{P \text{ or } n}}{\frac{1}{2}\rho V_e^2 \frac{\pi}{4} D^2}$$

$$C_Q = \frac{Q}{\frac{1}{2}\rho V_e^2 \frac{\pi}{4} D^2 D} \qquad \tau = \frac{T_P}{T} = \frac{C_{T_P}}{C_T}$$

where T, T_P, T_n and denote the total thrust, the impeller thrust, the nozzle thrust and the torque. The thrust and torque coefficients become:

$$C_{T_P} = \mu\bar{\gamma}\, C_1 + \bar{\gamma}^2 C_2 \qquad (4)$$

$$C_{T_n} = (\mu\bar{\gamma})^2 C_3 + \mu\bar{\gamma}\bar{\gamma}_1\, C_4 + \bar{\gamma}_1^2 C_5 \qquad (5)$$

$$C_T = C_{T_P} + C_{T_n} \qquad (6)$$

$$C_{T_Q} = \frac{1}{\mu}\left[\mu\bar{\gamma}\, C_6 + (\mu\bar{\gamma})^2 C_7 + \mu\bar{\gamma}\bar{\gamma}_1\, C_8\right] \qquad (7)$$

where, $C_1 = 2C_6 = 2(1-\lambda^2)$

$$C_2 = 4\int_{\lambda}^{1} A_3(0,\bar{r})\,d\bar{r}$$

$$C_3 = -\frac{2}{a\sqrt{1-a}}\int_{-a\eta}^{0} A_3(x,1)\sin\theta\,d\bar{x}$$

$$C_4 = -\frac{2}{a\sqrt{1-a}}\int_{-a\eta}^{(1-a)\eta} A_5(\bar{x},1)\sin\theta\,d\bar{x} - 4\int_{-a\eta}^{(1-a)\eta} A_4(\bar{x},1)\sin\theta\,d\bar{x}$$

$$C_5 = -4\int_{-a\eta}^{(1-a)\eta} A_5(\bar{x},1)\sin\theta\,d\bar{x}$$

$$C_7 = 2\int_{\lambda}^{1} A_1(0,\bar{r})\,\bar{r}\,d\bar{r}$$

$$C_p = 2\int_{\lambda}^{1} A_2(0,\bar{r})\,\bar{r}\,d\bar{r}$$

The efficiency of a ducted propeller system is defined by:

$$\eta_i = \frac{1}{2\mu}\cdot\frac{C_T}{C_Q} \qquad (8)$$

6. Presentation of the computation results:

The shape of the camberline of the nozzle profile, $S(\bar{x})$ the pressure distribution along the nozzle, $C_p^+(\bar{x})$ and $C_p^-(\bar{x})$, the thrust and torque coefficients C_{T_P}, C_{T_n}, C_T and C_Q and the ideal efficiency of the ducted propeller system were given in the relations (1) through (8). From these relations, it can be seen that $\bar{S}(\bar{x})$, $C_p^+(\bar{x})$, $C_p^-(\bar{x})$, C_{T_n} and μC_Q are completely determined by:

the main dimensions of the ducted propeller system, given by R_o, R_1, L and a.

The vortex density $\bar{\gamma}_1$

the product of the vortex density $\bar{\gamma}$ and the advance ratio μ

The thrust coefficient C_{T_p} and consequently the total thrust coefficient C_T and the ideal efficiency η_i depend not only on the product $\mu\bar{\gamma}$ but also on $\bar{\gamma}$

The impeller is represented by an actuator disk rotating with an <u>infinite</u> angular velocity if the undisturbed stream velocity V_e and the product $\mu\bar{\gamma}$ are kept constant and the advance coefficient μ becomes infinite. Then the vortex density $\bar{\gamma}$ goes to zero. Besides, the tangentially induced velocities and consequently the losses due to the rotation of fluid become zero. The case that the actuator disk rotates with an infinite angular velocity coincides with the case that the actuator disk or the impeller rotates with finite angular velocity while a stator is used to eliminate the rotational losses.
The total thrust coefficient C_T , the thrust ratio τ and the ideal efficiency η_i in that case are denoted by C_{T_o} , τ_o and η_{i_o}.

The shape of the camberline of the nozzle profile is also completely determined by the values of C_{T_o} , τ_o and the main dimensions of the ducted propeller system. Calculations of the thrust coefficient C_T , the thrust ratio τ and the ideal efficiency η_i , at various advance coefficients μ were made for a number of nozzle shape given by C_{T_o} , τ_o and the main dimensions of the ducted system λ , η and a In addition, the shapes of the camberline of the nozzle profiles and the pressure distributions along the nozzle surfaces were calculated. The data used for the computations and the results are given in the tables A_1, A_2 and A_3 respectively.

7. Effect of the thickness of the nozzle profile on the flow field

Hitherto, only nozzle profiles with zero thickness were considered. The thickness effect of the nozzle profile on the flow field can be taken into account in the linearized theory by representing the nozzle by a distribution of ring sources and sinks along a cylinder with radius R_4 (see Fig. 1). In the case of very thin nozzle profiles, the strength of the sink and source distributions representing the nozzle profile can be calculated by considering the flow around the profile as two-dimensional. Then the local source strength is equal to the derivative of the profile thickness:

$$q(\xi) = \frac{dh(\xi)}{d\xi}$$

where $h(\xi)$ denotes the local thickness of the nozzle profile. If the source strength $q(\xi)$ is made non-dimensional in the following way:

$$\bar{q}(\xi) = \frac{q(\xi)}{V_e}$$

the induced velocities in the point (x, r) of the flow field due to the ring sources representing the thickness of the nozzle become:

$$\bar{w}_a^{(6)}(\bar{x},\bar{r}) = \frac{1}{\pi}\int_{-a\eta}^{(1-a)\eta} d\bar{\xi} \int_0^{\pi/2} d\psi \; \bar{q}(\bar{\xi}) \frac{(\bar{x}-\bar{\xi})}{\left[(\bar{x}-\bar{\xi})^2 + (1+\bar{r})^2 - 4\bar{r}\sin^2\psi\right]^{3/2}}$$

$$\bar{w}_T^{(6)}(\bar{x},\bar{r}) = 0$$

$$\bar{w}_r^{(6)}(\bar{x},\bar{r}) = \frac{1}{\pi}\int_{-a\eta}^{(1-a)\eta} d\bar{\xi} \int_0^{\pi/2} d\psi \; \bar{q}(\bar{\xi}) \frac{(\bar{r}+\cos 2\psi)}{\left[(\bar{x}-\bar{\xi})^2 + (1+\bar{r})^2 - 4\bar{r}\sin^2\psi\right]^{3/2}}$$

and the effect of the thickness of the nozzle profile on the pressure distributions along the nozzle, the impeller thrust and torque, the nozzle thrust and so

on can be calculated in an easy way.
These calculations will not be given here in detail.

8. Tabulation of the results of the computations

The results of the computations are tabulated in the Tables A_1, A_2 and A_3. Table A_1 presents the thrust coefficients C_{T_0}, the thrust ratios τ_0 and the main dimensions of the ducted propeller systems for which computations were carried out. All the considered nozzle shapes had a NACA four-digit basic thickness form. Table A_2 gives the effect of the rotational velocity of the screw on the ideal efficiency η_i, the thrust coefficient C_T and the thrust ratio τ of the ducted propeller systems.
Finally, Table A_3 presents the mean lines and the pressure distributions along the nozzles of the various ducted propellers. In addition, the ideal efficiency η_i for $J=0$ (η_{i_0}) is given in this Table.

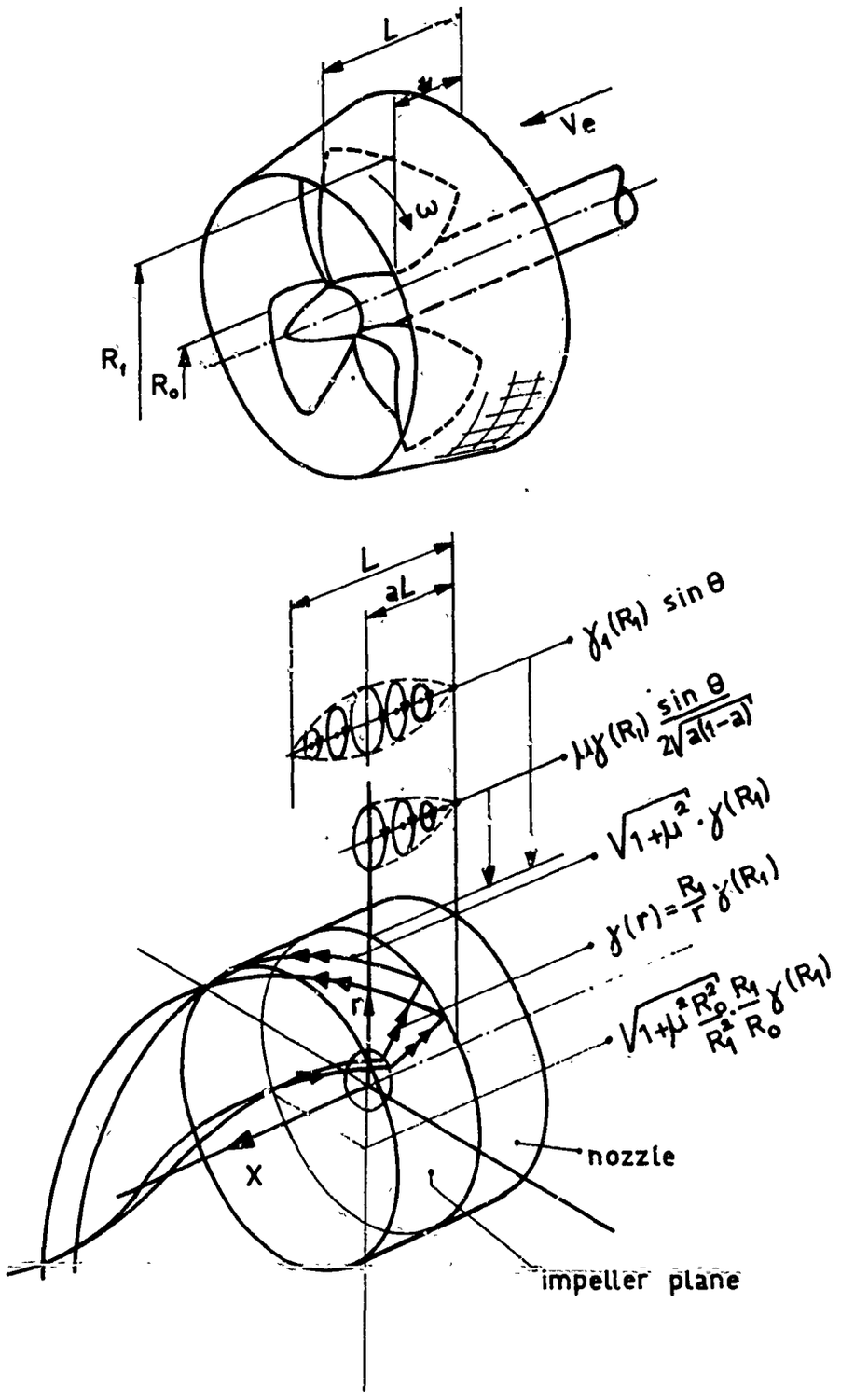

Fig.a Representation of ducted propeller by vortex distributions.

Table A_1 - Thrust coefficiency C_{T_o} , thrust ratio τ_o and main dimensions of nozzles for which computations were carried out.

nozzle number	C_{T_o}	τ_o	L/D	a/L	S/L	d/D
A, 1	0.5	1.0	0.6	0.5	0	0.2
2	0.5	1.0	0.6	0.5	0.15	0.2
3	0.5	1.0	0.3	0.5	0	0.2
4	0.5	1.0	0.3	0.5	0.15	0.2
5	0.5	1.0	0.9	0.5	0	0.2
6	0.5	1.0	0.9	0.5	0.15	0.2
B, 1	0.5	1.2	0.6	0.5	0	0.2
2	0.5	1.2	0.6	0.5	0.15	0.2
3	0.5	1.2	0.3	0.5	0	0.2
4	0.5	1.2	0.3	0.5	0.15	0.2
5	0.5	1.2	0.9	0.5	0	0.2
6	0.5	1.2	0.9	0.5	0.15	0.2
C, 1	0.5	1.4	0.6	0.5	0	0.2
2	0.5	1.4	0.6	0.5	0.15	0.2
3	0.5	1.4	0.3	0.5	0	0.2
4	0.5	1.4	0.3	0.5	0.15	0.2
5	0.5	1.4	0.9	0.5	0	0.2
6	0.5	1.4	0.9	0.5	0.15	0.2
D, 1	1.0	1.0	0.6	0.5	0	0.2
2	1.0	1.0	0.6	0.5	0.15	0.2
3	1.0	1.0	0.3	0.5	0	0.2
4	1.0	1.0	0.3	0.5	0.15	0.2
5	1.0	1.0	0.9	0.5	0	0.2
6	1.0	1.0	0.9	0.5	0.15	0.2
E, 1	1.0	1.2	0.6	0.5	0	0.2
2	1.0	1.2	0.6	0.5	0.15	0.2
3	1.0	1.2	0.3	0.5	0	0.2
4	1.0	1.2	0.3	0.5	0.15	0.2
5	1.0	1.2	0.9	0.5	0	0.2
6	1.0	1.2	0.9	0.5	0.15	0.2
F, 1	1.0	1.4	0.6	0.5	0	0.2
2	1.0	1.4	0.6	0.5	0.15	0.2
3	1.0	1.4	0.3	0.5	0	0.2
4	1.0	1.4	0.3	0.5	0.15	0.2
5	1.0	1.4	0.9	0.5	0	0.2
6	1.0	1.4	0.9	0.5	0.15	0.2

Table A_2 - Effect of the advance coefficient J on the thrust coefficient C_T and the thrust ratio τ of the considered nozzle shapes

$J=\frac{1}{\mu}$	Nozzles Nr. A		Nozzles Nr. B		Nozzles Nr. C	
	C_T/C_{T_o}	τ/τ_o	C_T/C_{T_o}	τ/τ_o	C_T/C_{T_o}	τ/τ_o
0	1.000	1.000	1.000	1.000	1.000	1.000
0.25	0.999	1.000	0.996	1.001	0.995	1.002
0.50	0.989	1.000	0.985	1.003	0.979	1.006
0.75	0.976	1.000	0.966	1.006	0.954	1.013
1.00	0.958	1.000	0.939	1.012	0.917	1.026
1.25	0.935	1.000	0.905	1.017	0.870	1.043
1.50	0.905	1.000	0.862	1.027	0.814	1.066
1.75	0.871	1.000	0.815	1.038	0.748	1.097
2.00	0.831	1.000	0.756	1.054	0.669	1.142

$J=\frac{1}{\mu}$	Nozzles Nr. D		Nozzles Nr. E		Nozzles Nr. F	
	C_T/C_{T_o}	τ/τ_o	C_T/C_{T_o}	τ/τ_o	C_T/C_{T_o}	τ/τ_o
0	1.000	1.000	1.000	1.000	1.000	1.000
0.25	0.995	1.000	0.992	1.002	0.990	1.003
0.50	0.979	1.000	0.970	1.005	0.959	1.012
0.75	0.953	1.000	0.932	1.013	0.907	1.029
1.00	0.915	1.000	0.878	1.023	0.834	1.057
1.25	0.868	1.000	0.810	1.039	0.741	1.100
.50	0.809	1.000	0.725	1.063	0.626	1.171
1.75	0.743	1.000	0.630	1.098	0.496	1.291
2.00	0.662	1.000	0.513	1.158	0.337	1.562

Table A_3 - Mean lines, pressure distributions along the nozzle profile and ideal efficiency of the considered ducted propeller systems.

nozzle number	η_{i_o}	x/R	$S(x)/R$	C_p^+	C_p^-
A, 1	0.889	- 0.600	+ 0.030	- 0.072	- 0.072
		- 0.540	+ 0.026	- 0.024	- 0.133
		- 0.480	+ 0.022	- 0.009	- 0.159
		- 0.240	+ 0.010	+ 0.009	- 0.220
		- 0	+ 0	+ 0	- 0.250
		+ 0	+ 0	+ 0	+ 0.250
		+ 0.240	- 0.010	- 0.010	+ 0.220
		+ 0.480	- 0.022	+ 0.009	+ 0.159
		+ 0.600	- 0.030	+ 0.072	+ 0.072
A, 2	0.898	- 0.600	- 0.011	+ 1.977	+ 1.977
		- 0.540	- 0.007	- 0.378	- 0.321
		- 0.480	- 0.003	- 0.431	- 0.353
		- 0.240	+ 0.005	- 0.481	- 0.362
		- 0	+ 0	- 0.387	- 0.258
		+ 0	- 0	- 0.387	+ 0.243
		+ 0.240	- 0.017	- 0.248	+ 0.329
		+ 0.480	- 0.047	- 0.073	+ 0.305
		+ 0.600	- 0.066	+ 0.121	+ 0.121
A, 3	0.889	- 0.300	+ 0.022	- 0.090	- 0.090
		- 0.270	+ 0.020	- 0.039	- 0.148
		- 0.240	+ 0.017	- 0.022	- 0.172
		- 0.120	+ 0.008	+ 0.003	- 0.226
		- 0	+ 0	+ 0	- 0.250
		+ 0	- 0	- 0	+ 0.250
		+ 0.120	- 0.008	- 0.003	+ 0.227
		+ 0.240	- 0.017	+ 0.002	+ 0.0172
		+ 0.300	- 0.022	+ 0.089	+ 0.089
A, 4	0.899	- 0.300	- 0.006	+ 1.952	+ 1.952
		- 0.270	- 0.004	+ 1.871	+ 1.960
		- 0.240	- 0.003	+ 1.815	+ 1.937
		- 0.120	- 0	+ 1.592	+ 1.778
		- 0	- 0	+ 1.326	+ 1.529
		+ 0	- 0	+ 1.321	+ 2.023
		+ 0.120	- 0.008	+ 0.981	+ 1.625
		+ 0.240	- 0.024	+ 0.361	+ 0.783
		+ 0.300	- 0.034	+ 0.115	+ 0.115

Table A_3 (continued)

nozzle number	η_{i_o}	x/R	$S(x)/R$	C_p^+	C_p^-
A, 5	0.890	- 0.900	+ 0.033	- 0.062	- 0.062
		- 0.855	+ 0.031	- 0.027	- 0.105
		- 0.810	+ 0.028	- 0.015	- 0.124
		- 0.720	+ 0.024	- 0.002	- 0.151
		- 0.360	+ 0.010	+ 0.012	- 0.216
		- 0	+ 0	+ 0	- 0.249
		+ 0	- 0	- 0	+ 0.251
		+ 0.360	- 0.010	- 0.013	+ 0.217
		+ 0.720	- 0.024	+ 0.001	+ 0.152
		+ 0.900	- 0.033	+ 0.062	+ 0.061
A, 6	0.901	- 0.900	- 0.032	+ 1.995	+ 1.995
		- 0.855	- 0.027	- 0.410	- 0.365
		- 0.810	- 0.023	- 0.449	- 0.386
		- 0.720	- 0.015	- 0.501	- 0.415
		- 0.360	+ 0.003	- 0.481	- 0.350
		- 0	+ 0	- 0.372	- 0.229
		+ 0	- 0	- 0.372	+ 0.272
		+ 0.360	- 0.024	- 0.241	+ 0.349
		+ 0.720	- 0.069	+ 0.037	+ 0.423
		+ 0.900	- 0.098	+ 0.398	+ 0.398
B, 1	0.850	- 0.600	- 0.008	- 0.009	- 0.009
		- 0.540	- 0.002	- 0.072	+ 0.058
		- 0.480	+ 0.001	- 0.097	+ 0.084
		- 0.240	+ 0.005	- 0.147	+ 0.130
		- 0	+ 0	- 0.175	+ 0.126
		+ 0	- 0	- 0.175	+ 0.726
		+ 0.240	- 0.018	- 0.169	+ 0.658
		+ 0.480	- 0.052	- 0.075	+ 0.466
		+ 0.600	- 0.076	+ 0.164	+ 0.164
B, 2	0.872	- 0.600	- 0.049	+ 2.046	+ 2.046
		- 0.540	- 0.037	- 0.431	- 0.113
		- 0.480	- 0.026	- 0.526	- 0.088
		- 0.240	- 0	- 0.649	+ 0.020
		- 0	+ 0	- 0.576	+ 0.153
		+ 0	- 0	- 0.576	+ 0.754
		+ 0.240	- 0.026	- 0.421	+ 0.798
		+ 0.480	- 0.079	- 0.164	+ 0.634
		+ 0.600	- 0.116	+ 0.219	+ 0.219

Table A_3 (continued)

nozzle number	η_{i_o}	x/R	$S(x)/R$	c_p^+	c_p^-
B, 3	0.849	- 0.300	- 0.005	- 0.027	- 0.027
		- 0.270	- 0.002	- 0.151	+ 0.100
		- 0.240	+ 0	- 0.196	+ 0.149
		- 0.120	+ 0.004	- 0.288	+ 0.240
		- 0	+ 0	- 0.323	+ 0.252
		+ 0	- 0	- 0.324	+ 0.852
		+ 0.120	- 0.014	- 0.295	+ 0.783
		+ 0.240	- 0.041	- 0.143	+ 0.562
		+ 0.300	- 0.058	+ 0.187	+ 0.187
B, 4	0.934	- 0.300	- 0.043	+ 2.040	+ 2.040
		- 0.270	- 0.034	+ 1.727	+ 2.295
		- 0.240	- 0.026	+ 1.588	+ 2.370
		- 0.120	- 0.004	+ 1.210	+ 2.404
		- 0	+ 0	+ 0.902	+ 2.204
		+ 0	- 0	+ 0.897	+ 2.799
		+ 0.120	- 0.016	+ 0.597	+ 2.341
		+ 0.240	- 0.054	+ 0.143	+ 1.284
		+ 0.300	- 0.080	+ 0.238	+ 0.238
B, 5	0.850	- 0.900	- 0.008	- 0.002	- 0.002
		- 0.855	- 0.006	- 0.032	+ 0.032
		- 0.810	- 0.005	- 0.043	+ 0.046
		- 0.720	- 0.002	- 0.058	- 0.064
		- 0.360	+ 0.004	- 0.092	+ 0.095
		- 0	+ 0	- 0.118	+ 0.086
		+ 0	- 0	- 0.118	+ 0.086
		+ 0.360	- 0.019	- 0.122	+ 0.015
		+ 0.720	- 0.059	- 0.055	+ 0.427
		+ 0.900	- 0.088	+ 0.147	+ 0.147
B, 6	0.877	- 0.900	- 0.077	+ 2.062	+ 2.062
		- 0.855	- 0.068	- 0.415	- 0.214
		- 0.810	- 0.059	- 0.479	- 0.199
		- 0.720	- 0.043	- 0.563	- 0.177
		- 0.360	- 0.003	- 0.596	- 0.007
		- 0	+ 0	- 0.501	+ 0.142
		+ 0	- 0	- 0.500	+ 0.742
		+ 0.360	- 0.034	- 0.361	+ 0.778
		+ 0.720	- 0.107	- 0.025	+ 0.721
		+ 0.900	- 0.157	+ 0.490	+ 0.490

Table A_3 (continued)

nozzle number	η_{i_o}	x/R	$S(x)/R$	C_p^+	C_p^-
C, 1	0.807	- 0.600	- 0.028	+ 0.032	+ 0.032
		- 0.540	- 0.020	- 0.110	+ 0.187
		- 0.480	- 0.014	- 0.160	+ 0.249
		- 0.240	+ 0.002	- 0.258	+ 0.366
		- 0	+ 0	- 0.300	+ 0.381
		+ 0	- 0	- 0.300	+ 1.081
		+ 0.240	- 0.025	- 0.283	+ 0.983
		+ 0.480	- 0.075	- 0.135	+ 0.694
		+ 0.600	- 0.111	+ 0.234	+ 0.233
C, 2	0.836	- 0.600	- 0.073	+ 2.090	+ 2.090
		- 0.540	- 0.057	- 0.469	+ 0.024
		- 0.480	- 0.041	- 0.592	+ 0.086
		- 0.240	- 0.003	- 0.765	+ 0.270
		- 0	+ 0	- 0.707	+ 0.422
		+ 0	- 0	- 0.707	+ 1.123
		+ 0.240	- 0.033	- 0.540	+ 1.137
		+ 0.480	- 0.103	- 0.227	+ 0.871
		+ 0.600	- 0.153	+ 0.291	+ 0.291
C, 3	0.805	- 0.300	- 0.023	+ 0.013	+ 0.013
		- 0.270	- 0.017	- 0.232	+ 0.269
		- 0.240	- 0.011	- 0.322	+ 0.369
		- 0.120	+ 0.002	- 0.496	+ 0.559
		- 0	+ 0	- 0.554	+ 0.597
		+ 0	- 0	- 0.554	+ 1.297
		+ 0.120	- 0.020	- 0.504	+ 1.193
		+ 0.240	- 0.058	- 0.260	+ 0.851
		+ 0.300	- 0.085	+ 0.263	+ 0.263
C, 4	0.919	- 0.300	- 0.065	+ 2.089	+ 2.089
		- 0.270	- 0.052	+ 1.633	+ 2.497
		- 0.240	- 0.040	+ 1.442	+ 2.631
		- 0.120	- 0.006	+ 0.968	+ 2.783
		- 0	+ 0	+ 0.633	+ 2.614
		+ 0	- 0	+ 0.628	+ 3.309
		+ 0.120	- 0.022	+ 0.355	+ 2.811
		+ 0.240	- 0.074	+ 0.006	+ 1.614
		+ 0.300	- 0.111	+ 0.323	+ 0.323

Table A_3 (continued)

nozzle number	η_{i_o}	x/R	S(x)/R	C_p^+	C_p^-
C, 5	0.808	- 0.900	- 0.036	+ 0.038	+ 0.038
		- 0.855	- 0.031	- 0.037	+ 0.124
		- 0.810	- 0.027	- 0.064	+ 0.160
		- 0.720	- 0.019	- 0.099	+ 0.209
		- 0.360	+ 0	- 0.166	+ 0.305
		- 0	+ 0	- 0.202	+ 0.312
		+ 0	- 0	- 0.202	+ 1.012
		+ 0.360	- 0.026	- 0.201	+ 0.911
		+ 0.720	- 0.085	- 0.095	+ 0.633
		+ 0.900	- 0.129	+ 0.211	+ 0.211
C, 6	0.842	- 0.900	- 0.107	+ 2.104	+ 2.104
		- 0.855	- 0.094	- 0.419	- 0.116
		- 0.810	- 0.082	- 0.500	- 0.077
		- 0.720	- 0.061	- 0.605	- 0.023
		- 0.360	- 0.007	- 0.674	+ 0.216
		- 0	+ 0	- 0.589	+ 0.381
		+ 0	- 0	- 0.589	+ 1.082
		+ 0.360	- 0.041	- 0.443	+ 1.088
		+ 0.720	- 0.134	- 0.067	+ 0.936
		+ 0.900	- 0.200	+ 0.557	+ 0.557
D, 1	0.801	- 0.600	+ 0.060	- 0.144	- 0.144
		- 0.540	+ 0.052	- 0.048	- 0.265
		- 0.480	+ 0.044	- 0.019	- 0.318
		- 0.240	+ 0.019	+ 0.018	- 0.439
		- 0	+ 0	- 0	- 0.499
		+ 0	- 0	- 0	+ 0.500
		+ 0.240	- 0.019	- 0.019	+ 0.441
		+ 0.480	- 0.044	+ 0.017	+ 0.318
		+ 0.600	- 0.059	+ 0.014	+ 0.144
D, 2	0.804	- 0.600	+ 0.021	+ 1.902	+ 1.902
		- 0.540	+ 0.020	- 0.400	- 0.461
		- 0.480	+ 0.020	- 0.438	- 0.522
		- 0.240	+ 0.015	- 0.466	- 0.595
		- 0	+ 0	- 0.382	- 0.522
		+ 0	- 0	- 0.381	+ 0.479
		+ 0.240	- 0.026	- 0.252	+ 0.536
		+ 0.480	- 0.068	- 0.062	+ 0.454
		+ 0.600	- 0.095	+ 0.190	+ 0.190

Table A_3 (continued)

nozzle number	η_{i_o}	x/R	$S(x)/R$	c_p^+	c_p^-
D, 3	0.801	- 0.300	+ 0.044	- 0.179	- 0.179
		- 0.270	+ 0.039	- 0.078	- 0.296
		- 0.240	+ 0.034	- 0.045	- 0.344
		- 0.120	+ 0.016	+ 0.006	- 0.452
		- 0	+ 0	- 0	- 0.500
		+ 0	- 0	- 0	+ 0.500
		+ 0.120	- 0.016	- 0.006	+ 0.453
		+ 0.240	- 0.034	+ 0.045	+ 0.345
		+ 0.300	- 0.044	+ 0.178	+ 0.178
D, 4	0.805	- 0.300	+ 0.020	+ 1.855	+ 1.855
		- 0.270	+ 0.018	+ 1.842	+ 1.785
		- 0.240	+ 0.016	+ 1.809	+ 1.731
		- 0.120	+ 0.010	+ 1.623	+ 1.503
		- 0	+ 0	+ 1.357	+ 1.226
		+ 0	- 0	+ 1.351	+ 2.221
		+ 0.120	- 0.015	+ 1.006	+ 1.802
		+ 0.240	- 0.039	+ 0.400	+ 0.921
		+ 0.300	- 0.053	+ 0.196	+ 0.196
D, 5	0.801	- 0.900	+ 0.067	- 0.124	- 0.124
		- 0.855	+ 0.061	- 0.054	- 0.209
		- 0.810	+ 0.057	- 0.030	- 0.247
		- 0.720	+ 0.048	- 0.003	- 0.302
		- 0.360	+ 0.019	+ 0.024	- 0.432
		- 0	+ 0	- 0	- 0.498
		+ 0	- 0	- 0	+ 0.501
		+ 0.360	- 0.019	- 0.026	+ 0.434
		+ 0.720	- 0.047	+ 0.002	+ 0.303
		+ 0.900	- 0.066	+ 0.123	+ 0.123
D, 6	0.805	- 0.900	+ 0.004	+ 1.929	+ 1.929
		- 0.855	+ 0.006	- 0.437	- 0.477
		- 0.310	+ 0.008	- 0.462	- 0.519
		- 0.720	+ 0.011	- 0.500	- 0.578
		- 0.360	+ 0.013	- 0.464	- 0.583
		- 0	+ 0	- 0.367	- 0.497
		+ 0	- 0	- 0.366	+ 0.504
		+ 0.360	- 0.033	- 0.249	+ 0.549
		+ 0.720	- 0.091	+ 0.040	+ 0.563
		+ 0.900	- 0.129	+ 0.456	+ 0.456

Table A_3 (continued)

nozzle number	η_{i_o}	x/R	$S(x)/R$	C_p^+	C_p^-
E, 1	0.738	- 0.600	+ 0.031	- 0.096	- 0.096
		- 0.540	+ 0.029	- 0.102	- 0.101
		- 0.480	+ 0.027	- 0.108	- 0.107
		- 0.240	+ 0.017	- 0.137	- 0.134
		- 0	+ 0	- 0.176	- 0.173
		+ 0	- 0	- 0.176	+ 1.026
		+ 0.240	- 0.029	- 0.180	+ 0.922
		+ 0.480	- 0.079	- 0.065	+ 0.656
		+ 0.600	- 0.112	+ 0.250	+ 0.250
E, 2	0.746	- 0.600	- 0.010	+ 1.954	+ 1.954
		- 0.540	- 0.004	- 0.456	- 0.288
		- 0.480	+ 0.002	- 0.530	- 0.300
		- 0.240	+ 0.012	- 0.627	- 0.274
		- 0	+ 0	- 0.563	- 0.179
		+ 0	- 0	- 0.563	+ 1.022
		+ 0.240	- 0.037	- 0.420	+ 1.033
		+ 0.480	- 0.104	- 0.148	+ 0.803
		+ 0.600	- 0.149	+ 0.300	+ 0.299
E, 3	0.737	- 0.300	+ 0.022	- 0.134	- 0.134
		- 0.270	+ 0.021	- 0.197	- 0.077
		- 0.240	+ 0.020	- 0.223	- 0.058
		- 0.120	+ 0.014	- 0.284	- 0.031
		- 0	+ 0	- 0.324	- 0.048
		+ 0	- 0	- 0.324	+ 1.152
		+ 0.120	- 0.024	- 0.298	+ 1.055
		+ 0.240	- 0.061	- 0.116	+ 0.769
		+ 0.300	- 0.085	+ 0.294	+ 0.294
E, 4	0.747	- 0.300	- 0.008	+ 1.911	+ 1.911
		- 0.270	- 0.004	+ 1.709	+ 2.042
		- 0.240	- 0	+ 1.607	+ 2.066
		- 0.120	+ 0.007	+ 1.293	+ 1.993
		- 0	+ 0	+ 0.990	+ 1.754
		+ 0	- 0	+ 0.984	+ 2.948
		+ 0.120	- 0.024	+ 0.674	+ 2.474
		+ 0.240	- 0.068	+ 0.216	+ 1.394
		+ 0.300	- 0.098	+ 0.323	+ 0.323

Table A_3 (continued)

nozzle number	η_{i_o}	x/R	$S(x)/R$	C_p^+	C_p^-
E, 5	0.738	- 0.900	+ 0.032	- 0.076	- 0.076
		- 0.855	+ 0.031	- 0.064	- 0.093
		- 0.810	+ 0.029	- 0.061	- 0.102
		- 0.720	+ 0.027	- 0.060	- 0.117
		- 0.360	+ 0.016	- 0.078	- 0.165
		- 0	+ 0	- 0.118	- 0.213
		+ 0	- 0	- 0.118	+ 0.987
		+ 0.360	- 0.030	- 0.138	+ 0.875
		+ 0.720	- 0.087	- 0.054	+ 0.609
		+ 0.900	- 0.127	+ 0.220	+ 0.220
E, 6	0.747	- 0.900	- 0.033	+ 1.981	+ 1.981
		- 0.855	- 0.027	- 0.447	- 0.355
		- 0.810	- 0.021	- 0.494	- 0.365
		- 0.720	- 0.012	- 0.559	- 0.382
		- 0.360	+ 0.009	- 0.571	- 0.300
		- 0	+ 0	- 0.490	- 0.194
		+ 0	- 0	- 0.489	+ 1.006
		+ 0.360	- 0.045	- 0.366	+ 1.005
		+ 0.720	- 0.132	- 0.018	+ 0.879
		+ 0.900	- 0.192	+ 0.557	+ 0.557
F, 1	0.674	- 0.600	+ 0.013	- 0.069	- 0.069
		- 0.540	+ 0.016	- 0.143	+ 0
		- 0.480	+ 0.017	- 0.173	+ 0.026
		- 0.240	+ 0.016	- 0.246	+ 0.059
		- 0	+ 0	- 0.301	+ 0.031
		+ 0	- 0	- 0.301	+ 1.431
		+ 0.240	- 0.038	- 0.296	+ 1.291
		+ 0.480	- 0.106	- 0.123	+ 0.916
		+ 0.600	- 0.153	+ 0.334	+ 0.334
F, 2	0.684	- 0.600	- 0.028	+ 1.981	+ 1.981
		- 0.540	- 0.017	- 0.498	- 0.182
		- 0.480	- 0.008	- 0.597	- 0.162
		- 0.240	+ 0.011	- 0.738	- 0.075
		- 0	+ 0	- 0.691	+ 0.033
		+ 0	- 0	- 0.691	+ 1.433
		+ 0.240	- 0.045	- 0.539	+ 1.408
		+ 0.480	- 0.132	- 0.207	+ 1.068
		+ 0.600	- 0.191	+ 0.385	+ 0.384

Table A_3 (continued)

nozzle number	η_{i_o}	x/R	$S(x)/R$	C_p^+	C_p^-
F, 3	0.673	- 0.300	+ 0.008	- 0.113	- 0.113
		- 0.270	+ 0.011	- 0.287	+ 0.062
		- 0.240	+ 0.013	- 0.353	+ 0.128
		- 0.120	+ 0.013	- 0.491	+ 0.243
		- 0	+ 0	- 0.554	+ 0.247
		+ 0	- 0	- 0.555	+ 1.646
		+ 0.120	- 0.031	- 0.508	+ 1.510
		+ 0.240	- 0.082	- 0.229	+ 1.092
		+ 0.300	- 0.116	+ 0.387	+ 0.287
F, 4	0.685	- 0.300	- 0.023	+ 1.937	+ 1.937
		- 0.270	- 0.016	+ 1.613	+ 2.197
		- 0.240	- 0.009	+ 1.468	+ 2.271
		- 0.120	+ 0.006	+ 1.069	+ 2.297
		- 0	+ 0	+ 0.740	+ 2.080
		+ 0	- 0	+ 0.735	+ 3.474
		+ 0.120	- 0.031	+ 0.448	+ 2.958
		+ 0.240	- 0.094	+ 0.094	+ 1.737
		+ 0.300	- 0.131	+ 0.421	+ 0.421
F, 5	0.675	- 0.900	+ 0.011	- 0.049	- 0.049
		- 0.855	+ 0.012	- 0.074	- 0.023
		- 0.810	+ 0.013	- 0.085	- 0.013
		- 0.720	+ 0.015	- 0.101	- 0.002
		- 0.360	+ 0.014	- 0.149	+ 0.002
		- 0	+ 0	- 0.202	- 0.037
		+ 0	- 0	- 0.203	+ 1.363
		+ 0.360	- 0.040	- 0.219	+ 1.215
		+ 0.720	- 0.118	- 0.094	+ 0.845
		+ 0.900	- 0.175	+ 0.297	+ 0.297
F, 6	0.686	- 0.900	- 0.055	+ 2.009	+ 2.009
		- 0.855	- 0.046	- 0.457	- 0.281
		- 0.810	- 0.038	- 0.519	- 0.272
		- 0.720	- 0.024	- 0.601	- 0.262
		- 0.360	+ 0.007	- 0.644	- 0.127
		- 0	+ 0	- 0.576	- 0.012
		+ 0	- 0	- 0.576	+ 1.389
		+ 0.360	- 0.054	- 0.449	+ 1.351
		+ 0.720	- 0.164	- 0.059	+ 1.120
		+ 0.900	- 0.241	+ 0.635	+ 0.635

Unclassified
Security Classification

DOCUMENT CONTROL DATA - R&D

(Security classification of title, body of abstract and indexing annotation must be entered when the overall report is classified)

1 ORIGINATING ACTIVITY (Corporate author) Netherlands Ship Model Basin Wageningen	2a REPORT SECURITY CLASSIFICATION Unclassified 2b GROUP —

3 REPORT TITLE

Series of Model Tests on Ducted Propellers

4 DESCRIPTIVE NOTES (Type of report and inclusive dates)

Final Report

5 AUTHOR(S) (Last name, first name, initial)

Oosterveld, Marinus W.C.

6 REPORT DATE October 1967	7a TOTAL NO. OF PAGES 89	7b NO. OF REFS 5
8a CONTRACT OR GRANT NO N 62558-4555 b PROJECT NO Subproject S-R 009-01-01 c Task d	9a ORIGINATOR'S REPORT NUMBER(S) 67-163-AH 9b OTHER REPORT NO(S) (Any other numbers that may be assigned this report) —	

10 AVAILABILITY/LIMITATION NOTICES "This document is subject to special export controls and each transmittal to foreign governments or foreign nationals may be made only with prior approval of the Naval Ship Research and Development Center, Washington, D.C. 20007".

11 SUPPLEMENTARY NOTES	12 SPONSORING MILITARY ACTIVITY Naval Ship Research and Development Center

13 ABSTRACT

This reports presents the results of open water tests and observation of the cavitation characteristics of systematic series of flow decelerating type of nozzles (or pumpjets). The tested nozzle shapes have been derived theoretically. The results of these theoretical calculations and of the experiments, are presented in a non-dimensional form in graphs and tables.
A discussion of the results is given.

DD FORM 1 JAN 64 1473
(ENCLOSURE 1)

Unclassified
Security Classification

Unclassified
Security Classification

14 KEY WORDS	LINK A		LINK B		LINK C	
	ROLE	WT	ROLE	WT	ROLE	WT
Ducted propellers Decelerating type of nozzle Pumpjet Open-water tests Cavitation tests						

INSTRUCTIONS

1. ORIGINATING ACTIVITY: Enter the name and address of the contractor, subcontractor, grantee, Department of Defense activity or other organization *(corporate author)* issuing the report.

2a. REPORT SECURITY CLASSIFICATION: Enter the overall security classification of the report. Indicate whether "Restricted Data" is included. Marking is to be in accordance with appropriate security regulations.

2b. GROUP: Automatic downgrading is specified in DoD Directive 5200.10 and Armed Forces Industrial Manual. Enter the group number. Also, when applicable, show that optional markings have been used for Group 3 and Group 4 as authorized.

3. REPORT TITLE: Enter the complete report title in all capital letters. Titles in all cases should be unclassified. If a meaningful title cannot be selected without classification, show title classification in all capitals in parenthesis immediately following the title.

4. DESCRIPTIVE NOTES: If appropriate, enter the type of report, e.g., interim, progress, summary, annual, or final. Give the inclusive dates when a specific reporting period is covered.

5. AUTHOR(S): Enter the name(s) of author(s) as shown on or in the report. Enter last name, first name, middle initial. If military, show rank and branch of service. The name of the principal author is an absolute minimum requirement.

6. REPORT DATE: Enter the date of the report as day, month, year, or month, year. If more than one date appears on the report, use date of publication.

7a. TOTAL NUMBER OF PAGES: The total page count should follow normal pagination procedures, i.e., enter the number of pages containing information.

7b. NUMBER OF REFERENCES: Enter the total number of references cited in the report.

8a. CONTRACT OR GRANT NUMBER: If appropriate, enter the applicable number of the contract or grant under which the report was written.

8b, 8c, & 8d. PROJECT NUMBER: Enter the appropriate military department identification, such as project number, subproject number, system numbers, task number, etc.

9a. ORIGINATOR'S REPORT NUMBER(S): Enter the official report number by which the document will be identified and controlled by the originating activity. This number must be unique to this report.

9b. OTHER REPORT NUMBER(S): If the report has been assigned any other report numbers *(either by the originator or by the sponsor)*, also enter this number(s).

10. AVAILABILITY/LIMITATION NOTICES: Enter any limitations on further dissemination of the report, other than those imposed by security classification, using standard statements such as:

(1) "Qualified requesters may obtain copies of this report from DDC."

(2) "Foreign announcement and dissemination of this report by DDC is not authorized."

(3) "U. S. Government agencies may obtain copies of this report directly from DDC. Other qualified DDC users shall request through _____."

(4) "U. S. military agencies may obtain copies of this report directly from DDC. Other qualified users shall request through _____."

(5) "All distribution of this report is controlled. Qualified DDC users shall request through _____."

If the report has been furnished to the Office of Technical Services, Department of Commerce, for sale to the public, indicate this fact and enter the price, if known.

11. SUPPLEMENTARY NOTES: Use for additional explanatory notes.

12. SPONSORING MILITARY ACTIVITY: Enter the name of the departmental project office or laboratory sponsoring *(paying for)* the research and development. Include address.

13. ABSTRACT: Enter an abstract giving a brief and factual summary of the document indicative of the report, even though it may also appear elsewhere in the body of the technical report. If additional space is required, a continuation sheet shall be attached.

It is highly desirable that the abstract of classified reports be unclassified. Each paragraph of the abstract shall end with an indication of the military security classification of the information in the paragraph, represented as *(TS), (S), (C), or (U)*

There is no limitation on the length of the abstract. However, the suggested length is from 150 to 225 words.

14. KEY WORDS: Key words are technically meaningful terms or short phrases that characterize a report and may be used as index entries for cataloging the report. Key words must be selected so that no security classification is required. Identifiers, such as equipment model designation, trade name, military project code name, geographic location, may be used as key words but will be followed by an indication of technical context. The assignment of links, rules, and weights is optional

Unclassified
Security Classification